Dynamic Modeling of a Small Modular Reactor for Control and Monitoring

A Thesis Presented for the

Master of Science

Degree

The University of Tennessee, Knoxville

Jeffrey Robert Kapernick

May 2015

© by Jeffrey Robert Kapernick, 2015
All Rights Reserved.

Acknowledgments

This research has been performed as part of a grant: STTR-Phase II Online monitoring in Small Modular Reactors, Grant award number: DE-SC0008282, sponsored by the U.S. Department of Energy, and mediated by the Analysis and Measurement Services Corporation.

The author would like to thank and acknowledge the advice, mentoring, and guidance provided by Dr. Belle R. Upadhyaya, and also the other members of the graduate committee Dr. J Wesley Hines and Dr. Arthur E. Ruggles.

Abstract

A system model of the Babcock & Wilcox Generation mPower small modular reactor (SMR) was developed within the MATLAB-Simulink environment. A detailed physical configuration of this SMR was established based on the limited information available for the mPower reactor. This is an important step in the development of the simulation model. Three mathematical models were combined to simulate the control dynamics. A lumped-parameter approximation of fuel-to-coolant heat transfer is combined with vessel upper plenum and lower plenum coolant masses to represent the core power and heat transfer dynamics. A nodalized moving boundary steam generator model balances mass, momentum, and energy for the sub-cooled, saturated, and superheated flow regimes. A component based balance-of-plant system calculates the feedwater temperature. Controllers for the system include a once-through steam generator program which maintains a constant average primary coolant temperature with reactor thermal power, and a constant steam pressure controller, which maintains the steam outlet pressure at the set point by throttling the main steam valve. The integrated plant model is used to generate normal operation data and simulation of plant operation under specified transients. These data are being used for developing and testing on-line monitoring techniques for small modular reactors.

Table of Contents

List of Tables

List of Figures

Acronyms

B&W	The Babcock & Wilcox Company
BOL	Beginning of Life
BOP	Balance of Plant Systems
CVCS	Chemical and Volume Control System
DOE	Department of Energy
DPA	Dislocations Per Atom
EOL	End of Life
FOA	Funding Opportunity Announcement
IEOTSG	Integral Economizer Once-Through Steam Generator
iPWR	Integral Pressurized Water Reactor
NRC	Nuclear Regulatory Commission
OTSG	Once-Through Steam Generator
REA	Rod Ejection Accident
RPV	Reactor Pressure Vessel
SMR	Small Modular Reactor
UTSG	U-Tube Steam Generator

Chapter 1

Introduction

1.1 Recent developments of small modular reactors

Renewed interest in the Small Modular Reactor (SMR) was prompted with the development of the NuScale Power reactor toward the late 2000's. As the project evolved and became more credible, competitors quickly emerged to ensure no single entity owned the market. Of the applicants, the four major companies pursuing design certification included NuScale Power, Babcock & Wilcox (B&W) Generation mPower, Holtec SMR-160, and the Westinghouse SMR. To further assist in the development and licensing of SMR technology, the United States Department of Energy (DOE) offered a Funding Opportunity Announcement (FOA) which would be awarded to two applicants. This announcement froze the financial activity of investors and venture capitalists who were now interested in monitoring the decision of the FOA unfold before committing to a design.

In January 2013 it was announced that B&W would be the lone recipient of the FOA for FY2013 (near 250 million USD provided over a period of 5 years, to be matched by the company) and that the second recipient would be awarded in FY2014. NuScale Power was subsequently awarded the FOA in January 2014. In April 2014, Generation mPower announced that it was significantly reducing its budget; effectively terminating the project. This announcement shocked the industry and community, especially the DOE as over 100 million taxpayer dollars had already been provided to that project. Part of the explanation included that B&W had no domestic customer for the near term. Tennessee Valley Authority had once been the proposed customer of the first Generation mPower reactor module, with a specified site. This arrangement has since disintegrated and the details have never been disclosed publicly.

NuScale Power remains the only entity to earnestly pursue design certification from the United States Nuclear Regulatory Commission (NRC). It has since received funding and support from FLUOR corporation, Rolls Royce, Western Initiative for Nuclear (support from several northwestern senators and politicians), Idaho National Laboratory and Enercon. Testing is being performed at Stern and SIET laboratories; there has been a proposed site for a prototype reactor module at Idaho National Laboratory.

1.2 The Role & Application of Load Following to the Nuclear Power Industry

A commercial nuclear power plant provides electricity to the power grid in the form of baseload: the amount of energy which is always consumed by the ratepayers. Throughout the course of a day, the grid will experience different levels of demand and consumption. For example the energy consumption during weekday evenings ramps to peak usage as a result of ratepayers returning home from work and using the HVAC, television, stove and other appliances. To provide the required energy for this demand, utilities will often burn natural gas. Natural gas plants may quickly be brought up to full power and do not have the same safety considerations associated with a nuclear chain reaction and decay heat.

Nuclear power plants have generally not been designed to accommodate grid demands. The reactor core is designed to operate at full power for the duration of the fuel cycle to ensure a uniform burnup of the fuel assemblies and maximize the economy of the plant. A sophisticated analysis of fuel assembly type and composition (enrichment and neutron poison within the fuel matrix) and assembly shuffling (relocation of partially spent fuel assemblies) is performed during each outage to achieve this purpose. The prospect of maneuvering reactor power levels to accommodate the grid undermines this effort. It also increases demand on the operators who may be required to configure the reactor within thin margins of its technical specifications. The extent of additional procedures for load following operations and their effects on human factors are not yet well defined.

The benefit of modular plants in terms of load following, however, is that it may be possible to configure the majority of modules to be at baseload while using a single module to handle load following. After a prescribed period, the module responsible for handling load following operations would be rotated, thus reducing the effects of inconsistent burnup within each module. The logistics for this strategy of modular load following is also currently being explored.

1.3 Online Monitoring

The general strategy for much of the nuclear power plant upkeep revolves around scheduled maintenance. After 18 months each unit is brought offline for refueling; during which time equipment is serviced and calibrated. This type of program prescribes maintenance for components which are still in good health. It also introduces the potential for a maintenance worker to inadvertently degrade a component through improper maintenance or human error. Furthermore, when equipment is calibrated according to a schedule and not monitored, there exists the possibility that a piece of equipment could be operating in a faulty state for up to a full maintenance cycle.

The use of online monitoring can help to eliminate these concerns. Online monitoring programs output a signal for each component to enable the user to observe degradation of the component over time. When the reactor is brought offline for refueling, degraded components, sensors, etc. may be replaced as need be, reducing the effort necessary for scheduled maintenance and the potential for human error.

1.4 Research Objective

The purpose of this research was to assemble a system model of the Babcock & Wilcox Generation mPower module including the reactor core and the once-through steam generator. The reactor core model is made up of a system of Ordinary Differential Equations (ODE) which approximate heat transfer from the nuclear fuel to the coolant. The solutions of the ODEs from the reactor core model are coupled to a similar system of ODEs which comprise the once-through steam generator model. Inputs which are made to the reactor core are coupled to the dynamics of the steam generator and vice versa.

A requirement of the model was to implement two reactor control systems. The first was the T-average control program, typical of a once-through steam generator, which maintains a constant average temperature of the core inlet and outlet to that of a user setpoint. As the average temperature deviates from the setpoint, a feedback mechanism introduces reactivity into the core (simulated rod manipulation) to bring the deviation back to the desired setpoint. The second control system maintains a constant steam outlet pressure by throttling the main steam control valve. As main steam pressure increases, the steam control valve is opened to relieve pressure back to the user setpoint. These two control systems drive the dynamics of the model.

Following completion of the model and its control systems, the model was used to generate normal operation data and simulation of small transients including an insertion of reactivity. The model had to be capable of generating data of large power excursions, associated with load following maneuvers. The data generated was submitted to the Analysis and Measurement Services Corporation for further development and testing of on-line monitoring techniques and algorithms for small modular reactors.

1.5 Project Tasks and Accomplishments

A comprehensive literature survey was conducted of the technical details of the Generation mPower to identify its physical characteristics, operating conditions, parameters and geometries. This effort proved to be limited in scope due to the competitive nature of the reactor design and its protected intellectual property, however sufficient design information was available through the company website, patent documents and submitted presentations to the NRC to produce an accurate collection of necessary input.

Following completion of the set of input parameters, the ODEs of the core model and the OTSG model had to be represented as signals within the Simulink environment. Although equations were provided by the source documentation, their representation for the conservation of mass, momentum and energy, did not explicitly solve for a specific state variable. The entire system of equations had to be reorganized for explicit solutions of each state variable prior to the implementation within the Simulink model.

The core model and steam generator model were successfully coupled, enabling the output of the core model (hotleg or core exit temperature) to feed directly into the steam generator model (Tp1 inlet temperature). For reactor control, the two control systems were implemented and tested. To improve the functionality of the model, a system of equations was added to simulate the Balance of Plant (BOP). The BOP has been implemented within the model, however its development requires additional verification before it will be coupled back to the dynamics of the steam generator. The BOP has been structured to generate an output of feedwater temperature when provided the main steam flow, temperature, and pressure from the steam generator model. The feedwater flow rate is the main user input for manual control of the reactor system.

The final deliverable and goal of the model was to produce output data for the Analysis and Measurement Services Corporation. The data provided included transients for a step insertion of positive reactivity and a sequence of reactor power excursions. The plots of these transients are provided in Chapter 7.

1.6 Thesis Organization

A general overview of the mPower reactor is provided in Chapter 2. This includes a description of the major components including the reactor core, reactor pressure vessel, steam generator, containment, and pressurizer. Some of the newer developments of the generation III+ reactor technology are discussed, including the history of the design changes and evolution of the once-through steam generator, implementation of integral control rod technology and its potential for the elimination of chemical shim, and design considerations which may assist in extending reactor power plant lifetimes beyond 80 years.

Chapter 3 illustrates the coupling of the mathematical models which comprise the full mPower system. It includes a brief discussion on the ODE solving routines available in Matlab-Simulink and provides justification for using the selected method.

A description of the reactor core modeling is provided in Chapter 4. This model is based primarily on Mann's core heat transfer model, of which the nodalization and assumptions are discussed. In addition, different reactor control strategies are introduced, highlighting the difference between once-through and u-tube steam generator control. The control strategy for the once-through steam generator (T-average controller) is discussed including its feedback mechanism. Equations for the reactor core module are also presented within Chapter 4.

The dynamics of the once-through steam generator are provided in Chapter 5. This includes the simplification and assumptions used in the flow regimes for the transitions from single phase subcooled liquid, to two-phase flow, to single phase superheated fluid. Source documentation of the data from Oconee nuclear station used to approximate fluid levels in the steam generator are provided. The second major control system of the model, the steam pressure controller, is described. Equations for the once-through steam generator are also presented within Chapter 5.

The development of the BOP is presented in Chapter 6. The arrangement of the components within the BOP are consistent with the source documentation. Equations for each component are presented within the corresponding subsection of the chapter. Many of the requirements for signals within this system of equations are based on polynomials and lookup tables relating temperature, pressure and enthalpy. The origin for each polynomial and table is referenced and discussed.

Simulations of the model are discussed in Chapter 7. Each simulation includes a series of output plots. The dynamics of the model may be observed in the response of each signal.

Concluding remarks, recommendations and future work are discussed in Chapter 8. A discussion of known issues, complications of the Matlab-Simulink environment, and suggestions for future development of the code and the BOP are provided.

Chapter 2

Description of the B&W Generation mPower Module

The B&W Generation mPower is an SMR which consists of two reactor units housed within a partially underground containment, both of which are operated from a single control room. Each unit generates 530 MWth and 180 MWe for a total plant output of 360 MWe. The reactor includes a forced flow primary coolant system, integral components, and a secondary system which produces superheated steam. Its notable departures from generation II commercial plants include a passive emergency core cooling system which takes advantage of natural circulation and also a four year, once through fuel cycle of the reactor core. Reactor specifics will be detailed in the following subsections.

2.1 Reactor Core

The Generation mPower reactor core is made up of 69 fuel assemblies (Figure 2.1). The assemblies are a standard Westinghouse 17 x 17 fuel pin, control rod and instrumentation tube lattice of conventional geometry (Figure 2.2), with the exception that the height of the active fuel is shorter than that of a standard assembly (approximately 7.9 feet tall). General reactor design parameters are provided in Appendix A.1.

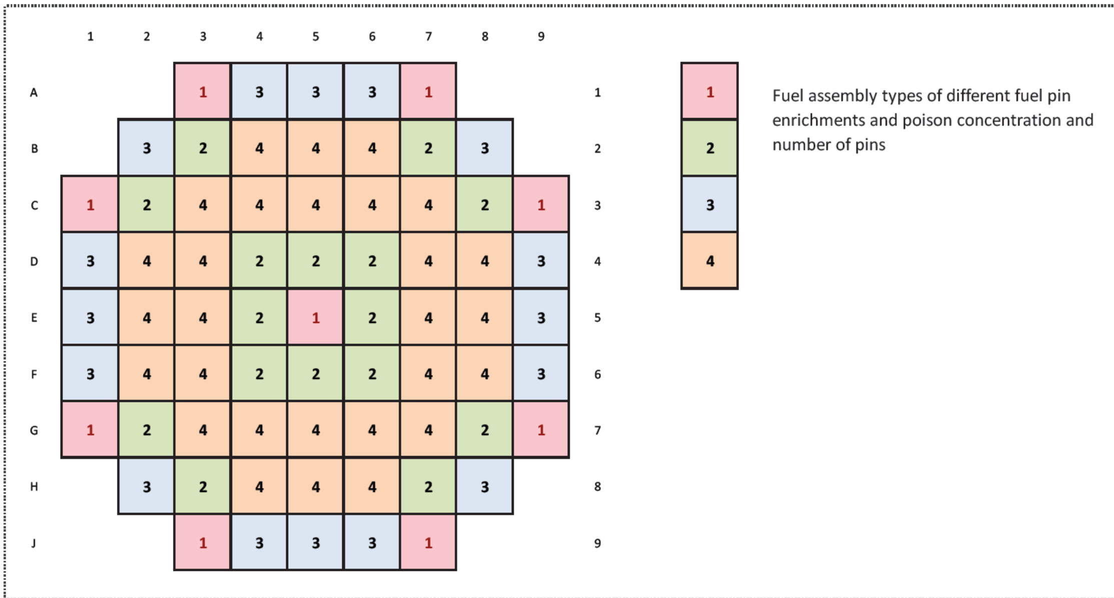

Figure 2.1: B&W Core Configuration [1] [2]

Of the 69 fuel assemblies, 61 contain removable control rods. This is made possible by the development of integral Control Rod Drive Mechanisms (CRDM). The majority of current generation plants use external CRDMs which are physically welded to the top of the reactor pressure vessel. The rod drive connects a shaft to the spider assembly which is then attached to a bundle of 24 boron or cadmium control rods. Therefore external rod drives span the entire length of the reactor pressure vessel and require the use of a support structure. In addition, the number of control rods are limited to the diameter of the central riser; meaning it is not physically possible to dedicate a rod drive to each fuel assembly. Fuel assemblies at the periphery of the core typically cannot accept control rods due to the compacted internals of the reactor module.

The integral control drive is much different in that the drive mechanism is submerged in the primary coolant and positioned directly above the fuel assembly. The mechanism has been designed to operate and withstand temperature and pressure of the primary coolant environment. The proximity of the rod drives eliminate the need for a support structure and significantly reduce any potential for the effects of control rod bow. Unlike external drives, integral drives are not confined to the window of the central riser which enables a

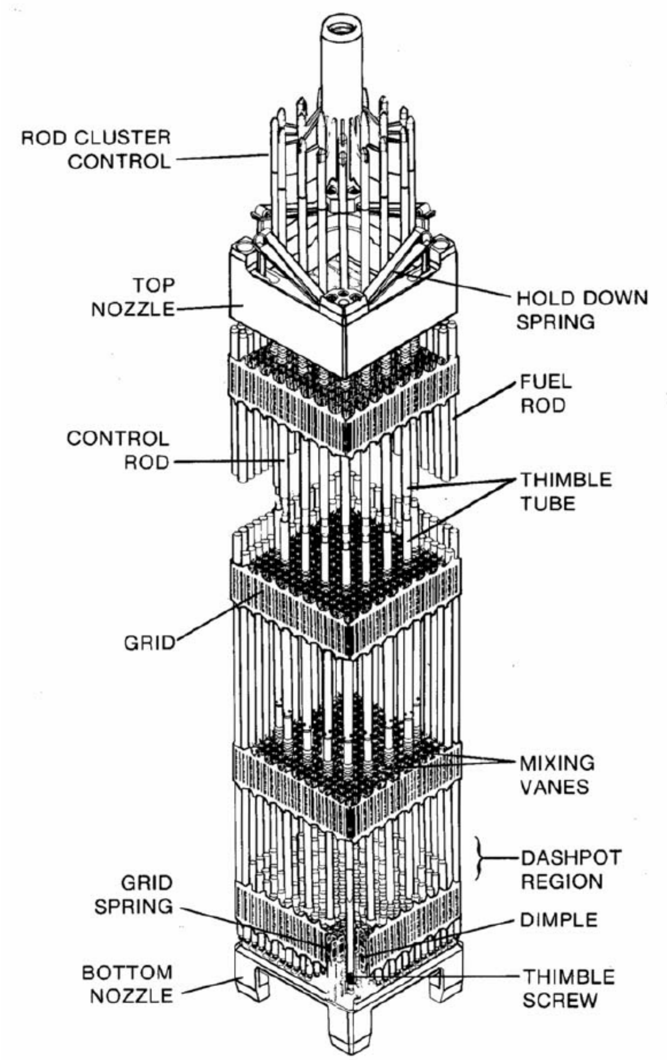

Figure 2.2: Westinghouse 17 x 17 fuel assembly [3]

much higher ratio of CRDMs to fuel assemblies. The additional rod drives provide a great advantage to the design of the plant for several reasons including increased reactor control, reduced licensing risk and the ability to operate the reactor without the need for chemical shim.

The increased level of control makes the reactor more licensable. The NRC mandates that applicants of a design certification perform a series of design basis calculations prescribed in Chapter 15 of NUREG-0800. One of the postulated accidents in Chapter 15 is the Rod Ejection Accident (REA), a measure directly attributed to the disaster which occurred in

Idaho at the SL-1 military reactor. The REA requires the applicant to evaluate the integrity of the core when the single highest worth rod bank is immediately and fully withdrawn. When this occurs, the worth of the remaining rods must be sufficient to ensure the reactor core may safely return to a controlled and stable configuration. As the ratio of control rod drives to fuel assemblies increases, the worth of each individual rod bank decreases, making this type of accident less credible.

The additional control rods also enable the plant to operate without the need for chemical shim of soluble boron. At the Beginning of Life (BOL) of the fuel cycle, it is common for commercial plants to introduce soluble boron into the primary water chemistry up to a concentration of 2000 ppm (maximum allowable; Figure 2.3). As the core burns, the operators will reduce this concentration through use of the Chemical and Volume Control System (CVCS). The CVCS includes a series of filters, gel beds, condensate polishers, and other equipment which will regulate primary water chemistry including boron concentration, pH, and filtration of particulate. As the core nears the End of Life (EOL), the concentration of soluble boron is reduced to enable as much burnup of the fuel as possible for the final months of the cycle. The ability to eliminate the need for chemical shim is advantageous as it simplifies reactor operations by reducing the involvement of the CVCS . Soluble boron is also very corrosive and leads to additional materials degradation issues within the reactor internals and the RPV dome; as experienced at the Davis-Besse Nuclear Power Station.

2.2 Reactor Pressure Vessel

The Reactor Pressure Vessel (RPV) is approximately 83 feet tall and 13 feet in diameter at the flange (Figure 2.4). The general configuration of the RPV may be classified by its internals above and below the flange as the upper and lower vessel respectively (Figure 2.5). The upper vessel contains the central riser, pressurizer, reactor coolant pumps, and steam generator. The lower vessel consists of the downcomer, reactor core, support plate, reactor internals and support structures, and the control rod drive mechanisms.

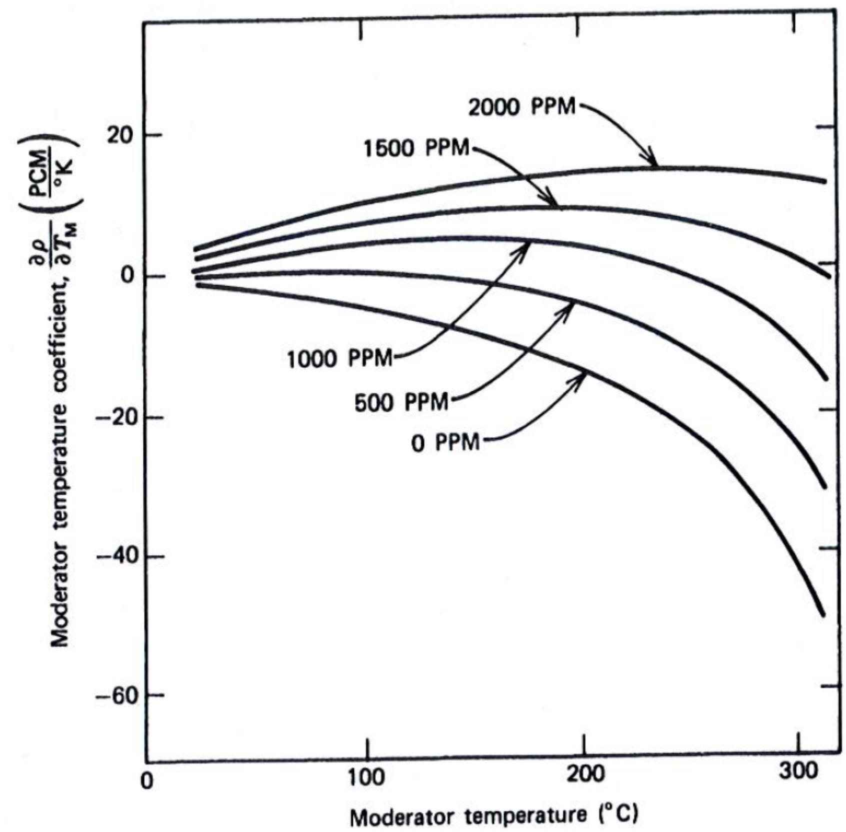

Figure 2.3: The effect of chemical shim on the moderator temperature coefficient in a PWR [4]

There are eight reactor coolant pumps, inverted and flanged to the top of the RPV. The pump impeller is included within the RPV pressure boundary while the motor, housing and serviceable components of the pump are excluded at the gasket. The steam generator is a straight tube, once-through design, discussed in detail in Section 2.3.

The primary system and secondary steam generator flow paths are illustrated in Figure 2.6. Primary coolant flows across the core and up through the central riser to the inlet of the reactor coolant pumps which force flow through the tube side of the steam generator. As the flow passes through the reactor coolant pumps it reaches the tube grid and endures a large pressure drop across the primary steam generator section. As the primary fluid leaves the steam generator tubes, the flow merges in the downcomer to complete the flow cycle by again moving across the core.

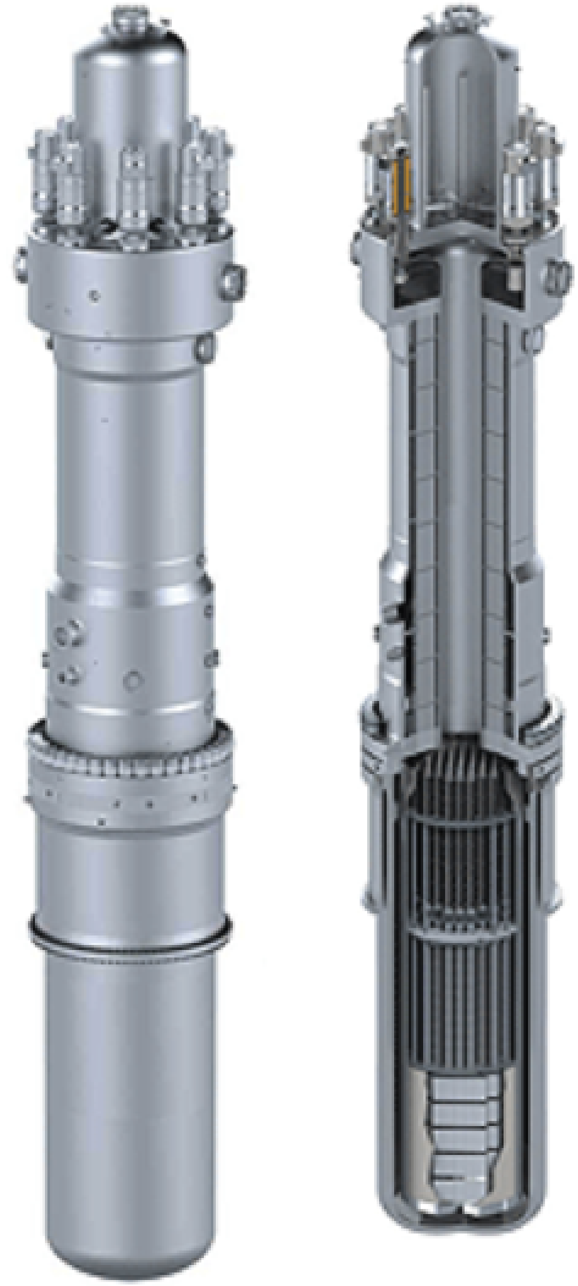

Figure 2.4: Babcock & Wilcox Generation mPower Reactor Pressure Vessel [5]

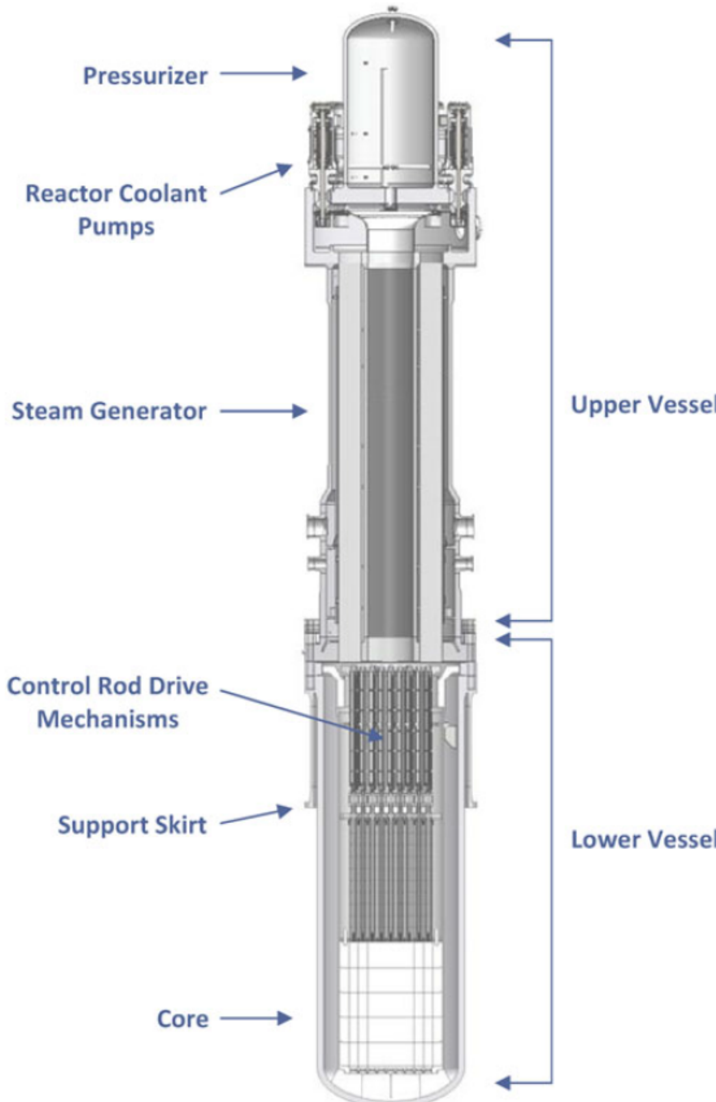

Figure 2.5: Upper & Lower Module Configuration [6]

On the secondary side of the steam generator (shell side) fluid flow makes an initial one half length downward pass within the feedwater plenum. As the flow reaches the bottom of the plenum it makes a 180 degree turn upward where it makes contact with the primary tube wall and begins to absorb heat from the primary system; this region is referred to as the integral economizer. The flow then makes a full upward pass across the span of the active steam generator tube length where the flow transitions from subcooled to the two-phase regimes to superheated steam. The superheated steam makes a 180 degree bend at the top of the active steam generator to proceed downward for the final half pass to the main steam nozzle and ultimately to the high pressure turbine system.

Additional important design characteristics of the mPower include flanged lower sections of the RPV. Currently the most substantial limiting factor to the lifetime of a nuclear power plant is the integrity of the RPV. After 60 years of neutron bombardment the beltline of the RPV takes a significant dose measured in Dislocations Per Atom (DPA), altering the characteristics of the material, reducing ductility. Certain levels of DPA actually strengthen the RPV steel, however, it also embrittles the material and reduces its ability to arrest cracks. Long term studies exploring the possibility of extending reactor operations from 60 year lifetime to 80 year lifetime are being conducted; however, the mPower design could bypass the issue entirely. Only a small portion of the RPV would need to be replaced (lower vessel shell), offering an economic solution for the extension of the lifetime of the plant.

2.3 Steam Generator

The Generation mPower Steam Generator (SG) is a counter flow shell and tube once-through design type, with primary fluid flowing top-down inside the straight tubes, and the feedwater flowing bottom-up in the active shell side (Figure 2.6). The steam generator feedwater inlet consists of subcooled water which at full power produces steam with 50 degrees Fahrenheit of superheat.

Knowledge and technical details for this design are extremely limited in the open source literature due to proprietary and competitive concerns. To calculate geometry, it was necessary to make assumptions for the diameter of the central riser (and its thickness), nominal tube diameter and schedule [7], triangular packing arrangement [8] (which includes the pitch and clearance; Figure 2.7) and the total number of SG tubes. With these assumptions and resources, realistic ratios of heat transfer surface area to cross sectional flow area within the SG (Figures 2.8 and 2.9) may be determined.

The following images were generated and subsequent calculations were performed using a computer code developed by the author. The user inputs the tube OD, tube ID, pitch,

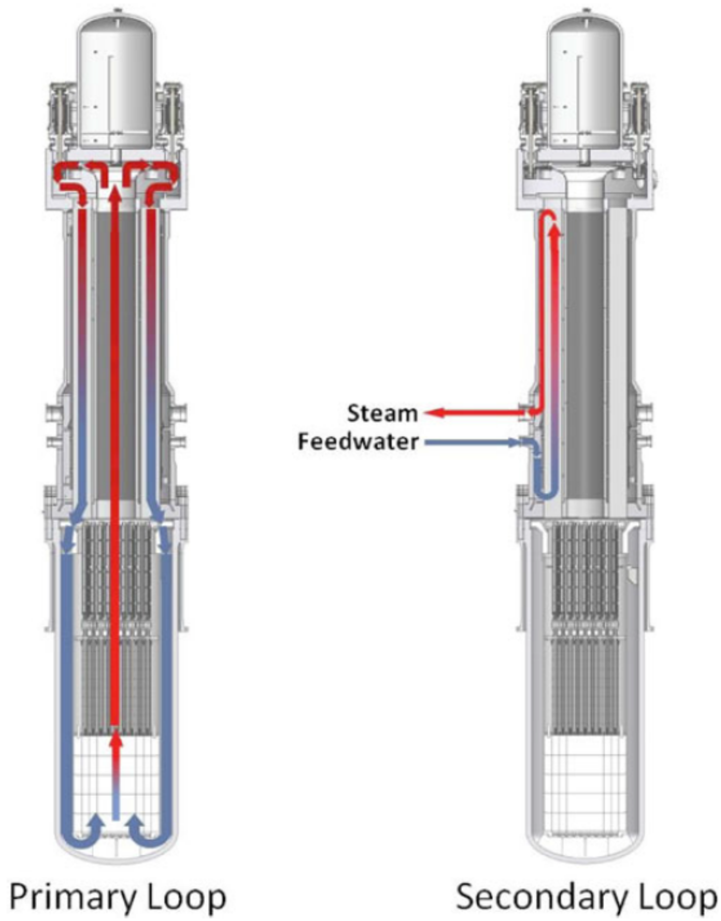

Figure 2.6: Generation mPower system flow [6]

inner barrel diameter and thickness, clearance of tube to barrel, and the minimum number of SG tubes. The code then begins plotting tube rings until the minimum number of SG tubes has been achieved. The final tube ring is then completed and the code then calculates the minimum outer shell diameter, the SG cross sectional flow area, heat transfer area, volume of tube metal, etc.

The once-through steam generator has been used for many applications, some of the earliest, and B&W designed, being the Otto Hahn submarine (Figure 2.10). Submarine technology lends well to the development of SMRs as the envelope and internal-design of a submarine propulsion power reactor is similar to that of an mPower reactor module.

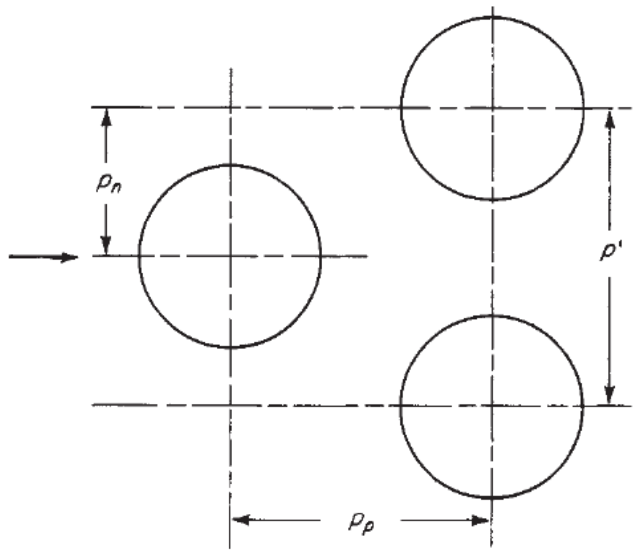

Tube O.D. D_o, in.	Tube pitch p', in.	Layout	p_p, in.	p_n, in.
0.625	0.812	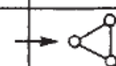	0.704	0.406
0.750	0.938	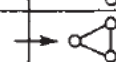	0.814	0.469
0.750	1	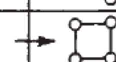	1.000	1.000
0.750	1	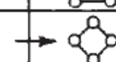	0.707	0.707
0.750	1	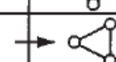	0.866	0.500
1.000	1.250	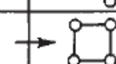	1.250	1.250
1.000	1.250	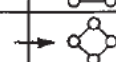	0.884	0.884
1.000	1.250	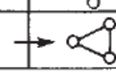	1.082	0.625

Figure 2.7: Values of tube pitch for common tube layouts [8]

The term once-through steam generator is in reference to the primary coolant which enters the steam generator from the top. The primary flow is forced against a grid plate which distributes the flow to the inside of the individual steam generator tubes. This process induces a considerable pressure drop. Primary flow continues through the length of the tubes to the lower grid plate where the flow merges. Depending on the design and type of OTSG there may be one primary inlet and two primary outlets. The primary fluid leaving through the outlet is then recirculated through the core.

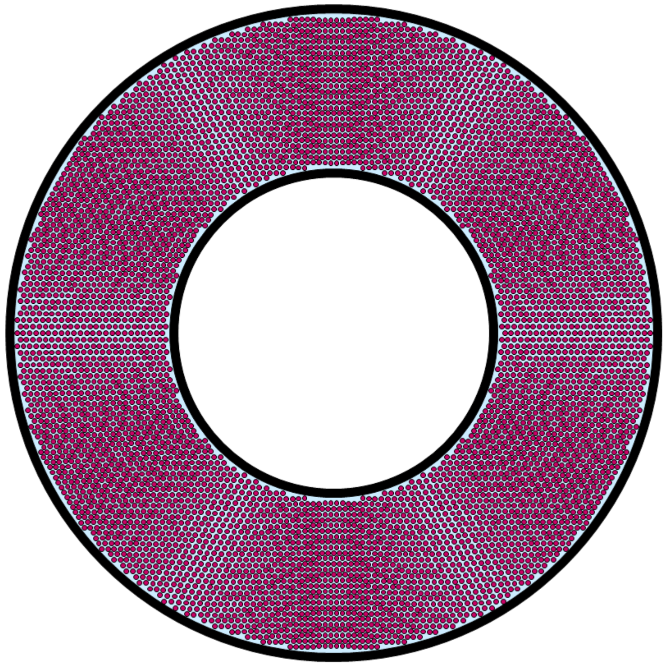

Figure 2.8: Calculated steam generator tube arrangement and geometry

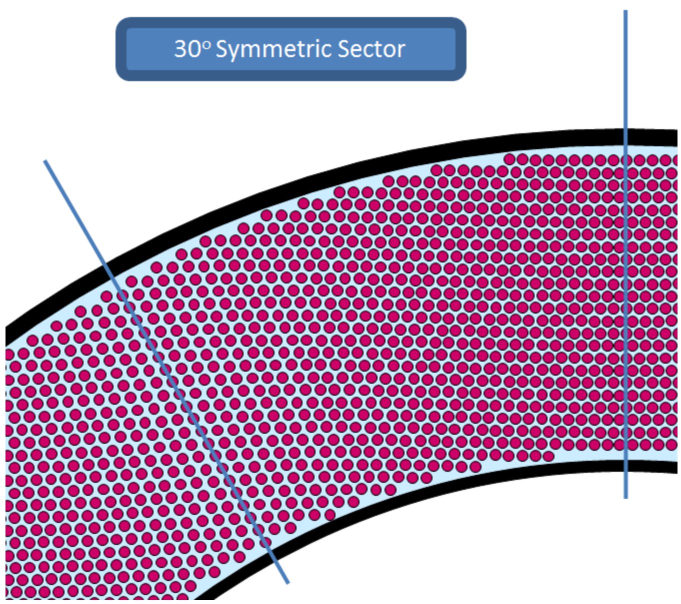

Figure 2.9: Cut-out section of the steam generator tube grid

The secondary fluid in a OTSG is generally not once through, but rather dual pass: a partial downward pass in the plenum, full length upward pass in the shellside region of the heat exchanger, and a second partial downward pass in the plenum. This pathway is

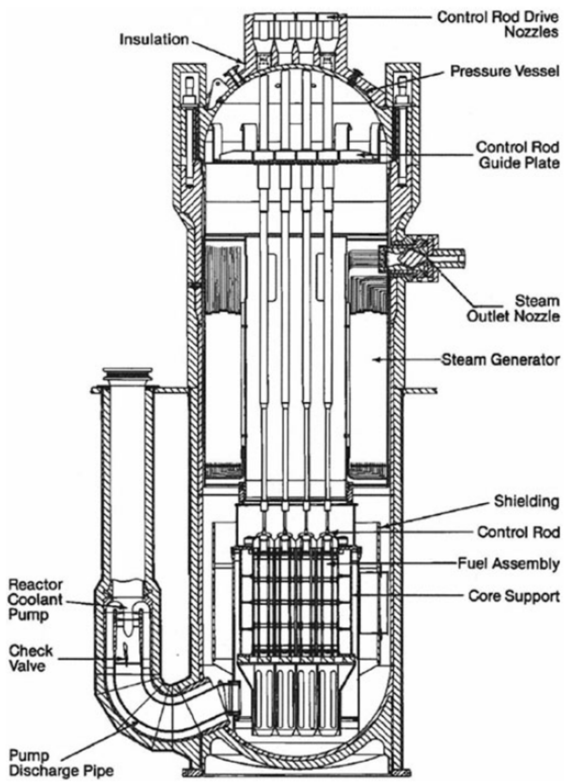

Figure 2.10: Otto Hahn Steam Generator Design [6]

illustrated in Figure 2.6. Early designs of OTSGs have a bleedport (Figures 2.11 and 2.12) about halfway up the active length of the steam generator (adjacent to the feedwater inlet).

Through the bleedport, a small amount of steam is aspirated into the downcomer plenum where it is mixed with feedwater. The feedwater has two main nozzles which are connected to a torus that uniformly distributes flow to the downcomer region. As subcooled feedwater enters the downcomer, it mixes with the steam aspirated from the shellside and preheats as it makes the first partial downward pass. As the flow enters the shellside, heat transfer from the primary system takes place. As the flow continues upward through the shellside, the fluid is almost entirely saturated (i.e., there is little or no subcooled region within the active shellside). As the saturated steam continues its upward pass it transitions to a single phase superheated fluid. As the steam travels upward against the forces of gravity, the final turn at the top of the steam generator acts as a passive moisture separator. Microdroplets of water which migrate upward are in contact with the superheated steam and undergo phase

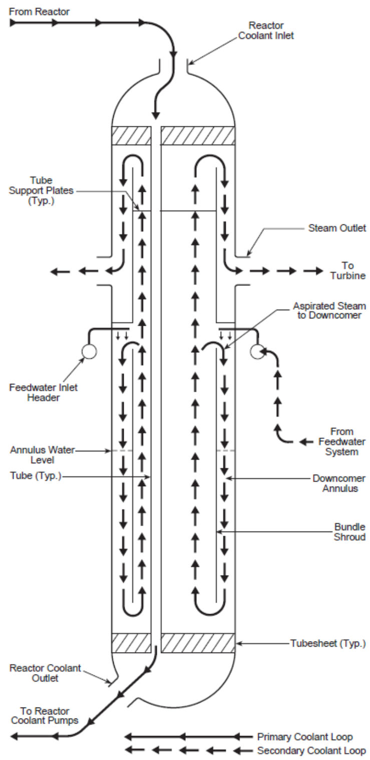

Figure 2.11: Simple Diagram of a OTSG [7]

change prior to exiting the main steam lines. As the superheated steam makes its final downward pass there is some heat transfer which contributes to the overall enthalpy of the steam, however it is much less significant than the upward pass.

One of the problems of using a bleedport is that the efficiency of the system is reduced by aspirating the steam. B&W has developed an improved technology which does not rely on steam for preheating. Instead, both the feedwater and mainsteam nozzles have been lowered from about 60% the height of the active steam generator length to about 20% above the bottom. With this configuration, subcooled feedwater flows directly into the shell side where it maintains a certain level before transitioning into the saturated and superheated regions, thus negating any need for a bleedport. The region containing subcooled fluid is referred to as the integral economizer (Figure 2.13) and similarly the distinction between this design type and the bleedport type is noted as the Integral Economizer Once-Through Steam Generator (IEOTSG).

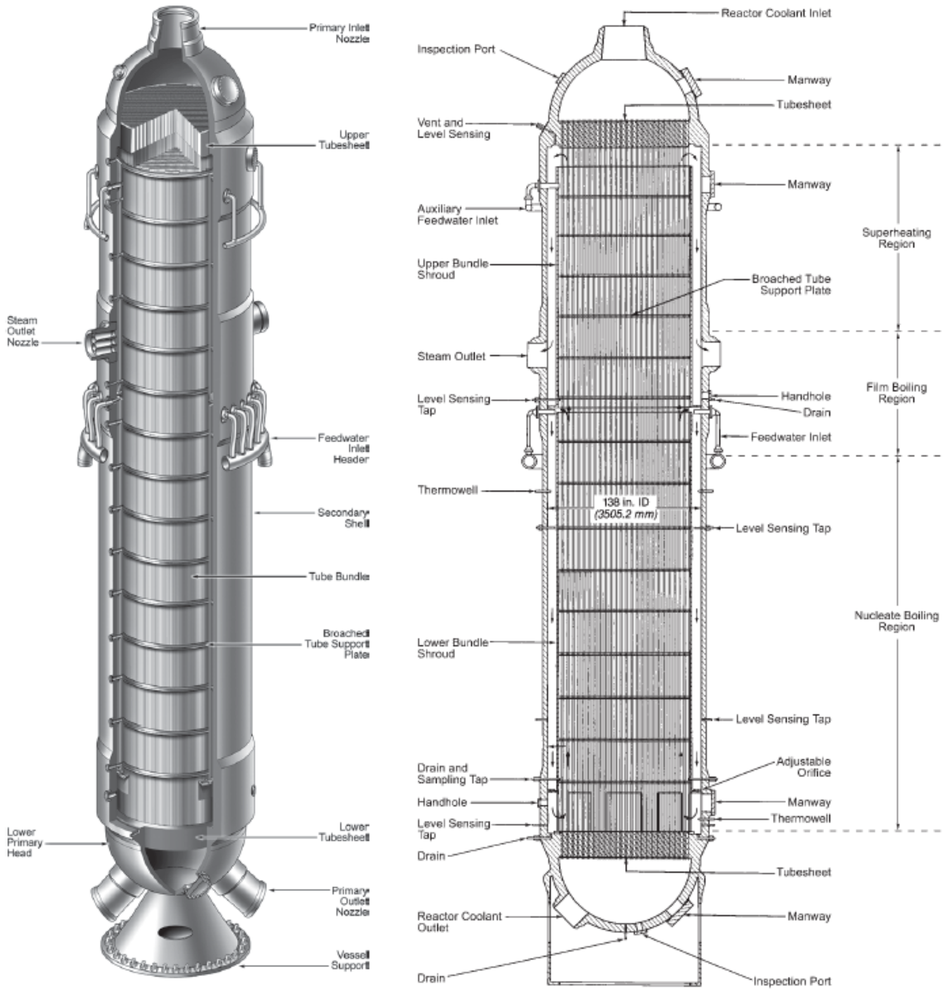

Figure 2.12: External OTSG Unit [7]

2.4 Containment

The containment is a conventional structure of reinforced concrete which is approximately 50% below grade. The containment does take credit for additional passive safety features, mainly due to its below grade positioning which include improved retention of water inventory and a reinforced cap protecting from avaiation and external events. Specifics of the containment will not be addressed in this document and are beyond the scope of the dynamic modeling.

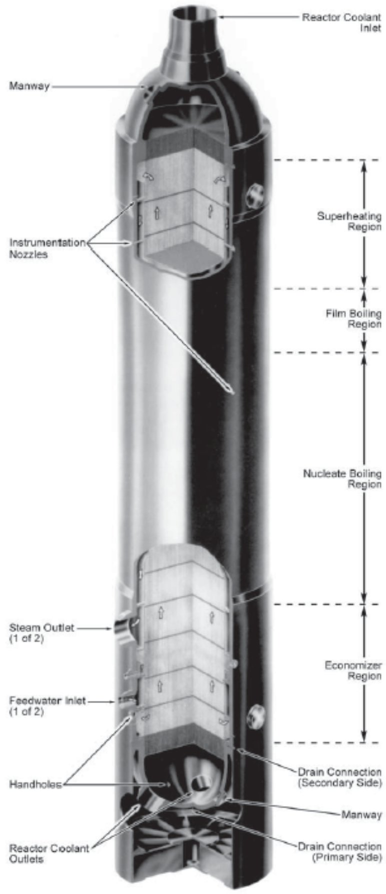

Figure 2.13: Integral Economizer OTSG [7]

2.5 Pressurizer

The reactor module features an integral pressurizer which is mounted at the top of the vessel head. There is a baffle plate with several small penetrations which separates the primary fluid from the fluid within the pressurizer. The pressurizer contains a spray and heater system, consistent to an external unit, which is used to maintain pressure within the technical specification. The amount of coolant either introduced by the spray system or vaporized by the heaters is balanced through the bleed and charging lines of the CVCS to maintain constant primary coolant inventory.

2.6 Balance of Plant

The Balance Of Plant (BOP) has a reduced size to accommodate smaller power levels of the reactor, but otherwise contains a general infrastructure and layout. A portion of steam is routed from the main steam line to the reheaters, the remainder is channelled to the nozzle chest; this component regulates steam delivery to the high pressure turbine. An inline series of four turbines (one high pressure and three low pressure) are connected to a single shaft which is coupled to the electric generator. In between the high and low pressure turbines are a moisture separator and reheater which sufficiently increase the enthalpy of steam from the high pressure turbine outlet such that it may pass through the low pressure turbines without inducing cavitation of the blades. The low pressure turbine outlets are condensed into feedwater via the ultimate heat sink, reheated and pumped back to the steam generator to complete the thermodynamic cycle. The equations for the BOP system model are presented in Chapter 6.

Chapter 3

Development of the Dynamic Model

Simulink is a block diagram environment used for the simulation and analysis of dynamic systems. It has been developed to couple together three separate physics models into a full systems code. These include Mann's model of primary heat transfer (Chapter 4), once-through steam generator model (Chapter 5), and the balance of plant model (Chapter 6).

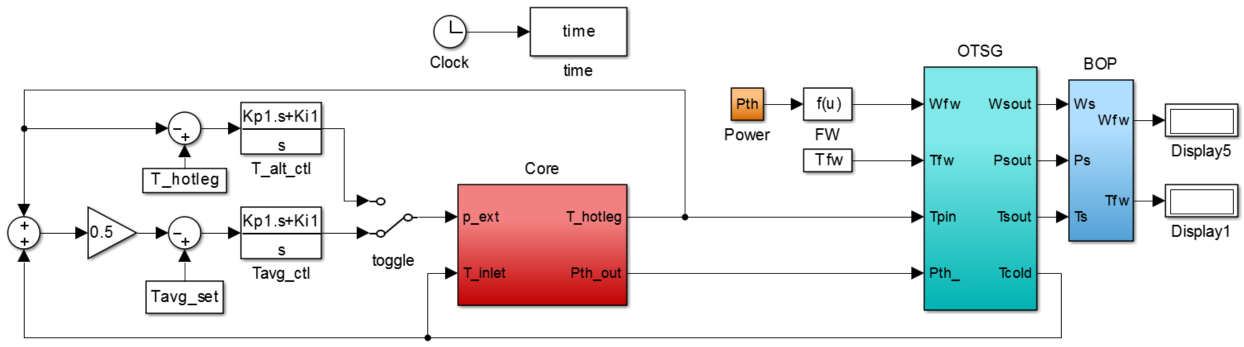

Figure 3.1: Babcock & Wilcox Generation mPower Reactor Pressure Vessel

3.1 Solving Routines

The following variable step ODE solvers are available in MATLAB-Simulink version 2014b. A description of each solver type is provided in Table 3.1.

Table 3.1: Simulink ODE Solvers

Solver	**Problem Type**	**Method**	**When to use**
ode45	Nonstiff	Runge-Kutta	Most of the time. This should be the first solver you try (Dormand-Prince, Medium accuracy).
ode23	Nonstiff	Runge-Kutta	For problems with crude error tolerances or for solving moderately stiff problems (Bogacki-Shampine, Low accuracy).
ode113	Nonstiff	Adams	For problems with stringent error tolerances or for solving computationally intensive problems (Adams, Low to high accuracy).
ode15s	Stiff & DAEs	NDFs (BDFs)	If ode45 is slow because the problem is stiff (Stiff/NDF, Low to med accuracy).
ode23s	Stiff	Rosenbrock	If using crude error tolerances to solve stiff systems and the mass matrix is constant (Stiff/Mod. Rosenbrock, Low accuracy).

Continued on next page

Table 3.1 – *Continued from previous page*

Solver	Problem Type	Method	When to use
ode23t	Mod stiff & DAEs	Trapezoidal	For moderately stiff problems if you need a solution without numerical damping (mod. Stiff/Trapezoidal, Low accuracy).
ode23tb	Stiff	TR-BDF2	If using crude error tolerances to solve stiff systems (Stiff/TR-BDF2, Low accuracy).
ode15i	Fully implicit	BDFs	N/A (Accuracy N/A)

The solver used for this research was ode23s, the Rosenbrock method. This solver was selected for its ability to perform calculations efficiently. MathWorks developers suggest that the user first try solver ode45 due to its trade-off between accuracy and computational expense. Ode45 is not a possibility for use on the mPower model. After a lengthy simulation, Simulink reported a generic error message and yielded no data. This error message is reproducible. Additional justification for the ordinary differential equation solver selected for the model would be required for a verification and validation effort, and is beyond the scope of this research.

3.2 Variation between Solving Routines

To illustrate variation between the different solvers, plots for some of the more sensitive equations have selected on a fixed scale. The four stiff equation solvers have been evaluated with the same user input which was a power ramp (Section 7.2). Figures 3.2 & 3.3 plot the rate of change of pressure and total reactivity, respectively for solver ode15, Figures 3.4 & 3.5 for solver ode23s, Figures 3.6 & 3.7 for solver ode23t, Figures 3.8 & 3.9 for the first simulation of solver ode23tb, and Figures 3.10 & 3.11 for the second simulation of solver ode23tb. Plots for solver ode23tb illustrate how two independent simulations of the same input yield distinct and random, computational noise.

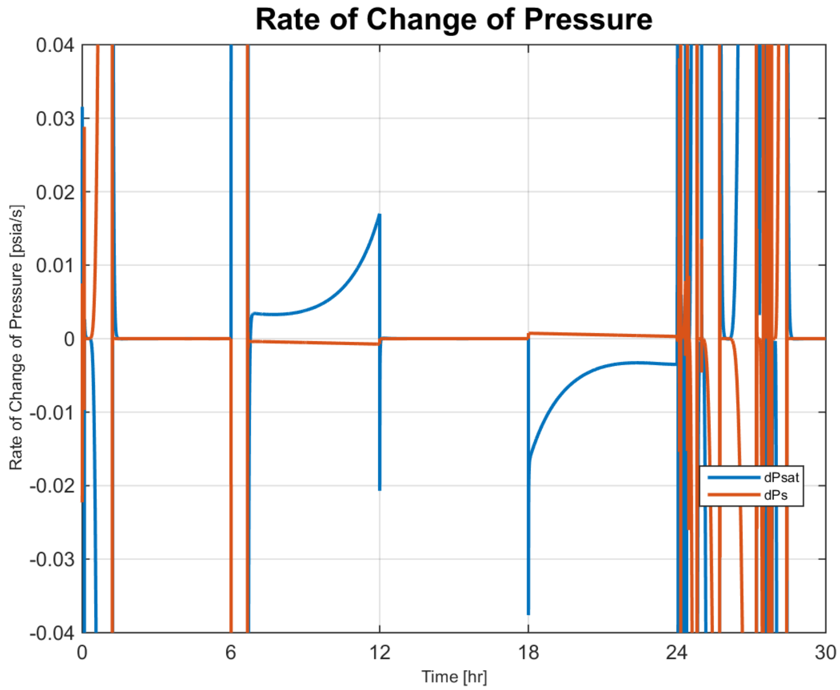

Figure 3.2: Rate of change of pressure using ode15s

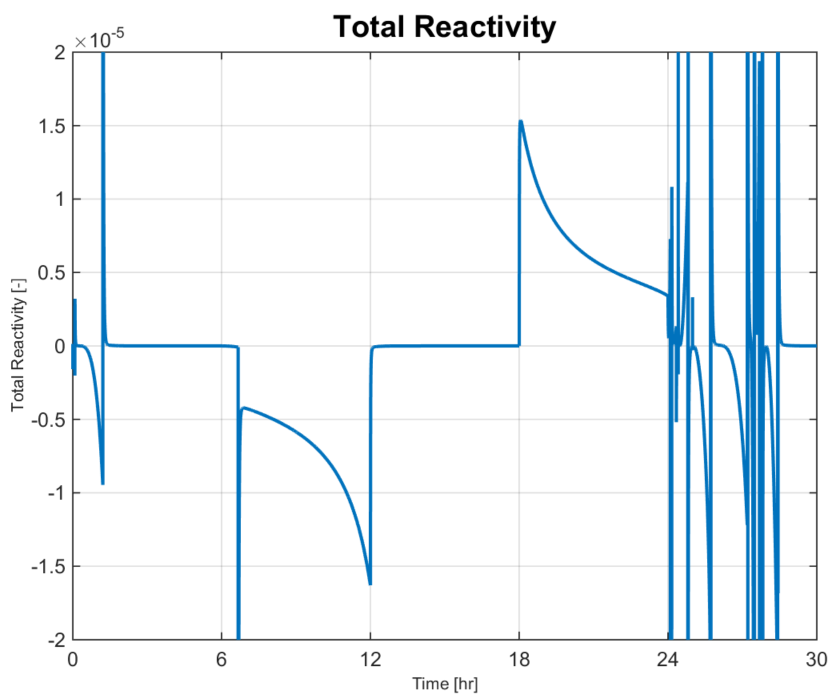

Figure 3.3: Total reactivity using ode15s

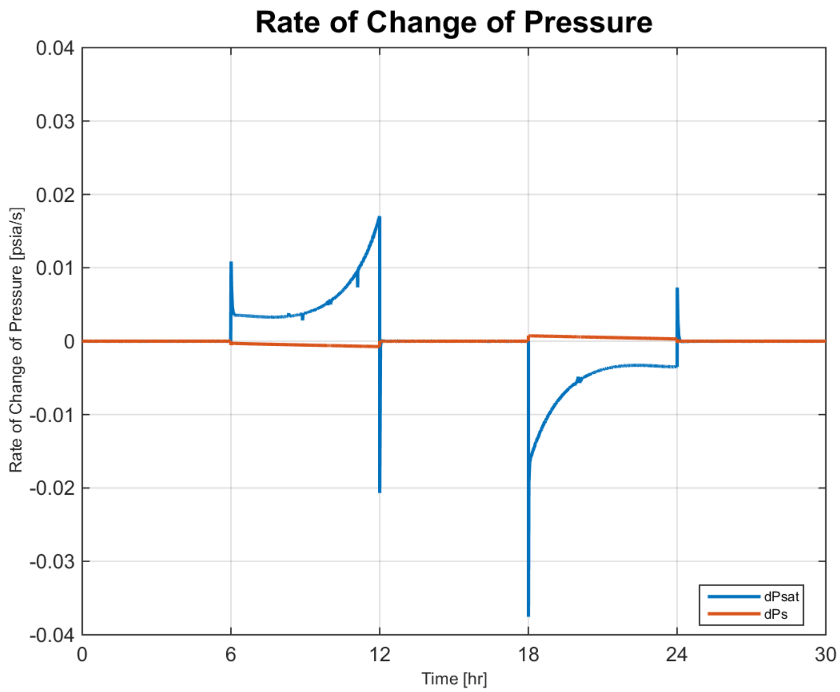

Figure 3.4: Rate of change of pressure using ode23s

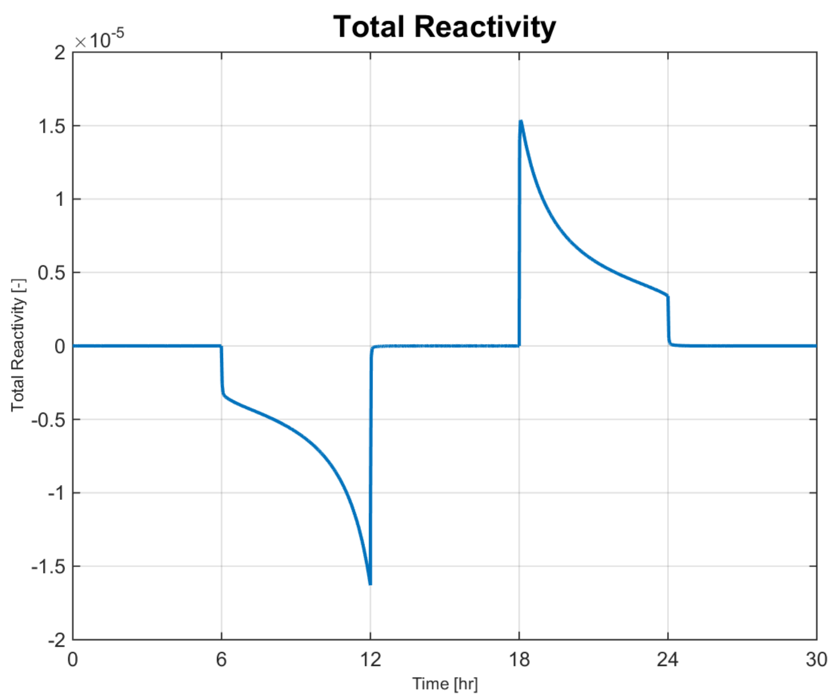

Figure 3.5: Total reactivity using ode23s

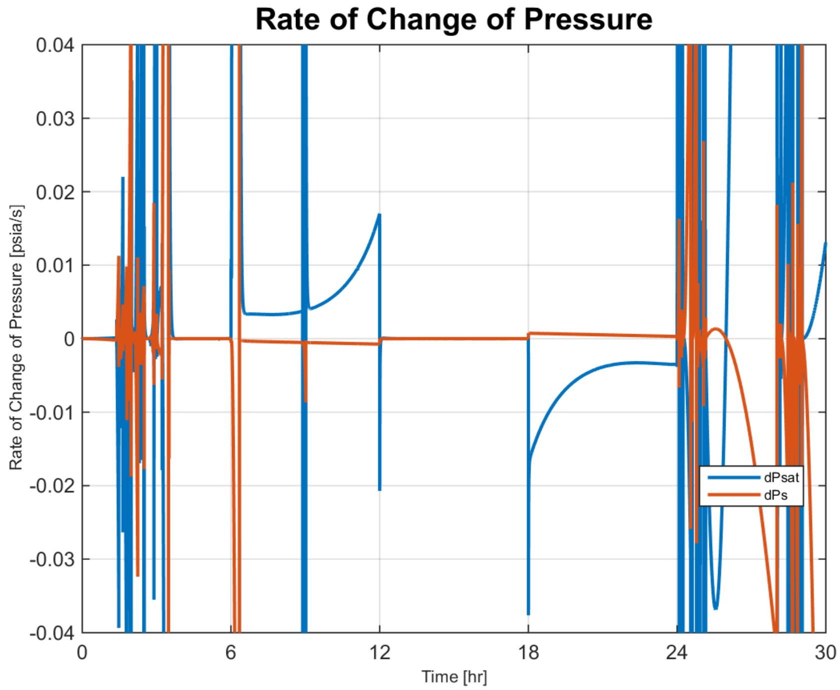

Figure 3.6: Rate of change of pressure using ode23t

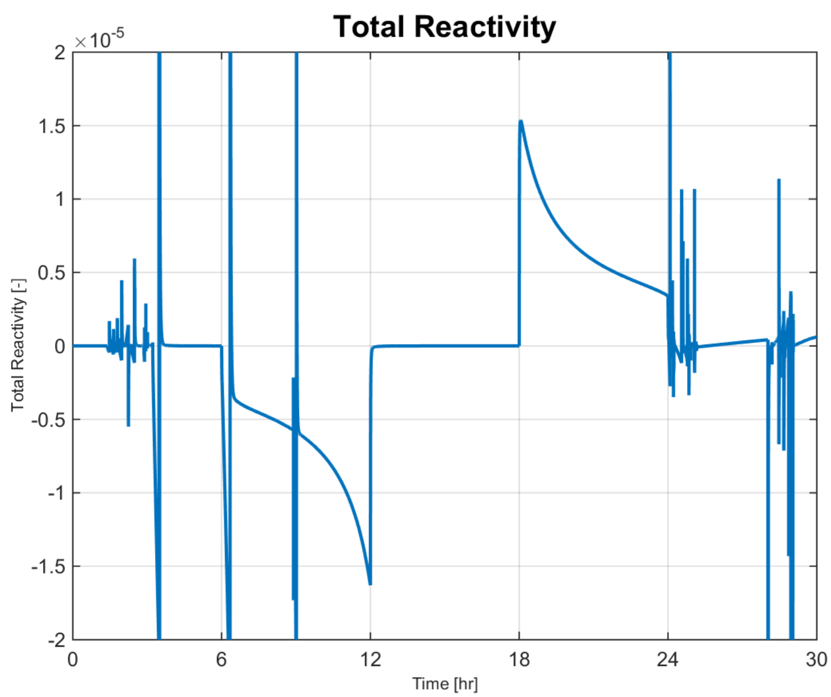

Figure 3.7: Total reactivity using ode23t

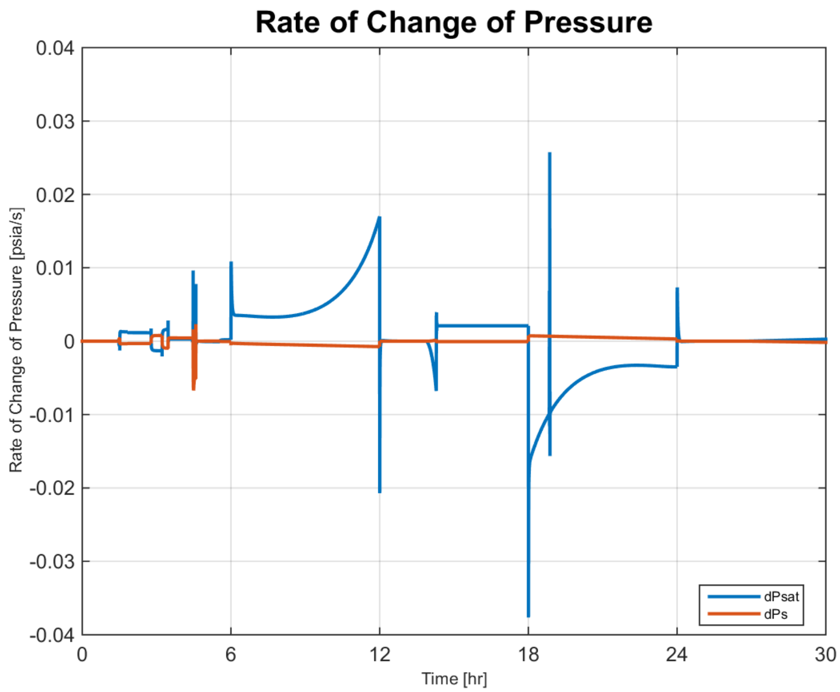

Figure 3.8: Rate of change of pressure using ode23tb

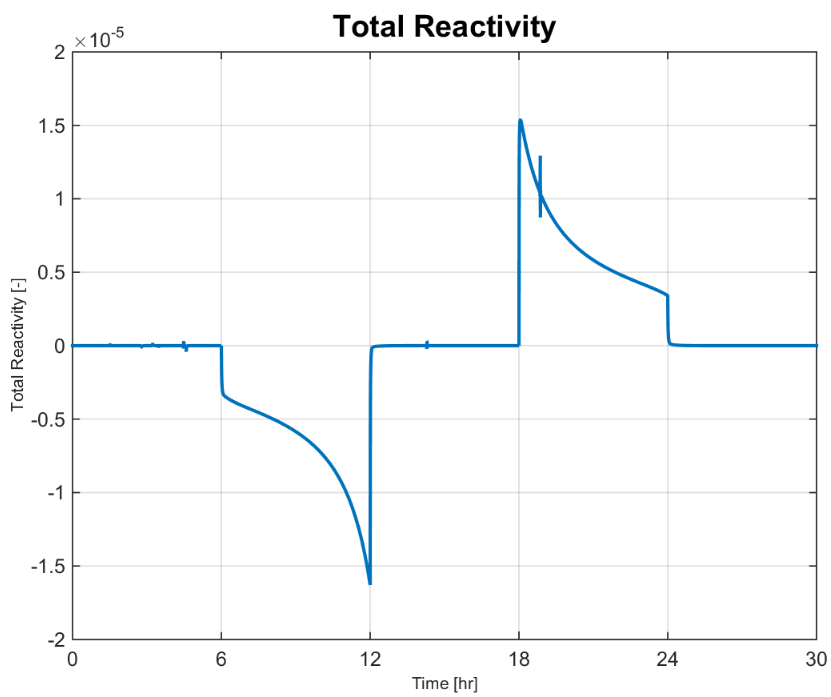

Figure 3.9: Total reactivity using ode23tb

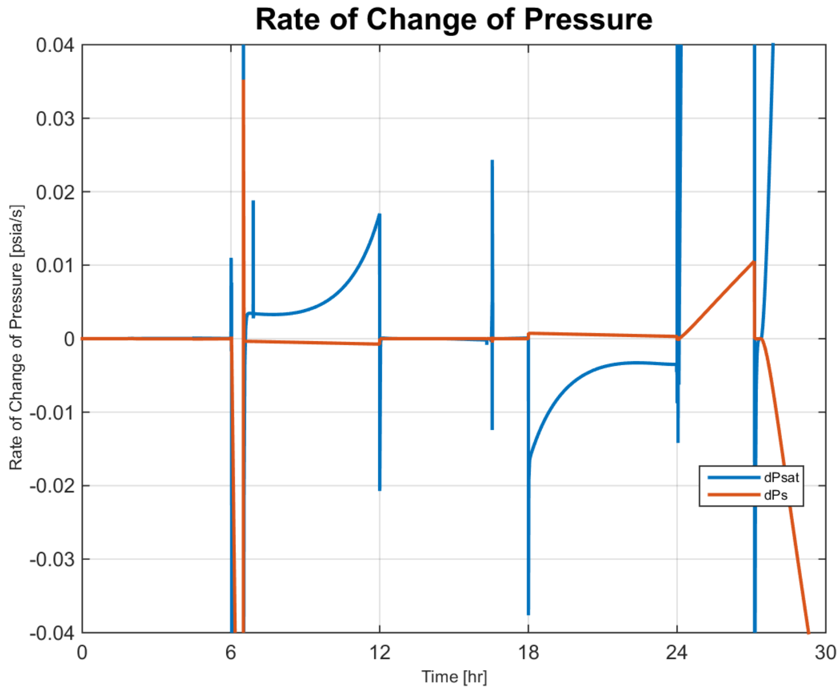

Figure 3.10: Rate of change of pressure using ode23tb

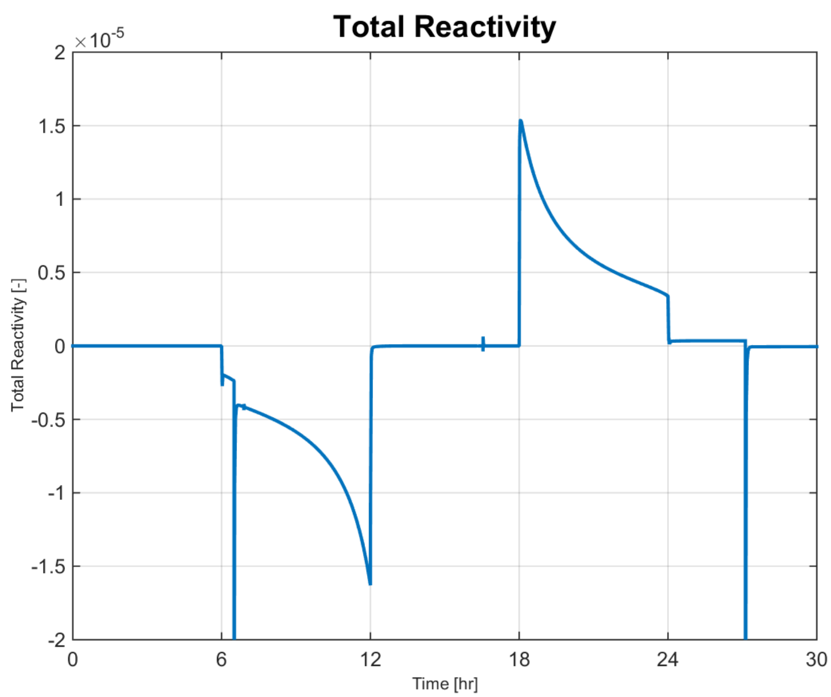

Figure 3.11: Total reactivity using ode23tb

Chapter 4

Reactor Core & Neutron Physics

4.1 Neutron Kinetics & Core Heat Transfer

The physics of the reactor core are modeled after a simplified one speed diffusion equation, neutron precursor concentrations and the fuel and moderator temperature feedback coefficients. The point kinetics equation used in the core module is provided by Duderstadt and Hamilton [4], page 239.

$$\frac{dn}{dt} = \left[\frac{\rho\left(t\right) - \beta}{\Lambda}\right] n\left(t\right) + \sum_{i=1}^{6} \lambda_i C_i\left(t\right)$$

$$\frac{dC_i}{dt} = \frac{\beta_i}{\Lambda} n\left(t\right) - \lambda_i C_i\left(t\right), i = 1, ..., 6$$

where,

$\Lambda \equiv \frac{l}{k} \equiv$ mean generation time

$\rho\left(t\right) \equiv \frac{k(t)-1}{k(t)} \equiv$ reactivity

λ_i = decay constant (β-decay) of the ith delayed neutron precursor

β_i = ith delayed neutron fraction

$\beta = \Sigma_i \beta_i$ = Total fraction of fission neutrons which are delayed

C_i = ith delayed neutron precursor concentration

Data for the delayed neutron parameters (Table 4.1) are provided by Stacey [9] (page 144).

Table 4.1: Delayed Neutron Parameters for ^{235}U [9]

	Fast Neutrons		Thermal Neutrons	
	Decay Constant	Relative Yield	Decay Constant	Relative Yield
Group	$\lambda_i(s^-1)$	β_i/β	$\lambda_i(s^-1)$	β_i/β
^{235}U		$\nu_d = 0.01673$ $\beta = 0.0064$		$\nu_d = 0.01668$ $\beta = 0.0067$
1	0.0127	0.038	0.0124	0.033
2	0.0317	0.213	0.0305	0.219
3	0.115	0.188	0.111	0.196
4	0.311	0.407	0.301	0.395
5	1.40	0.128	1.14	0.115
6	3.87	0.026	3.01	0.042

4.2 Feedback Coefficients

There are two major coefficients of feedback which are important to light water reactor physics. These are the fuel temperature coefficient of feedback and the moderator temperature coefficient of feedback. The fuel temperature coefficient of feedback is also referred to as the "prompt" (or doppler) coefficient. As fission occurs in the nuclear fuel, the fission products are released with kinetic energy. The fission products slow down through collisions of neighbouring atoms; transferring the kinetic energy to heat distributed within the fuel matrix. This process happens instantaneously, relative to the time required for the effects of the moderator temperature coefficient to take place.

The temperature coefficient relation provided by Lamarsh [10]:

$$\alpha_T = \frac{d\rho}{dT}$$

Where,

ρ = reactivity of the system

T = temperature of a specific component

The two specific components in a light water reactor are the fuel and the coolant which is also the moderator. Therefore the fuel temperature coefficient of feedback is represented:

$$\alpha_f = \frac{d\rho}{dT_{\text{fuel}}}$$

and the moderator temperature coefficient of feedback:

$$\alpha_c = \frac{d\rho}{dT_{\text{coolant}}}$$

The moderator temperature coefficient is important for light water reactors, as the moderator is affected by temperature and pressure. As the localized temperature increases, the density of the moderator decreases and sometimes leads to the onset of net void generation. When the moderator density decreases, neutrons receive less thermalizing and remain relatively fast. The fast neutron has a smaller probability to cause an additional fission and reactivity of the system decreases.

Temperature feedback coefficients are an important phenomenon in the design of a nuclear reactor, as it can be used as an inherent physical safety system to assist the reactor in avoiding the potential of reaching a prompt supercritical state. A negative temperature coefficient means that as the temperature of the fuel and moderator increases, the reactivity of the system decreases and helps the system to return to a nominal safe temperature. For this very reason, the U.S. NRC mandates that all applicants of a design certification have negative reactivity coefficients.

4.3 Core Heat Transfer Model

Typical analysis of a thermal fluids system involves conservation of mass, momentum and energy. This analysis is simplified by first assuming that the reactor coolant is at constant density, pressure and mass flow rate; eliminating state equations for mass and momentum. The energy balance accounts for the heat transfer from the nuclear fuel to the coolant using

Mann's model [11] [12] [13] (developed by E.R. Mann at the Oak Ridge National Laboratory): a lumped-parameter approximation of a counter flow heat exchanger (Figure 4.1). The nodal model makes the following assumptions:

- Fluid transport in each stream is represented by a "two well-stirred tanks in series" approximation.
- The primary heat transfer from fuel to coolant is in the radial direction.
- There is negligible heat transfer in the axial direction in the fuel.
- Heat transfer between the fuel node and the coolant node is proportional to the difference between the fuel node temperature and the mean temperature of the fluid in the inlet "tank" or the upstream coolant node (same as upstream node outlet temperature).
- Explicit transport times are not included in the model. It is not a continuous model and is not spatially dependent. The nodal model is a first order approximation which has a certain resident time ($\frac{\dot{m}}{m}$) as a function of node size.

The reactor core may be subdivided into as many nodes as desired by the user. For the purposes of this model, the fuel mass remains as a single node. The model requires a minimum of two coolant nodes for each fuel node. This enables variation in the coolant temperature and also provides driving force as the core outlet temperature is greater than the average core temperature. Additional assumptions for the core model include a constant mass flow rate, density and pressure of the primary coolant. If desired the user may incorporate a pressurizer and pump modules to control these parameters: for the purposes of this project steady flow and pressure is sufficient.

4.4 Reactor Average Temperature Controller

The typical control program for a OTSG is to maintain an average temperature of the hot leg (core outlet or central riser) and cold leg (core inlet or downcomer) constant as a function

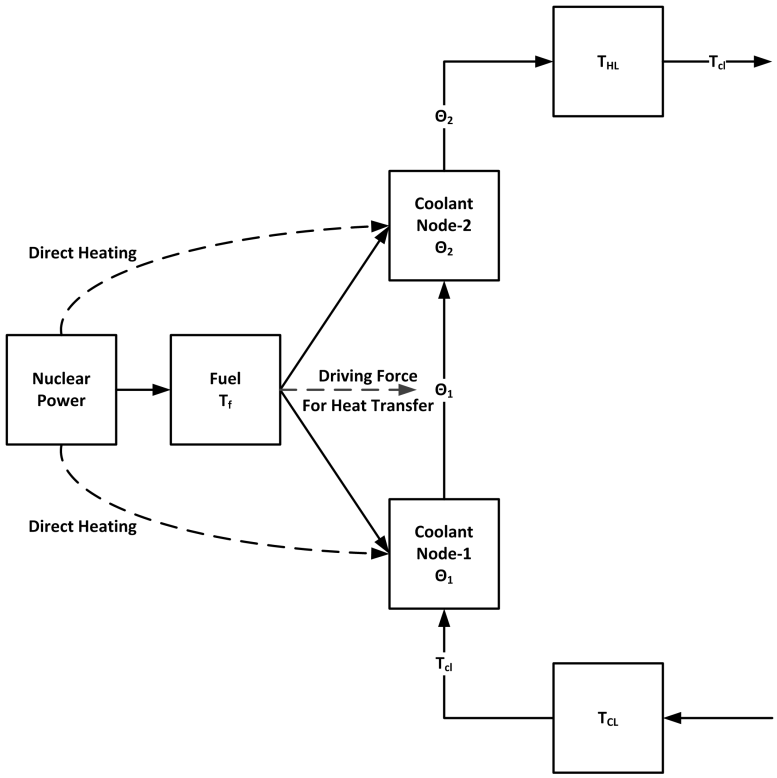

Figure 4.1: Mann's heat transfer model [13]

of thermal power (Figure 4.2). This type of control action is referred to in the literature as a temperature averaged controller (T-avg control) [14]. One of the benefits of using T-avg control is that it reduces the amount of volume change in the primary coolant as a function of thermal power. This enables the pressurizer to maintain a relatively constant fluid level over large power surges, and alleviates involvement of the heater and spray systems.

B&W has identified an alternate strategy for reactor control which is based on a constant hotleg temperature as a function of thermal power [15] (Figure 4.3). This control strategy has evolved out of the design considerations for elimination of chemical shim. As poison is eliminated from the primary coolant, the moderator temperature and void coefficients remain negative however their absolute values become greater in magnitude. Consequently the volume of primary coolant varies more as a function of thermal power, affecting the fluid level in the pressurizer. The dynamics of pressurizer control are designed to prevent an overpressurization or underpressurization event.

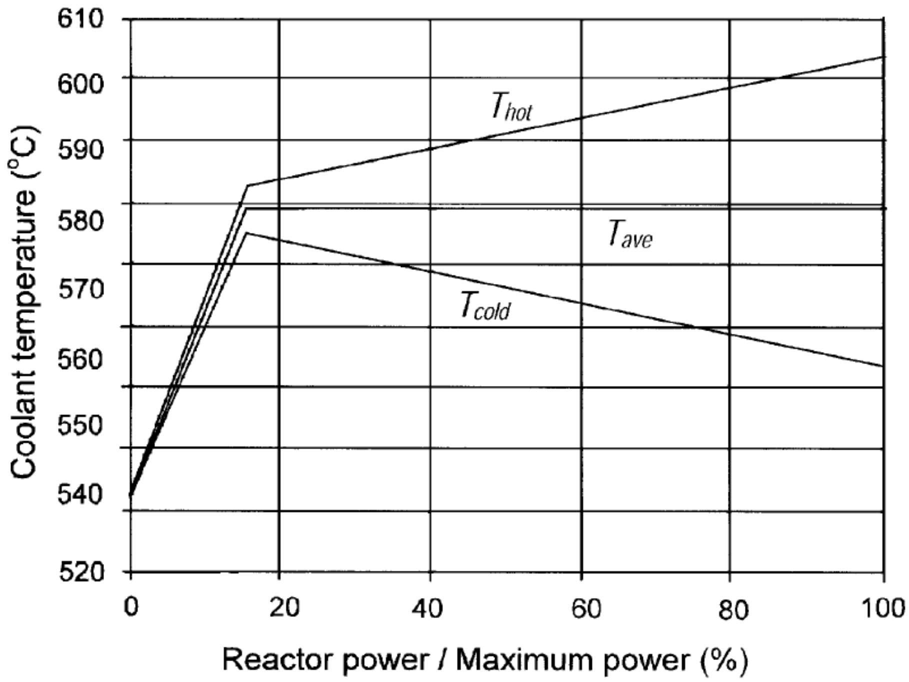

Figure 4.2: T-average control program for a OTSG [15]

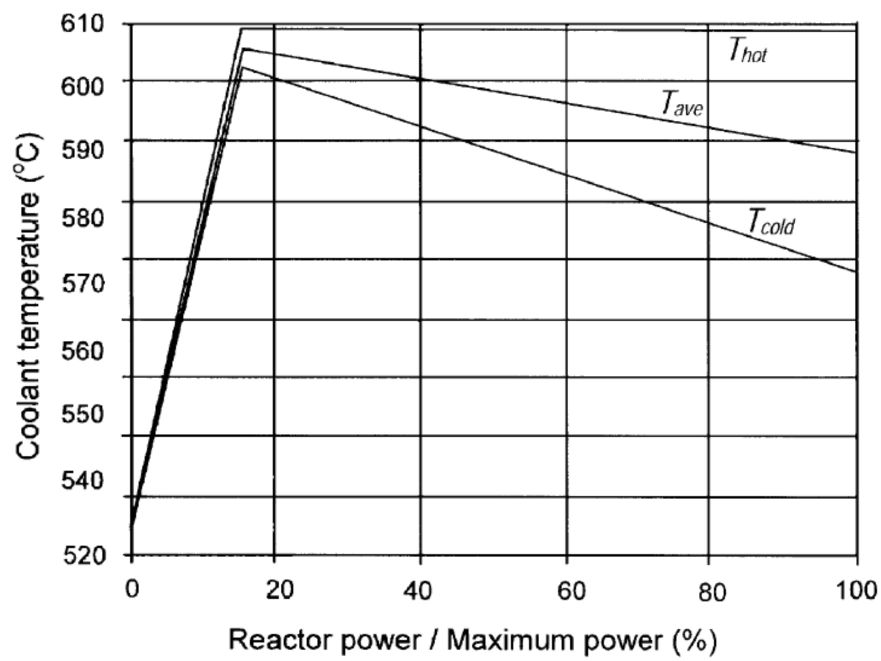

Figure 4.3: OTSG Alternative Control Program [15]

T-average control for a U-Tube Steam Generator (UTSG) works the same way in principle as the OTSG, the difference being in the manner in which its power program operates. Instead of maintaining a constant T-average temperature, there is a near constant cold leg temperature with a linearly increasing hotleg temperature as a function of percent power (Figure 4.4). The T-average setpoint for a given power level must then be calculated.

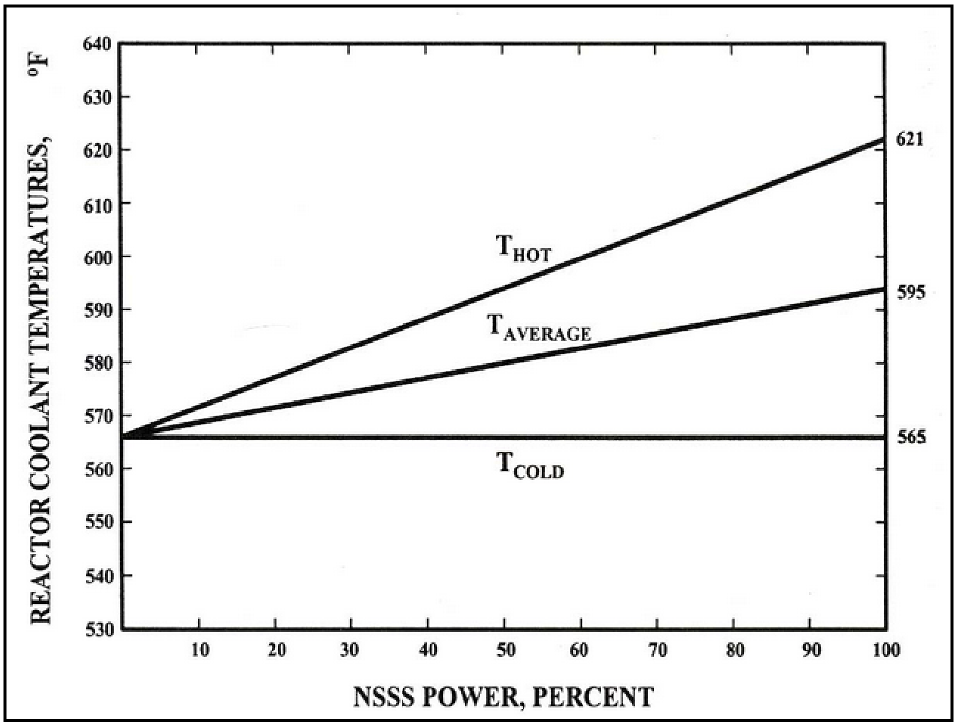

Figure 4.4: UTSG T-average Control Program [14]

To model the T-avg control system, a nominal average temperature is assigned as a set point. As the average temperature deviates from the set point an error signal is output to the proportional-integral transfer function block. Depending on the magnitude and polarity of the mismatch, the proportional-integral transfer function introduces positive or negative external reactivity into the core model (Figure 4.5). The dynamics of the reactivity insertion (magnitude of overshoot, and settling time) depend on the time constants of the proportional and integral components of the controller.

The core model, T-average control program and proportional-integral transfer function collectively solve the calculation as follows. First the core model solves for the hot

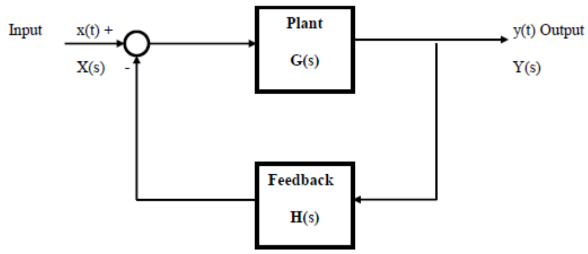

Figure 4.5: Transfer Function

leg temperature. That solution is input to the OTSG model to calculate the cold leg temperature. The cold leg and hot leg temperatures are then averaged to apply a mismatch to a nominal T-average set point. The mismatch is applied to the transfer function which introduces external reactivity for the next time step. As the next time step begins, together the reactivity and cold leg temperature inputs yield the newest solution for the hot leg temperature and the iterative process continues until the calculation has reached a user specified termination.

4.5 Core Parameters & Calculations

The geometry of the core is estimated using standard parameters as well as engineering judgement and assumptions. The geometries of the 17 x 17 fuel array have been acquired from appendix K of Duderstadt and Hamilton [4], and include diameters and thickness of the pellet, cladding, core barrel, and pitch. Additional parameters including the fuel density and number of fuel pins have been estimated. Reactor parameters are referenced in Appendix A.2.

4.5.1 Fuel mass calculation

The following calculation shows how the mass of fuel has been determined.

$$m_f = \left(\frac{\pi OD_{pellet}^2}{4} \times L_{fuel}\right) N_{fuel} \rho_{\mathrm{UO_2}}$$

$$m_f = \left(\frac{\pi(0.0269ft)^2}{4} \times 7.9ft\right) \times 18216 \times 658.2\frac{lbm}{ft^3} \approx 53850.5lbm$$

4.5.2 Mass of coolant in core

The calculation for the mass of coolant in the core begins with the pin-cell geometry of the fuel assembly (Figure 4.6). The fuel pitch (P_{fuel}) is defined as the distance from one fuel pin centerline to another within the fuel assembly. The area of the fuel pin may be determined by using its outermost boundary, the outer diameter of the cladding (OD_{clad}). The cross sectional area of coolant for each pin-cell flow channel may be determined by squaring the fuel pitch and subtracting the area of each fuel pin. The total cross sectional area within the fuel assemblies may be approximated by multiplying the flow channel by the total number of fuel pins (N).

$$\text{Flow area within fuel assemblies} \approx \left(P_{fuel}^2 - \frac{\pi OD_{clad}^2}{4}\right) N_{total}$$

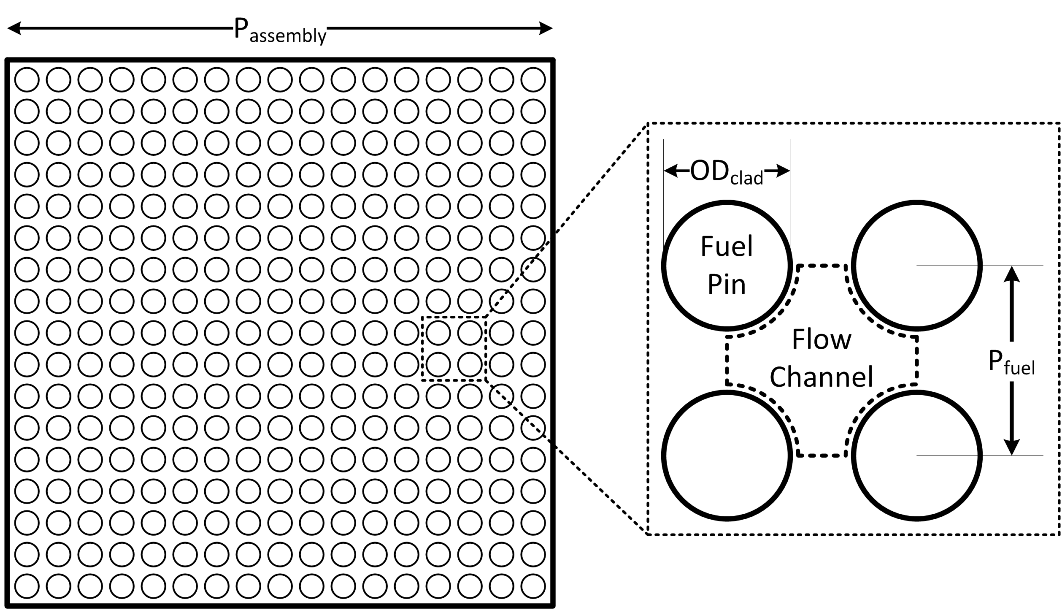

Figure 4.6: Fuel assembly and pin cell geometries

There is a fluid region between the fuel assemblies and the core barrel known as the core bypass (Figure 4.7). This region may be approximated by subtracting the area of the fuel assemblies from the total core barrel area. The fuel assembly pitch ($P_{assembly}$) is defined as the the distance from the center of one fuel assembly to the center of an adjacent fuel assembly. The outer diameter of the core barrel (OD_{barrel}) may be used to determine the entire area of the core barrel. The core bypass area may be approximated by subtracting the area from all 69 fuel assemblies from the total area of the core barrel.

$$\text{Core barrel flow area} \approx \left(\frac{\pi OD_{barrel}^2}{4} - N_{assembly} \times P_{assembly}^2 \right)$$

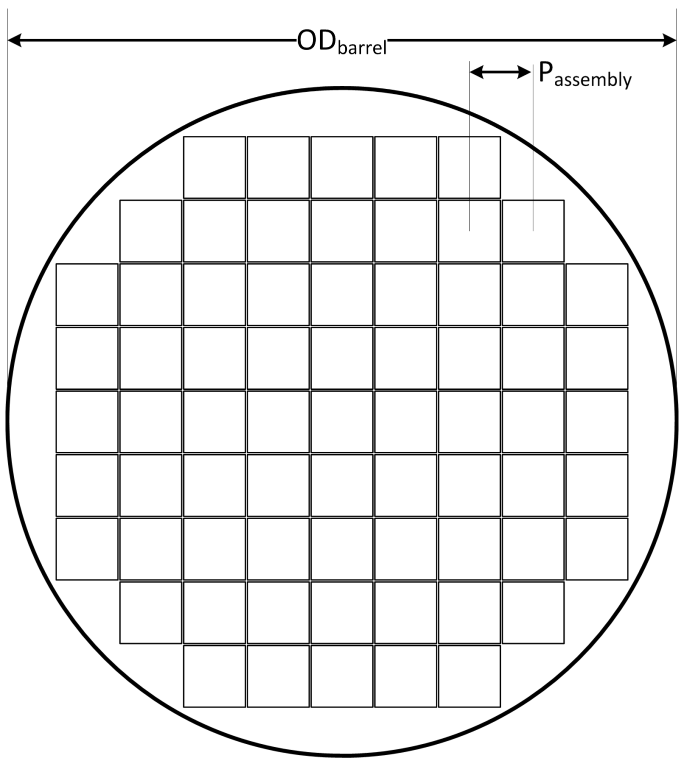

Figure 4.7: Core barrel

Therefore the total cross sectional flow area in the core is,

$$\text{Core cross sectional flow area} \approx \left[\left(P_{fuel}^2 - \frac{\pi OD_{clad}^2}{4} \right) N_{total} + \frac{\pi OD_{barrel}^2}{4} - N_{assembly} \times P_{assembly}^2 \right]$$

To determine mass, the flow area must be multiplied by the active fuel length and the coolant density,

$$m_c = \left[\left(P_{fuel}^2 - \frac{\pi OD_{clad}^2}{4}\right)N_{total} + \frac{\pi OD_{barrel}^2}{4} - N_{assembly} \times P_{assembly}^2\right]L_{fuel} \times \rho_{coolant}$$

Applying parameters found in Appendix A1 (Table 4.2), the mass of the coolant in the core may be calculated as follows,

Table 4.2: Parameters for determining the mass of coolant in the core

Parameter	Description	Value	Unit
L_{fuel}	active length of fuel	7.9	[ft]
N	number of fuel pins	18216	[-]
OD_{barrel}	core barrel diameter	6.701	[ft]
OD_{clad}	fuel cladding diameter	0.0312	[ft]
$\rho_{coolant}$	coolant density	44.01	$[\frac{\text{lbm}}{\text{ft}^3}]$
$P_{assembly}$	assembly pitch	0.705	[ft]
P_{fuel}	fuel pin pitch	0.0413	[ft]

$$m_c = \left[\left((0.0413ft)^2 - \frac{\pi(0.0312ft)^2}{4}\right)19941 + \frac{\pi(6.701ft)^2}{4} - 69 \times (0.705ft)^2\right]7.9ft \times 44.01\frac{lbm}{ft^3}$$

$$m_c \approx 6898.3lbm$$

4.6 Neutronics model and equations

To determine total reactivity (Equation 4.1), the effects of the fuel and moderator temperature coefficients and the external reactivity (ρ_{ext}) generated by the T-average controller are summed. Parameters for the total reactivity equation are provided in Table 4.3.

Table 4.3: Parameters for determining total reactivity

Parameter	Description	Value	Unit
α_c	moderator temperature coefficient	-0.0002	$[\frac{1}{\mathrm{F}}]$
α_f	fuel temperature coefficient	-0.165e-05	$[\frac{1}{\mathrm{F}}]$
β	Total delayed neutron group fraction	0.0067	[-]
θ_1	Theta 1 node calculated temperature	Equation 4.11	[ft]
θ_{1_0}	Theta 1 node nominal temperature	586.3	[ft]
θ_2	Theta 2 node calculated temperature	Equation 4.12	[ft]
θ_{2_0}	Theta 2 node nominal temperature	608.0	[ft]
ρ_{ext}	external reactivity	T-avg ctl	[ft]
T_f	fuel temperature	Equation 4.10	[ft]
T_{f_0}	nominal fuel temperature	608.0000	[ft]

$$\rho = (T_f - T_{f_0})\alpha_f + \Big((\theta_1 + \theta_2) - (\theta_{1_0} + \theta_{2_0})\Big)\frac{1}{2}\alpha_c + \rho_{ext}\beta \tag{4.1}$$

Core inlet temperature is calculated in the steam generator model (Equation 5.6). It is imported to the core model and used as an input for solving temperature of coolant node 1 (θ_1) (Equation 4.11).

$$T_{inlet} = \text{Input from Steam Generator} \tag{4.2}$$

Fractional Reactor Power:

$$\frac{dP_{\mathrm{th}}}{dt} = \frac{(\rho - \beta)P_{th}}{\Lambda} + \lambda_1 C_1 + \lambda_2 C_2 + \lambda_3 C_3 + \lambda_4 C_4 + \lambda_5 C_5 + \lambda_6 C_6 \tag{4.3}$$

The neutron precursor concentrations for each of the six groups (C_i) are calculated according to the following equation:

$$\frac{dC_i}{dt} = \frac{\beta_i}{\Lambda}\frac{\delta P}{P_0} - \lambda_i C_i, \text{ i=1,...,6}$$

The parameters for each constituent are provided in Table 4.4. Values for decay constants were previously reported in Table 4.1. Values for the delayed neutron fraction of each group may be determined by multiplying the relative yield by the total delayed neutron fraction.

Table 4.4: Parameters for determining neutron precursor concentrations

Parameter	Description	Value	Unit
β	Total delayed neutron group fraction	0.0067	$[-]$
β_1	delayed neutron frac group 1	0.000221	$[-]$
β_2	delayed neutron frac group 2	0.001467	$[-]$
β_3	delayed neutron frac group 3	0.001313	$[-]$
β_4	delayed neutron frac group 4	0.002647	$[-]$
β_5	delayed neutron frac group 5	0.000771	$[-]$
β_6	delayed neutron frac group 6	0.000281	$[-]$
Λ	Mean prompt neutron generation time	0.0001	[s]
λ_1	decay const group 1	0.0124	$[\frac{1}{\mathrm{s}}]$
λ_2	decay const group 2	0.0305	$[\frac{1}{\mathrm{s}}]$
λ_3	decay const group 3	0.111	$[\frac{1}{\mathrm{s}}]$
λ_4	decay const group 4	0.301	$[\frac{1}{\mathrm{s}}]$
λ_5	decay const group 5	1.14	$[\frac{1}{\mathrm{s}}]$
λ_6	decay const group 6	3.01	$[\frac{1}{\mathrm{s}}]$
P_{th}	fractional reactor power	Equation 4.3	$[-]$

$$\frac{dC_1}{dt} = \frac{\beta_1}{\Lambda} P_{th} - \lambda_1 C_1 \tag{4.4}$$

$$\frac{dC_2}{dt} = \frac{\beta_2}{\Lambda} P_{th} - \lambda_2 C_2 \tag{4.5}$$

$$\frac{dC_3}{dt} = \frac{\beta_3}{\Lambda} P_{th} - \lambda_3 C_3 \tag{4.6}$$

$$\frac{dC_4}{dt} = \frac{\beta_4}{\Lambda} P_{th} - \lambda_4 C_4 \tag{4.7}$$

$$\frac{dC_5}{dt} = \frac{\beta_5}{\Lambda} P_{th} - \lambda_5 C_5 \tag{4.8}$$

$$\frac{dC_6}{dt} = \frac{\beta_6}{\Lambda} P_{th} - \lambda_6 C_6 \tag{4.9}$$

There are many parameters required for the calculation of the fuel temperature, coolant nodes θ_1 and θ_2, and the hotleg temperature. These parameters are provided in Table 4.5.

Table 4.5: Parameters for determining core nodal temperatures

Parameter	Description	Value	Unit
A_{fc}	fuel-to-coolant heat transfer area	14120.6	$[\text{ft}^2]$
A_{fc_1}	node 1 fuel-to-coolant heat transfer area	7060.3	$[\text{ft}^2]$
A_{fc_2}	node 2 fuel-to-coolant heat transfer area	7060.3	$[\text{ft}^2]$
c_{p_c}	coolant heat capacity	1.376	$[\frac{\text{BTU}}{\text{lbm-}^\circ\text{F}}]$
c_{p_f}	fuel heat capacity	0.059	$[\frac{\text{BTU}}{\text{lbm-}^\circ\text{F}}]$
f	fraction of reactor power deposited in fuel	0.97	$[-]$
m_c	mass of coolant in core	6898.3	[lbm]
m_{c_1}	coolant mass node 1	3449.1	[lbm]
m_{c_2}	coolant mass node 2	3449.1	[lbm]
m_f	mass of fuel	53850.5	[lbm]
P_0	nominal power output	502343	$[\frac{\text{BTU}}{\text{s}}]$
T_f	fuel cladding temperature	962.672	$[^\circ\text{F}]$
T_{f_0}	nominal fuel cladding temperature	962.741	$[^\circ\text{F}]$
U_{fc}	overall heat transf coeff	0.0909	$[\frac{\text{BTU}}{\text{s-ft}^2\text{-}^\circ\text{F}}]$
W_c	primary coolant mass flow rate	8333.3	$[\frac{\text{lbm}}{\text{s}}]$

Fuel Temperature:

$$\frac{d}{dt}\delta T_f = \frac{fP_0}{m_f c_{p_f}}\frac{\delta P}{P_0} + \frac{U_{fc}A_{fc}}{m_f c_{p_f}}\left(\delta T_f - \delta\theta_1\right)$$

$$\frac{dT_f}{dt} = \frac{fP_0}{m_f c_{p_f}}P_{th} + \frac{U_{fc}A_{fc}}{m_f c_{p_f}}(\theta_1 - T_f) \tag{4.10}$$

Theta 1 Temperature

$$\frac{d}{dt}\left(m_{c_1}c_{p_c}\delta\theta_1\right) = \left(\frac{1-f}{2}\right)P_0\frac{\delta P}{P_0} + U_{fc}A_{fc_1}\left(\delta T_f - \delta\theta_1\right) + W_c c_{p_c}\left(\delta T_{inlet} - \delta\theta_1\right)$$

where,

$$\frac{d\theta_1}{dt} = (1-f)\frac{P_0}{m_{c_1}c_{p_c}}P_{th} + \frac{U_{fc}A_{fc_1}}{m_{c_1}cp_c}\left(T_f - \theta_1\right) + \frac{W_c}{m_{c_1}}\left(T_{inlet} - \theta_1\right) \tag{4.11}$$

Theta 2 Temperature

$$\frac{d}{dt}\left(m_{c_2}c_{p_c}\delta\theta_2\right) = \left(\frac{1-f}{2}\right)P_0\frac{\delta P}{P_0} + U_{fc}A_{fc_2}\left(\delta T_f - \delta\theta_1\right) + W_c c_{p_c}\left(\delta\theta_1 - \delta\theta_2\right)$$

where,

$$\frac{d\theta_2}{dt} = \left(\frac{1-f}{2}\right)\frac{P_0}{m_{c_2}c_{p_c}}P_{th} + \frac{U_{fc}A_{fc_2}}{m_{c2}c_{p_c}}\left(T_f - \theta_1\right) + \frac{W_c}{m_{c_2}}\left(\theta_1 - \theta_2\right) \tag{4.12}$$

Core outlet temperature

$$\frac{dT_{outlet}}{dt} = \frac{W_c(\theta_2 - T_{outlet})}{m_c} \tag{4.13}$$

Chapter 5

Once Through Steam Generator

The steam generator model uses three regions to approximate the transitions from single phase liquid, to two phase flow and to single phase vapor: they are the subcooled, boiling and superheated regions. Feedwater is pumped through the inlet nozzle to the subcooled region where it is heated. It is assumed that no subcooled boiling occurs. As the fluid is heated, it becomes saturated and transitions to the boiling region where two phase heat transfer takes place. The boiling region is grossly simplified and does not account for many of the complex phenomena that occur in two phase flow dynamics. All flow regimes (nucleate boiling, churn, bubbly, slug, annular, etc.) are lumped to a single node and provided an approximate heat transfer coefficient from the tube wall to the liquid and vapor. As the boiling region transitions to the superheated region, again the superheated node is considered ubiquitous and well mixed, and is provided an approximate heat transfer coefficient to calculate heat transfer from the tube wall to the superheated vapor.

The subcooled region of the steam generator is also referred to in the literature as the integral economizer [7], thus distinguishing the Integral Economizer Once-Through Steam Generator (IEOTSG) from the previous generation OTSG. Prior to the incorporation of the integral economizer, process steam of high quality would be aspirated through bleedports to mix with and preheat the feedwater in the downcomer region. This process was inefficient due to the steam loss, and the bleed ports were phased out during the development of the next generation steam generator unit.

The OTSG Simulink model consists of a system of algebraic and ordinary differential equations outlined by Chen [16]. Chen's system of equations is nodalized consistent to the three steam generator regions previously mentioned: sub-cooled, boiling, and superheated. The subcooled and superheated regions each contain two nodes of equal volume which are variable boundary (e.g., as sub-cooled length increases, both sub-cooled nodes increase by the same volume). The entirety of the boiling node is lumped into a single node. The system of ordinary differential equations for the OTSG is much more involved than what is used for the core model, as it accounts for the conservation of mass, momentum, and energy. Although fluid density is constant within each node, the density of the nodes would change according to the temperature and pressure of the fluid. As the volume of the node changes, that small change is accounted for in the overall mass flow rate of the system. Again, heat transfer is assumed to occur only in the radial direction and four heat transfer coefficients are applied to capture the dynamics for the different regions (primary to wall, wall to sub-cooled, boiling and superheated). A representation of the nodalized model and its coupling to core heat transfer model is shown in Figure 5.2.

Figure 5.2 illustrates the coupling between the Mann's model and steam generator model. The θ_2 node temperature is the input to the primary temperature node 1. Primary temperature node 6 is the input to the θ_1 node. For primary temperature nodes one through six, their geometry is defined by the lengths of each individual fluid regime. The entire steam generator model is a coupled system of differential and algebraic equations. Therefore the volume of nodes one and two, three and four, five and six is always equal. Each flow regime has two nodes to drive heat transfer similar to that of Mann's model.

5.1 Fluid Level Dynamics

The fluid levels of the steam generator are based on data from Oconee Nuclear Generating Station [14], a plant designed by B&W which has once-through steam generators. While at full power, the lower 15% of the active tube length of the steam generator makes up the integral economizer region, the upper 15% represents the superheated steam region, and the remaining tube length is where saturated boiling occurs. These levels are ideal in that the majority 70% of tube length takes advantage of boiling (saturated region) where the more efficient two phase heat transfer is occurring. The 15% buffer on the top and bottom help ensure that small transients will not cause the active tube region to dry out or to vent wet steam to the turbine. As the power decreases, the sub-cooled level remains relatively constant; however the boiling and superheated regions tradeoff almost linearly (Figure 5.1). At low power not as much boiling is required to remove heat from the primary system, and therefore the majority of heat transfer surface area is taken in the form of superheat. This program has been implemented in the model which calculates the steam generator fluid level as a function of core thermal power.

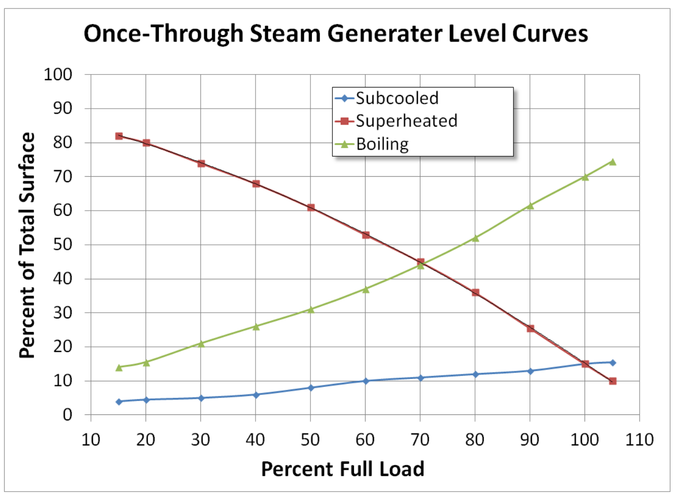

Figure 5.1: OSTG Fluid Regions [14]

5.2 Steam Pressure Controller

In addition to the T-average controller, the second control mechanism regulates steam pressure. The pressure of the superheated steam is maintained at a constant set point value by throttling a valve on the main steam line.

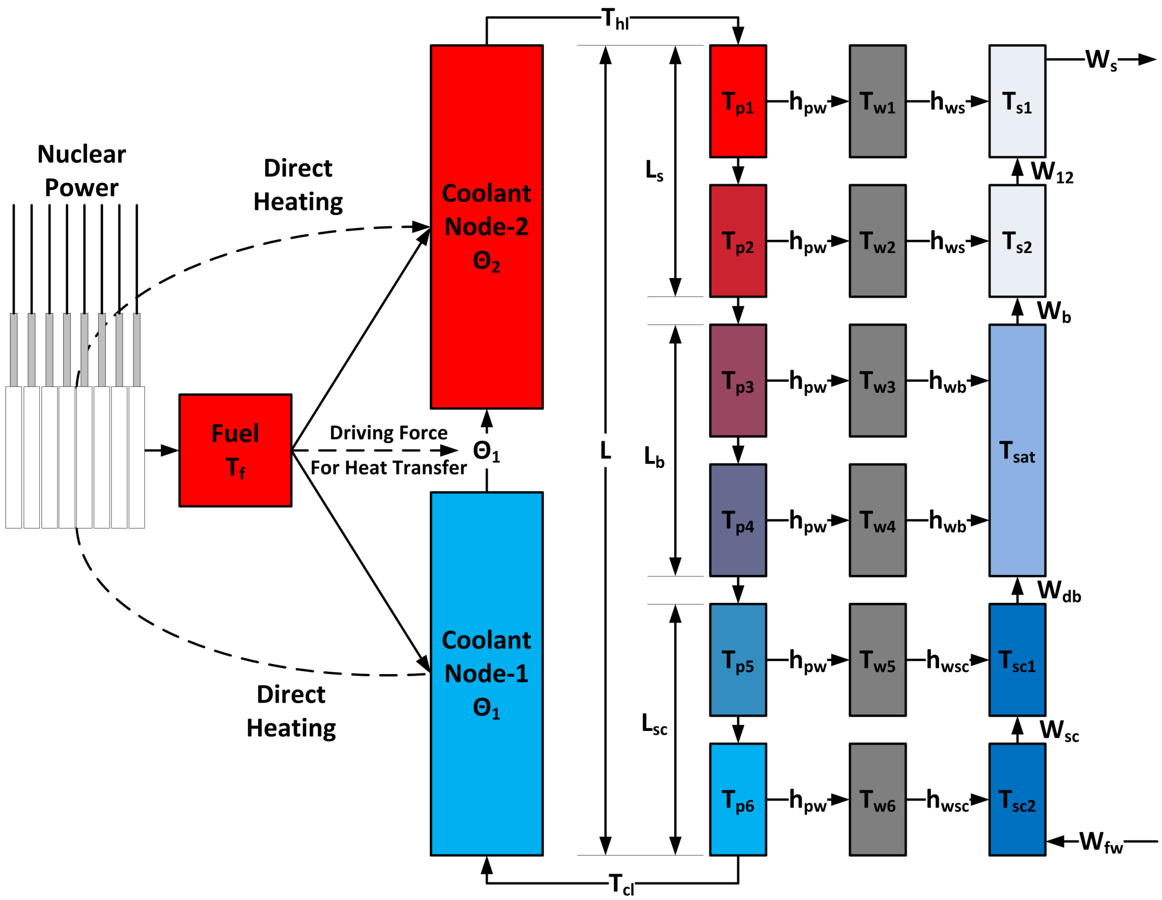

Figure 5.2: Mann's Model Coupled to the Steam Generator

5.3 State Equations

This section contains the state equations for the steam generator. The equations have been numbered such that they are consistent in the order found within the Simulink model. Design parameters for the equations may be referred to in Appendix B.

5.3.1 Primary Node Temperature

The generic form of the primary node temperature equation is:

$$\frac{dT_{pi}}{dt} = \frac{W_{pi-1}c_{p_p}\left(T_{pi-1} - T_{pi}\right) - h_{pw}A_{pwi}\left(T_{pi} - T_{wi}\right)}{M_{pi}c_{p_p i}} \text{ i} = 1, ..., 6$$

where,

$$A_{pwi} = \left(N\pi D_{it}\frac{1}{2}L_i\right)$$

$$M_{pi} = \left(N\pi\frac{D_{it}^2}{4}\frac{1}{2}L_i\right)\rho_p$$

The expanded nodal equations are as follows,

$$\frac{dT_{p1}}{dt} = \frac{W_p c_{p_p}\left(T_{pin} - T_{p1}\right) - h_{pw}\left(N\pi D_{it}\frac{1}{2}L_s\right)\left(T_{p1} - T_{w1}\right)}{\left(N\pi\frac{D_{it}^2}{4}\frac{1}{2}L_s\right)\rho_p c_{p_p}} \tag{5.1}$$

$$\frac{dT_{p2}}{dt} = \frac{W_p c_{p_p}\left(T_{p1} - T_{p2}\right) - h_{pw}\left(N\pi D_{it}\frac{1}{2}L_s\right)\left(T_{p2} - T_{w2}\right)}{\left(N\pi\frac{D_{it}^2}{4}\frac{1}{2}L_s\right)\rho_p c_{p_p}} \tag{5.2}$$

$$\frac{dT_{p3}}{dt} = \frac{W_p c_{p_p}\left(T_{p2} - T_{p3}\right) - h_{pw}\left(N\pi D_{it}\frac{1}{2}L_b\right)\left(T_{p3} - T_{w3}\right)}{\left(N\pi \frac{D_{it}^2}{4}\frac{1}{2}L_b\right)\rho_p c_{p_p}} \tag{5.3}$$

$$\frac{dT_{p4}}{dt} = \frac{W_p c_{p_p}\left(T_{p3} - T_{p4}\right) - h_{pw}\left(N\pi D_{it}\frac{1}{2}L_b\right)\left(T_{p4} - T_{w4}\right)}{\left(N\pi \frac{D_{it}^2}{4}\frac{1}{2}L_b\right)\rho_p c_{p_p}} \tag{5.4}$$

$$\frac{dT_{p5}}{dt} = \frac{W_p c_{p_p}\left(T_{p4} - T_{p5}\right) - h_{pw}\left(N\pi D_{it}\frac{1}{2}L_{sc}\right)\left(T_{p5} - T_{w5}\right)}{\left(N\pi \frac{D_{it}^2}{4}\frac{1}{2}L_{sc}\right)\rho_p c_{p_p}} \tag{5.5}$$

$$\frac{dT_{p6}}{dt} = \frac{W_p c_{p_p}\left(T_{p5} - T_{p6}\right) - h_{pw}\left(N\pi D_{it}\frac{1}{2}L_{sc}\right)\left(T_{p6} - T_{w6}\right)}{\left(N\pi \frac{D_{it}^2}{4}\frac{1}{2}L_{sc}\right)\rho_p c_{p_p}} \tag{5.6}$$

5.3.2 Steam Generator Tube Wall Temperature

The generic form of the tube wall temperature equation is:

$$\frac{dT_{wi}}{dt} = \frac{h_{pw}A_{pwi}\left(T_{pi} - T_{wi}\right) - h_{ws}A_{wsi}\left(T_{wi} - T_{si}\right)}{M_{wi}c_{p_{wi}}} \text{ i} = 1, ..., 6$$

where,

$$A_{pwi} = \left(N\pi D_{it}\frac{1}{2}L_i\right)$$

$$A_{wsi} = \left(N\pi D_{ot} \frac{1}{2} L_i \right)$$

$$M_{wi} = \left(N\pi \frac{D_{ot}^2 - D_{it}^2}{4} \frac{1}{2} L_i \right) \rho_w$$

The expanded nodal equations are as follows,

$$\frac{dT_{w1}}{dt} = \frac{h_{pw}\left(N\pi D_{it}\frac{1}{2}L_s \right)(T_{p1} - T_{w1}) - h_{ws}\left(N\pi D_{ot}\frac{1}{2}L_s \right)(T_{w1} - T_{s1})}{\left(N\pi \frac{D_{ot}^2 - D_{it}^2}{4}\frac{1}{2}L_s \right)\rho_w c_{p_w}} \tag{5.7}$$

$$\frac{dT_{w2}}{dt} = \frac{h_{pw}\left(N\pi D_{it}\frac{1}{2}L_s \right)(T_{p2} - T_{w2}) - h_{ws}\left(N\pi D_{ot}\frac{1}{2}L_s \right)(T_{w2} - T_{s2})}{\left(N\pi \frac{D_{ot}^2 - D_{it}^2}{4}\frac{1}{2}L_s \right)\rho_w c_{p_w}} \tag{5.8}$$

$$\frac{dT_{w3}}{dt} = \frac{h_{pw}\left(N\pi D_{it}\frac{1}{2}L_b \right)(T_{p3} - T_{w3}) - h_{ws}\left(N\pi D_{ot}\frac{1}{2}L_b \right)(T_{w3} - T_{sat})}{\left(N\pi \frac{D_{ot}^2 - D_{it}^2}{4}\frac{1}{2}L_b \right)\rho_w c_{p_w}} \tag{5.9}$$

$$\frac{dT_{w4}}{dt} = \frac{h_{pw}\left(N\pi D_{it}\frac{1}{2}L_b \right)(T_{p4} - T_{w4}) - h_{ws}\left(N\pi D_{ot}\frac{1}{2}L_b \right)(T_{w4} - T_{sat})}{\left(N\pi \frac{D_{ot}^2 - D_{it}^2}{4}\frac{1}{2}L_b \right)\rho_w c_{p_w}} \tag{5.10}$$

$$\frac{dT_{w5}}{dt} = \frac{h_{pw}\left(N\pi D_{it}\frac{1}{2}L_{sc} \right)(T_{p5} - T_{w5}) - h_{ws}\left(N\pi D_{ot}\frac{1}{2}L_{sc} \right)(T_{w5} - T_{sat})}{\left(N\pi \frac{D_{ot}^2 - D_{it}^2}{4}\frac{1}{2}L_{sc} \right)\rho_w c_{p_w}} \tag{5.11}$$

$$\frac{dT_{w6}}{dt} = \frac{h_{pw}\left(N\pi D_{it}\frac{1}{2}L_{sc}\right)(T_{p6} - T_{w6}) - h_{ws}\left(N\pi D_{ot}\frac{1}{2}L_{sc}\right)(T_{w6} - T_{sc2})}{\left(N\pi\frac{D_{ot}^2 - D_{it}^2}{4}\frac{1}{2}L_{sc}\right)\rho_w c_{p_w}} \tag{5.12}$$

5.3.3 Superheat Temperature

$$\frac{dT_{s1}}{dt} = \frac{h_{ws}N\pi D_{ot}\frac{1}{2}L_s(T_{w1} - T_{s1}) - \left(W_s c_{ps}(T_{s1} - T_{s2})\right)}{A_s\frac{1}{2}L_s\rho_s c_{ps}} \tag{5.13}$$

$$\frac{dT_{s2}}{dt} = \frac{h_{ws}N\pi D_{ot}\frac{1}{2}L_s(T_{w2} - T_{s2}) - \left(W_s c_{ps}(T_{s2} - T_{sat})\right)}{A_s\frac{1}{2}L_s\rho_s c_{ps}} \tag{5.14}$$

5.3.4 Subcooled Temperature

Subcooled temperature is calculated for Node 2 only. The inlet node (Node 1) is assumed to be well mixed at the feedwater temperature.

$$\begin{aligned} \frac{dT_{sc}}{dt} = & \\ & \left[h_{wsc}\pi D_{ot}\frac{L_{sc}}{2}\left(T_{w6} - T_{sc2}\right) + c_{p_{sc}}\left(W_{fw}T_{fw} - W_{sc}T_{sc2}\right) + \right. \\ & \left.\frac{1}{778}\frac{A_s L_{sc}}{2}\dot{P}_{sc} - \frac{T_{sc2}\dot{L}_{sc}A_s\rho_{sc}c_{p_{sc}}}{2}\right]\left[\frac{L_{sc}A_s\rho_{sc}c_{p_{sc}}}{2}\right]^{-1} \end{aligned} \tag{5.15}$$

5.3.5 Primary Inlet Temperature

Primary inlet temperature is read as an output from the core model. This value is used for calculations in each timestep of the steam generator and is therefore imported as a dedicated signal.

$$T_{pin} = \text{input from core model} \tag{5.16}$$

5.3.6 Fluid Levels

Fluid levels are determined based on power, as explained in Section 5.1. The derivative of the fluid level is approximated by taking the mismatch from the current timestep with that of the previous timestep.

$$\frac{dL_{sc}}{dt} = f(Power) \tag{5.17}$$

$$L_{sc} = f(Power) \tag{5.18}$$

$$\frac{dL_b}{dt} = f(Power) \tag{5.19}$$

$$L_b = f(Power) \tag{5.20}$$

$$\frac{dL_s}{dt} = f(Power) \tag{5.21}$$

$$L_s = f(Power) \tag{5.22}$$

5.3.7 Subcooled Pressure

$$\frac{dP_{sc}}{dt} = \frac{W_{fw} - W_{db} - \rho_{sc} A_s \frac{dL_{sc}}{\mathrm{dt}}}{A_s L_{sc} K_{sc}} \tag{5.23}$$

$$P_{sc} = \int \frac{dP_{sc}}{dt} \tag{5.24}$$

5.3.8 Saturation Pressure

$$\frac{dP_{sat}}{dt} = \frac{h_{wsc} A_{wsc} (T_{w5} - T_{sat}) + 2c_{p_{sc}}(W_{sc} T_{sc2} - W_{db} T_{sat}) - A_s \rho_{sc} c_{p_{sc}} (T_{sat} \frac{dL_{sc}}{dt})}{A_s \rho_{sc} c_{p_{sc}} K_1 L_{sc}} \tag{5.25}$$

where,

h_{wsc} = heat transfer coefficient from SG tube wall to subcooled fluid. This heat transfer coefficient has been approximated from data provided of the Oconee nuclear station (designed by B&W which has once-through steam generators).

$A_{wsc} = \left(N \pi D_{ot} \frac{L_{sc}}{2} \right)$

$A_s = \left(\pi \frac{D_{os}^2}{4} \right) - \left(N \pi \frac{D_{ot}^2}{4} \right) - \left(\pi \frac{D_{is}^2}{4} \right)$

$$P_{sat} = \int \frac{dP_{sat}}{dt} \tag{5.26}$$

5.3.9 Saturation Temperature

Saturation temperature is calculated using the saturation pressure. Steam tables [17] have been used to generate a polynomial; providing saturation temperature given saturation pressure.

$$T_{sat} = f(P_{sat}) \tag{5.27}$$

5.3.10 Steam Pressure

$$\frac{dP_s}{dt} = \frac{Z_{ss}(W_b - W_s)R\frac{(T_{s1}+458.67+T_{s2}+458.67)}{2M_{stm}}}{A_s L_s} \tag{5.28}$$

$$P_s = \int \frac{dP_s}{dt} \tag{5.29}$$

5.3.11 Feedwater Temperature

$$T_{fw} = \text{user defined constant} \tag{5.30}$$

5.3.12 Mass flow rates

Feedwater flow

$$W_{fw} = \text{Input from Balance of Plant} \tag{5.31}$$

Subcooled Flow

$$W_{sc} = W_{FW} + \frac{1}{2}\frac{dL_{sc}}{\mathrm{dt}}A_s\rho_{sc} \tag{5.32}$$

Transition to Boiling Flow

$$W_{db} = W_{sc} + \frac{1}{2}\frac{dL_{sc}}{\mathrm{dt}}A_s\rho_{sc} \tag{5.33}$$

Boiling Flow

$$W_b = W_{db} + \frac{dL_{sc}}{dt}A_s\rho_b \tag{5.34}$$

Flow between superheated nodes

$$W_{12} = W_b + \frac{1}{2}\frac{dL_s}{dt}A_s\rho_s \tag{5.35}$$

Steam flow

$$W_s = W_{12} + \frac{1}{2}\frac{dL_s}{dt}A_s\rho_s \tag{5.36}$$

5.3.13 Coefficients of the OTSG model

Kb is a coefficient which represents the partial change of the boiling fluid density (ρ_{b}) to the partial change in saturation pressure ($\mathrm{P}_{\mathrm{sat}}$).

$$K_b = \frac{\partial\bar{\rho}_b}{\partial P}$$

Kb is approximated as the average slope of the boiling fluid density to saturation pressure over the range of 500-600 F.

$$K_b \approx -0.000053 \tag{5.37}$$

K1 is a coefficient which represents the partial change in saturation temperature to the partial change in saturation pressure.

$$K_1 = \frac{\partial T_{sat}}{\partial P}$$

K1 is approximated as the average slope of the saturation temperature to saturation pressure over the range of 500-600 F.

$$K_1 \approx 8.02299324E-04 \tag{5.38}$$

Inverse signal of K1

$$\frac{1}{K_1} \approx \frac{1}{8.02299324E-04} \tag{5.39}$$

Ksc is a coefficient which represents the partial change of the subcooled fluid density (ρ_{sc}) to the partial change in saturation pressure ($\mathrm{P}_{\mathrm{sat}}$).

$$K_{sc} = \frac{\partial \rho_{sc}}{\partial P} = \frac{\partial}{\partial P}\frac{(\rho_{fw} + \rho_f)}{2}$$

where,

$\rho_{fw} =$ density of feedwater

$\rho_f =$ density of saturated water

Ksc is approximated as the average slope of the subcooled fluid density to saturation pressure over the range of 500-600 F.

$$K_{sc} \approx -0.000053 \tag{5.40}$$

Inverse signal of Ksc

$$\frac{1}{K_{sc}} \approx \frac{1}{-0.000053} \tag{5.41}$$

5.3.14 Steam Pressure Controller

Steam Pressure Control

$$\frac{\mathrm{dW}_s}{\mathrm{dt}} = \frac{W_{s_0}\left[1 - C_{st}\left(k_c(1 - \frac{P_s}{P_{set}}) + \frac{k_c\left(1 - \frac{P_s}{P_{set}}\right)}{t_s}\right)\right] - W_s}{t_s} \tag{5.42}$$

5.3.15 Imported signals and inverse signals

Thermal fractional power (Pth) is imported from the core model and is used to calculate SG levels.

$$P_{th} = \text{ input from core model} \tag{5.43}$$

MATLAB-Simulink will not process division by a signal. In a strange workaround however, if the signal is inversed and then multiplied, the code will continue to run. This issue has been brought to the attention of the administrators of MathWorks.
The inversed signal of saturation temperature

$$\frac{1}{T_{sat}} \tag{5.44}$$

The inversed signal of subcooled fluid level within the steam generator

$$\frac{1}{L_{sc}} \tag{5.45}$$

Chapter 6

Balance of Plant

The Balance Of Plant (BOP) systems have been developed according to the system of ordinary differential equations outlined by Shankar [18] and Dutta [19] and Naghedolfeizi [20]. The BOP equations have been numbered within this document such that they correspond to the signal number found within the Simulink model. Subsequently, each signal from the code is linked to a prefix (Table 6.1) which provides it unique identifier. The code output is structured according to the unique identifiers. A list of all parameters may be referred to in Appendix C. Code output at steady state is provided in Appendix D.

Shankar's model (Figure 6.1), contains the following components: nozzle chest, high and low pressure turbines, moisture separator and reheater, and two feedwater heaters. Each component is provided a set of ODEs to calculate the output state variables. In order to fully define the system, numerous constants and variables need to be identified by the user. For several of these, there are no units listed; many of these parameters are best estimate and need be revisited to ensure validity of the model. The Simulink model (Figure 6.2) has been assembled to be representative of the physical layout of Shankar's model.

Table 6.1: Balance of Plant Output

Identifier	Description
cor	reactor core
stg	steam generator
cst	steam chest
hpt	high pressure turbine
msr	moisture separator
rhr	reheater
lpt	low pressure turbine
cnd	condenser
fha	feedwater heater 1
fhb	feedwater heater 2

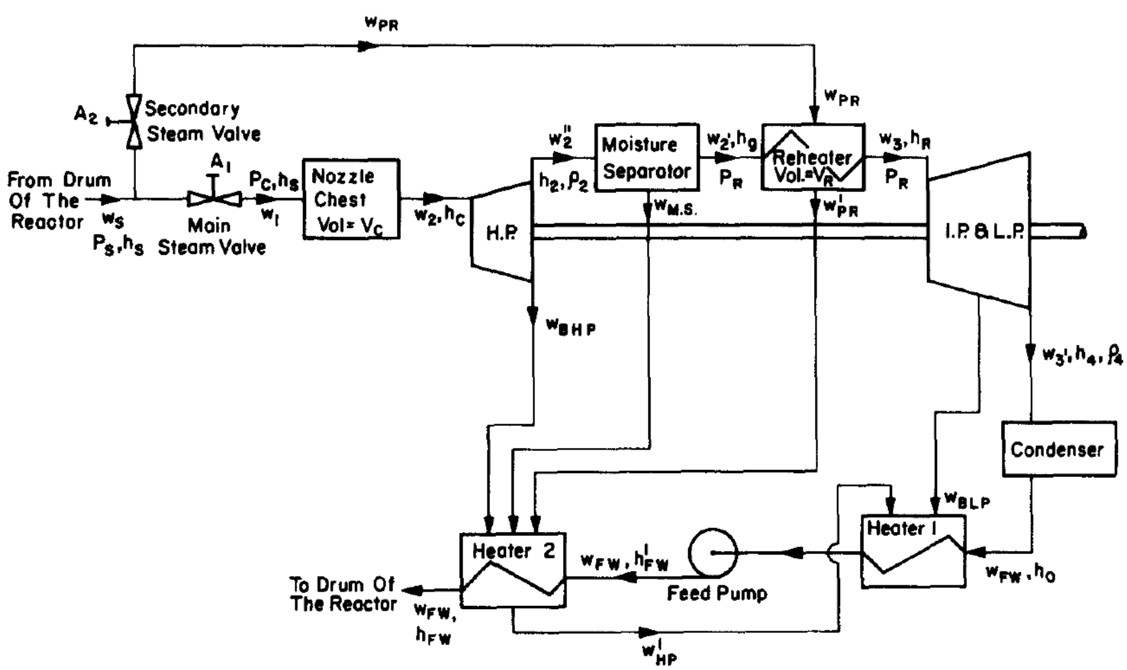

Figure 6.1: Balance of Plant Flow Diagram [18][19][20]

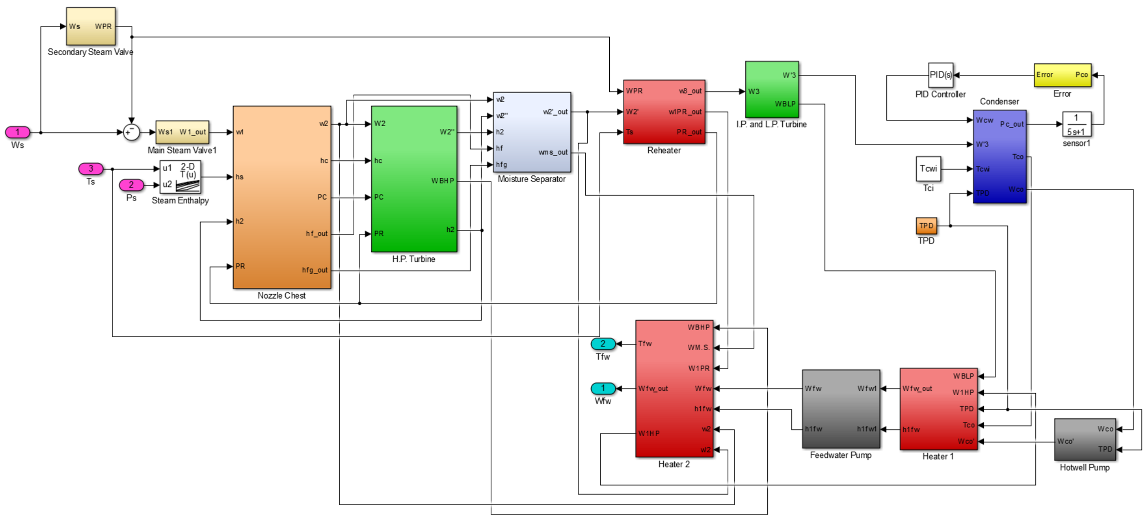

Figure 6.2: Balance of Plant Simulink Model

6.1 Main Steam Valve

The main steam valve diverts 16% of the steam flow for use of process heat in the reheater and feedwater heaters one and two.

$$w_1 = 0.84W_s \tag{6.1.1}$$

6.2 Nozzle Chest

Rate of change of enthalpy in the nozzle chest

$$\frac{dh_c}{dt} = \left(\frac{w_1 h_s - w_2 hc}{\rho_c V_c} + \frac{JP_c}{\rho_c^2}\frac{d\rho_c}{dt}\right) \tag{6.2.1}$$

There is a integral block in simulink which is used to calculate the enthalpy in the nozzle chest (h_c)

$$h_c = \int \frac{dh_c}{dt} \tag{6.2.2}$$

Rate of change of steam density in the nozzle chest.

$$\frac{d\rho_c}{dt} = \frac{w_1 - w_2}{V_c} \tag{6.2.3}$$

The integral block calculates steam density in the nozzle chest.

$$\rho_c = \int \frac{d\rho_c}{dt} \tag{6.2.4}$$

Inverted density

$$\frac{1}{\rho_c} \tag{6.2.5}$$

Steam flow from the nozzle chest to the high pressure turbine

$$w_2 = A_{K2}(P_C\rho_c - P_R\rho_2) \tag{6.2.6}$$

Nozzle chest pressure $\mathrm{P_C}$ is determined through superheated steam properties and is a function of density and enthalpy. There is a steam function in MATLAB (Xsteam) which was used to produce a 2-D lookup table (Figure 6.3). Signals for steam chest enthalpy ($\mathrm{h_c}$) and steam chest density (ρ_c) are inputs to the lookup table; the output yields nozzle chest pressure in units of pounds per square foot.

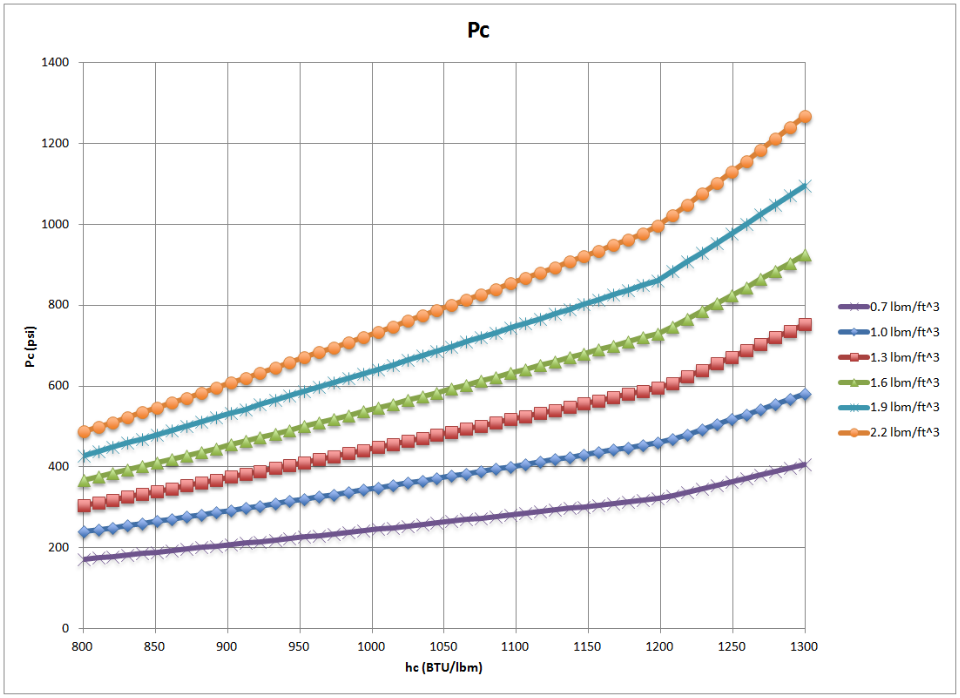

Figure 6.3: Nozzle chest pressure steam curves

$$\mathrm{P_C} = f(\mathrm{h_c}, \rho_\mathrm{c}) \tag{6.2.7}$$

Steam quality input for calculation of density (ρ_2).

$$x = \frac{h_2 - h_f}{h_{fg}} \tag{6.2.8}$$

Steam density between nozzle chest and high pressure turbine.

$$\rho_2 = \frac{1}{x\nu_g + (1-x)\nu_f} \tag{6.2.9}$$

The specific volume of saturated steam (ν_g) is calculated by a polynomial (Figure 6.4) based off of steam property data (Xsteam). The specific volume is a function of reheater pressure ($\mathrm{P_R}$).

Table 6.2: ν_g Polynomial coefficients

Power	Coefficient
$\mathrm{P_R^6}$	3.16015E-28
$\mathrm{P_R^5}$	-1.06919E-22
$\mathrm{P_R^4}$	1.47784E-17
$\mathrm{P_R^3}$	-1.07591E-12
$\mathrm{P_R^2}$	4.43489E-08
$\mathrm{P_R^1}$	-1.03385E-03
$\mathrm{P_R^0}$	1.27494E+01

$$\nu_g = f(\mathrm{P_R}) \tag{6.2.10}$$

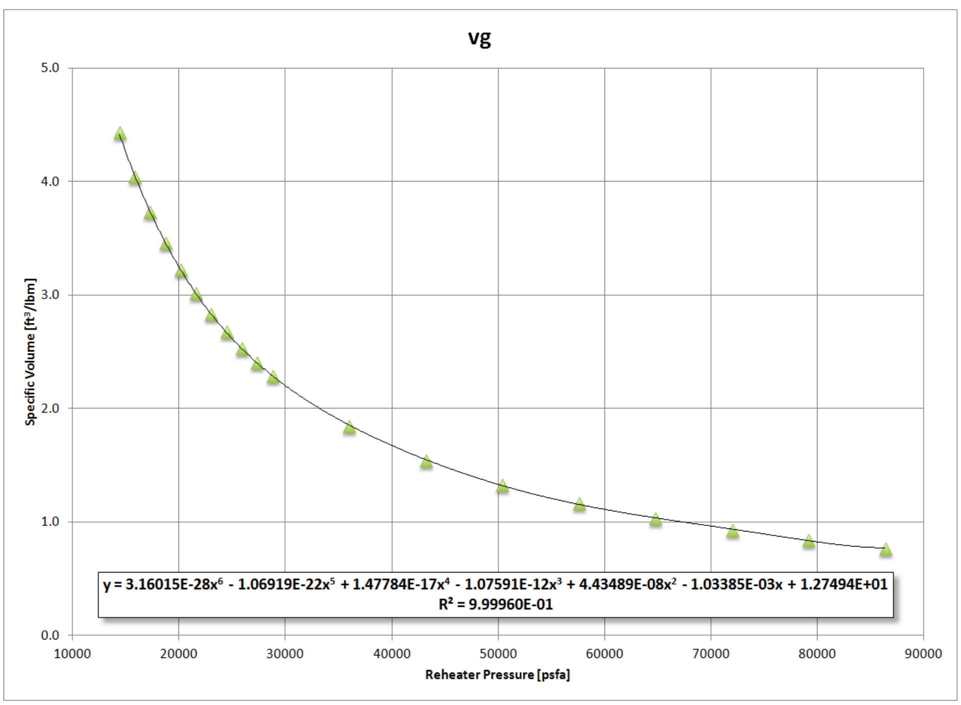

Figure 6.4: Specific volume of saturated steam curve

The enthalpy of saturated water in the reheater feedwater ($\mathrm{h_f}$) is calculated by a polynomial (Figure 6.5) as a function of reheater pressure ($\mathrm{P_R}$).

Table 6.3: $\mathrm{h_f}$ Polynomial coefficients

Power	Coefficient
$\mathrm{P_R^4}$	-4.63411E-18
$\mathrm{P_R^3}$	1.20033E-12
$\mathrm{P_R^2}$	-1.23684E-07
$\mathrm{P_R^1}$	7.74471E-03
$\mathrm{P_R^0}$	2.09721E+02

$$h_f = f(\mathrm{P_R}) \tag{6.2.11}$$

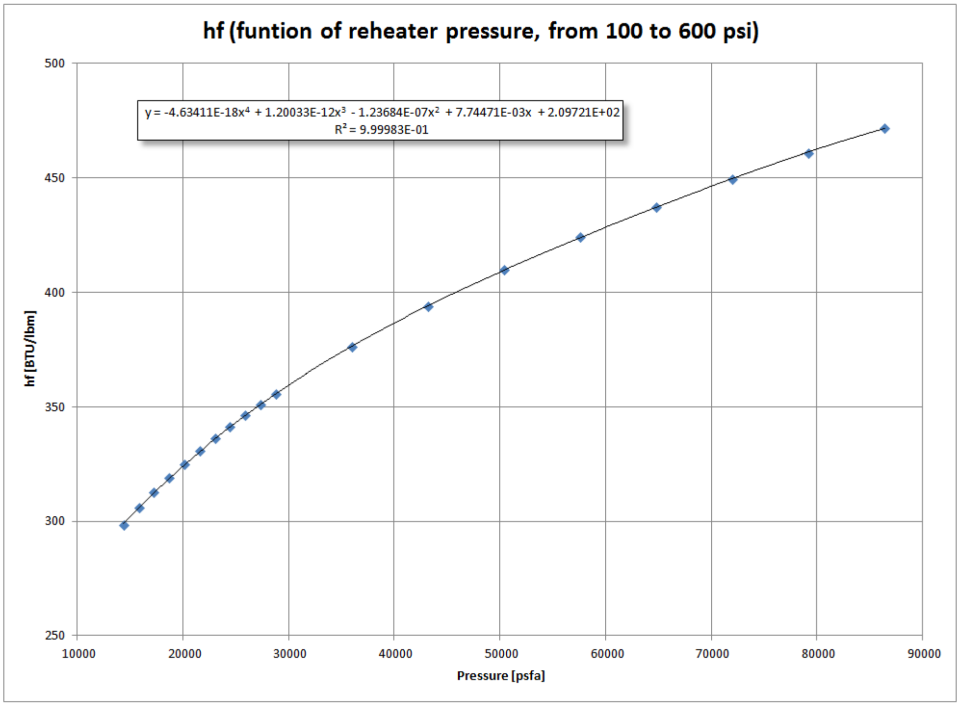

Figure 6.5: Enthalpy of saturated water in the reheater feedwater

The latent heat of vaporization in the reheater feedwater (h_{fg}) is calculated by a polynomial (Figure 6.6) as a function of reheater pressure (P_R). It can be observed that there is some instability of the polynomial at high pressures which greatly influences the slope. The Simulink model however, uses only the corresponding value of the latent heat of vaporization (h_{fg}) as a function of reheater pressure and not its derivative ($\frac{dh_{fg}}{dP}$).

Table 6.4: h_{fg} Polynomial coefficients

Power	Coefficient
P_R^6	3.353614E-26
P_R^5	-9.257963E-21
P_R^4	9.864059E-16
P_R^3	-5.121756E-11
P_R^2	1.364869E-06
P_R^1	-2.062660E-02
P_R^0	1.016796E+03

$$h_{fg} = f(P_R) \tag{6.2.12}$$

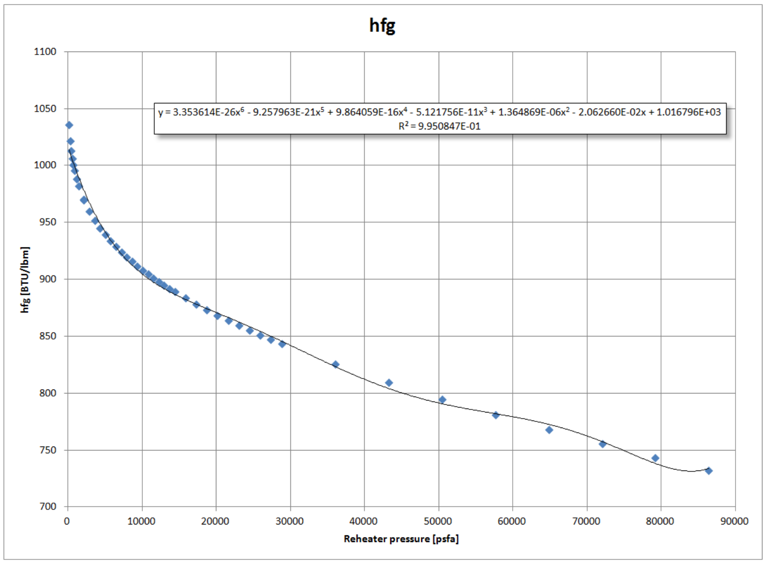

Figure 6.6: Specific enthalpy change of evaporation in the reheater feedwater

6.3 High Pressure Turbine

Flow rate of change from the high pressure turbine to the moisture separator.

$$\frac{dw_2''}{dt} = \frac{(w_2 - w_{BHP}) - w_2''}{T_{w2}} \tag{6.3.1}$$

Flow from the high pressure turbine to the moisture separator.

$$w_2'' = \int \frac{dw_2''}{dt} \tag{6.3.2}$$

Bleed flow from the high pressure turbine to the moisture separator.

$$w_{BHP} = K_{BHP} w_2 \tag{6.3.3}$$

Enthalpy of main steam at moisture separator.

$$\mathrm{h}_2 = \left[\frac{(\mathrm{h}_2' - \mathrm{h_c})}{\eta^*_{\mathrm{HP}}}\right] + \mathrm{h_c} \tag{6.3.4}$$

Enthalpy of main steam at isentropic end points from pressure $\mathrm{P_C}$.

$$\mathrm{h}_2' = 1067 + 0.37(\mathrm{P_R} - 200) - 0.0011(\mathrm{P_R} - 200)^2 - 0.1(\mathrm{P_C} - 1000) \tag{6.3.5}$$

6.4 Moisture Separator

Flow from moisture separator to heater 2.

$$W_{MS} = (w_2 - K_{BHP} w_2) - w_2' \tag{6.4.1}$$

Flow from moisture separator to reheater.

$$w_2^{'} = \frac{\mathrm{h}_2 - \mathrm{h}_\mathrm{f}}{\mathrm{h}_\mathrm{fg}} w_2'' \tag{6.4.2}$$

6.5 Reheater

Rate of change of density of steam in reheater.

$$\frac{d\rho_R}{dt} = \frac{(w_2^{'} - w_3)}{V_R} \tag{6.5.1}$$

Density of steam in reheater.

$$\rho_\mathrm{R} = \int \frac{d\rho_\mathrm{R}}{dt} \tag{6.5.2}$$

Inverse density of steam in reheater.

$$\frac{1}{\rho_\mathrm{R}} \tag{6.5.3}$$

Rate of change in enthalpy of steam in reheater.

$$\frac{dh_R}{dt} = \left\{ \frac{(Q_R + w_2^{'} h_g - w_3 h_R)}{\rho_R V_R} + \frac{J P_R (w_2^{'} - w_3)}{\rho_R^2 V_R} \right\} \tag{6.5.4}$$

Enthalpy of steam in reheater.

$$\mathrm{h_R} = \int \frac{dh_R}{dt} \tag{6.5.5}$$

Inverse enthalpy of steam in reheater.

$$\frac{1}{\mathrm{h_R}} \tag{6.5.6}$$

The pressure in the reheater is generated through a look up table (Figure 6.7).

$$\mathrm{P_R} = f(\rho_\mathrm{R} \mathrm{h_R}) \tag{6.5.7}$$

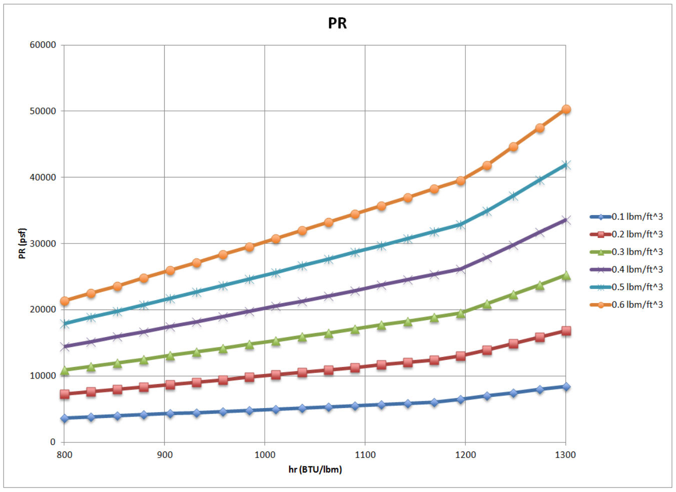

Figure 6.7: Reheater pressure

Flow from reheater to low pressure turbine.

$$w_3 = K_3(\mathrm{P_R}\rho_\mathrm{R})^{\frac{1}{2}} \tag{6.5.8}$$

The enthalpy of saturated steam in the reheater feedwater is calculated by a polynomial.

Table 6.5: $\mathrm{h_g}$ Polynomial coefficients

Power	Coefficient
$\mathrm{P_R^4}$	-1.78516E-18
$\mathrm{P_R^3}$	4.57484E-13
$\mathrm{P_R^2}$	-4.63042E-08
$\mathrm{P_R^1}$	2.19275E-03
$\mathrm{P_R^0}$	1.16443E+03

$$h_g = f(\mathrm{P_R}) \tag{6.5.9}$$

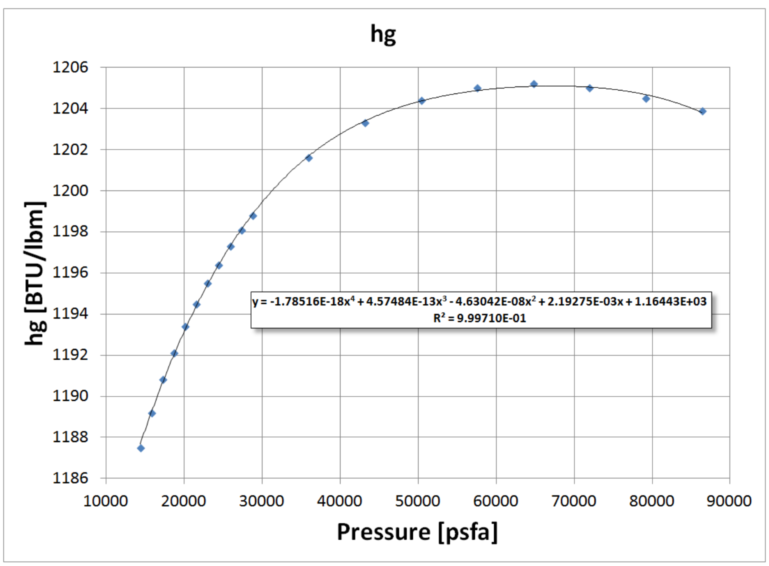

Figure 6.8: Enthalpy of saturated vapor in reheater

Rate of change of flow from reheater to heater 2.

$$\frac{\mathrm{dw}'_{\mathrm{PR}}}{\mathrm{dt}} = \frac{w_{\mathrm{PR}} - w'_{\mathrm{PR}}}{\mathrm{T_{R1}}} \tag{6.5.10}$$

Flow from reheater to heater 2.

$$\mathrm{w}'_{\mathrm{PR}} = \int \frac{\mathrm{dw}'_{\mathrm{PR}}}{\mathrm{dt}} \tag{6.5.11}$$

Rate of change in the heat transfer rate in the reheater.

$$\frac{dQ_R}{dt} = \frac{w_P R + w'_{PR} H_R}{2T_{R2}}(T_S - T_R) - \frac{Q_R}{T_{R2}} \tag{6.5.12}$$

Heat transfer rate in the reheater.

$$\mathrm{Q_R} = \int \frac{dQ_R}{dt} \tag{6.5.13}$$

Temperature of the shell side steam

$$\mathrm{T_S} = \text{ input from OTSG model} \tag{6.5.14}$$

Temperature of the tube side steam

$$T_R = \frac{P_R}{\rho_R R} \tag{6.5.15}$$

Gas constant

$$R = \frac{201.7}{0.365(520 + 460)} \tag{6.5.16}$$

6.6 Low Pressure Turbine

Rate of change of flow from low pressure turbine to condenser.

$$\frac{dw_3^{'}}{dt} = (1 - K_{BLP})w_3 - \frac{w_3^{'}}{T_{w3}} \tag{6.6.1}$$

Flow from low pressure turbine to condenser.

$$w_3^{'} = \int \frac{dw_3^{'}}{dt} \tag{6.6.2}$$

Bleed flow from low pressure turbine to heater 1.

$$w_{BLP} = K_{BLP} w_3 \tag{6.6.3}$$

6.7 Heater 1

$$\frac{dh'_{FW}}{dt} = \frac{Q_{H1}}{T_{H1}w_{FW}} + \frac{h_0 - h'_{FW}}{T_{H1}} \tag{6.7.1}$$

$$h'_{FW} = \int \frac{dh'_{FW}}{dt} \tag{6.7.2}$$

$$h_0 = 69.0(\text{a constant}) \tag{6.7.3}$$

$$Q_{H1} = H_{FW}(w'_{HP} + w_{BLP}) \tag{6.7.4}$$

6.8 Heater 2

$$\frac{dh_{FW}}{dt} = \frac{Q_{H2}}{T_{H2}w_{FW}} + \frac{h'_{FW} - h_{FW}}{T_{H2}} \tag{6.8.1}$$

$$h_{FW} = \int \frac{dh_{FW}}{dt} \tag{6.8.2}$$

$$Q_{H2} = H_{FW}(w_{BHP} + w_{MS} + w'_{PR}) \tag{6.8.3}$$

$$\frac{dw'_{HP}}{dt} = \frac{w_2 - w_2^{'}}{T_{H2P}} + \frac{w'_{PR} w'_{HP}}{T_{H2P}} \tag{6.8.4}$$

$$w'_{HP} = \frac{dw'_{HP}}{dt} \tag{6.8.5}$$

Chapter 7

Results of SMR Simulation

7.1 Reactivity Insertion

The following transient simulates the system response to a 10 cent step insertion of positive reactivity (e.g., immediate control rod withdrawal). The reactor is operating at steady state when at time $t = 0$, the reactivity insertion occurs. As a result, the reactivity insertion causes the average reactor coolant temperature to increase, creating a mismatch to the average temperature setpoint. The mismatch drives the feedback mechanism of the T-average controller to introduce negative reactivity (representative of control rod manipulation) to compensate for the effects of the step insertion. Over time, external reactivity stabilizes and the reactor parameters return to their nominal values. To illustrate the effects of the T-average controller, plots of the core model include profiles for when the controller is engaged and disengaged.

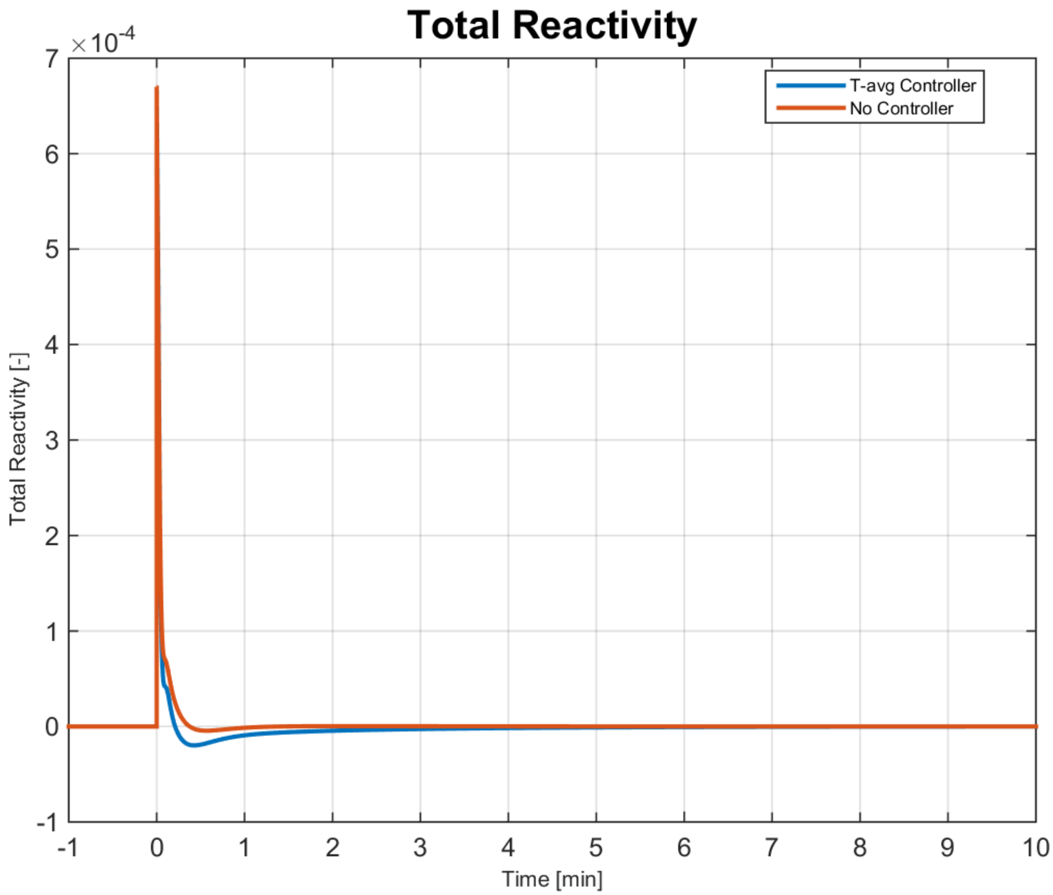

Figure 7.1: Positive reactivity insertion: total reactivity

The reactivity plot of the insertion (Figure 7.1) is indicated with the large spike at time zero. The effects of an insertion for both the T-average controller engaged and disengaged are plotted with the blue and red lines respectively. Note that the plot with the controller engaged remains negative for long after the spike, slowly trending back to zero. As a result, the negative reactivity over time brings the state variables back to their nominal values.

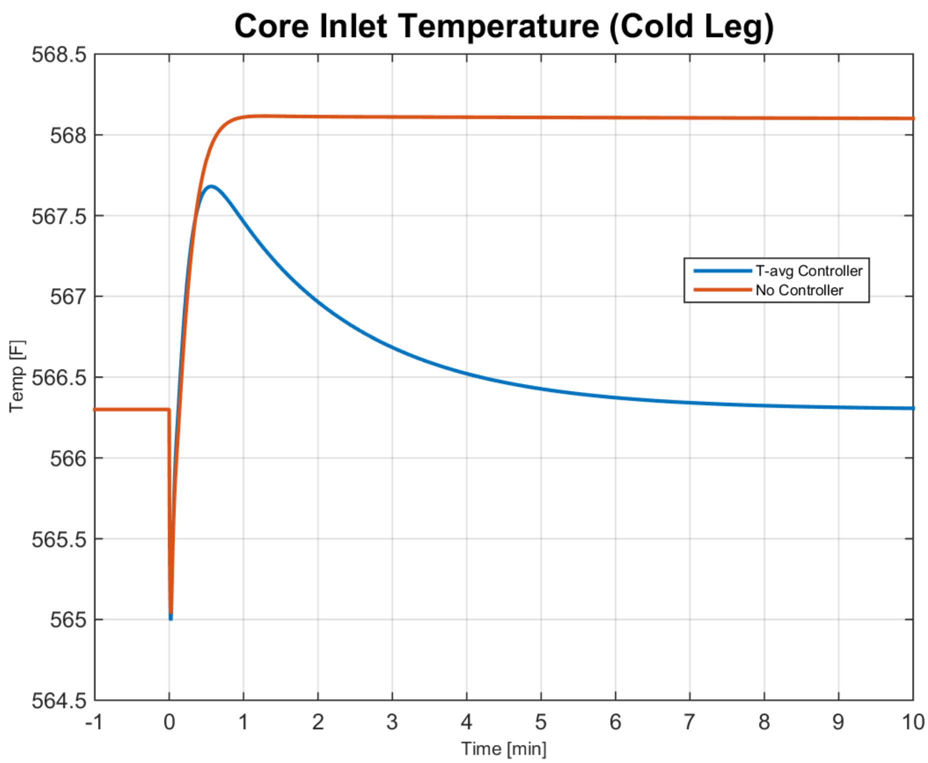

Figure 7.2: Positive reactivity insertion: core inlet temperature

The core inlet temperature plot after insertion (Figure 7.2) indicates an immediate decrease in temperature, a non-physical response resultant from the manner in which the steam generator fluid levels are calculated (Figure 7.12). Fluid levels are calculated as a function of thermal fractional power (Figure 7.3), for immediate power excursions this means the fluid level changes are also immediate. In reality, the fluid level dynamics in response to thermal power are far more delayed. Following the immediate decrease in temperature, the overall response is an increase in core inlet temperature. The plot of the red line indicates the response with no T-average controller engaged, resulting in a core inlet temperature about two degrees higher than nominal. The plot of the blue line indicates the response with the T-average controller engaged, returning the core inlet temperature to the nominal value. The effects of the initial decrease in temperature carry over to other nodes in the model including the θ_1 node (Figure 7.6), the SG primary node temperatures (Figure 7.9), SG wall node temperatures (Figure 7.10), and SG secondary fluid temperatures (Figure 7.11).

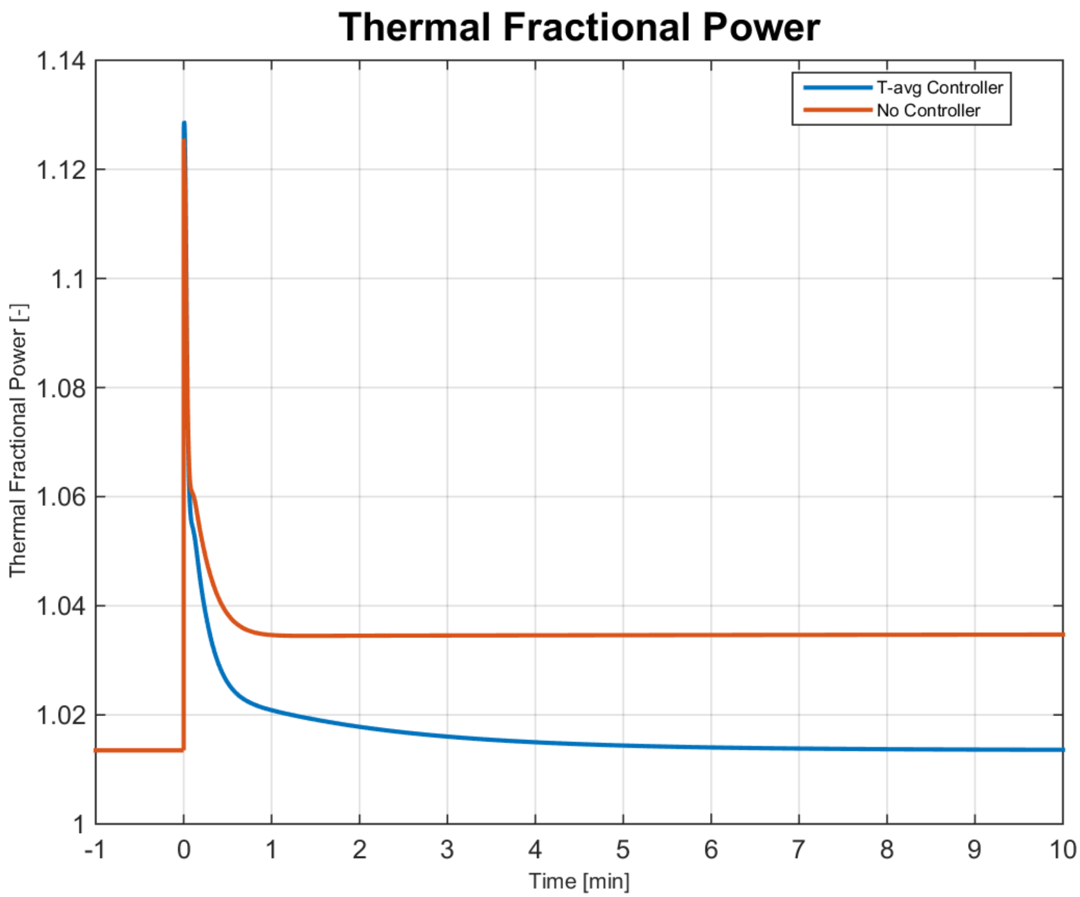

Figure 7.3: Positive reactivity insertion: thermal fractional power

Fractional thermal power following the insertion (Figure 7.3) indicates an initial power surge. The red plot, no T-average controller engaged, shows an overall increase in reactor power by about 2%. The blue plot, T-average controller engaged, shows the power level return to the initial steady state value.

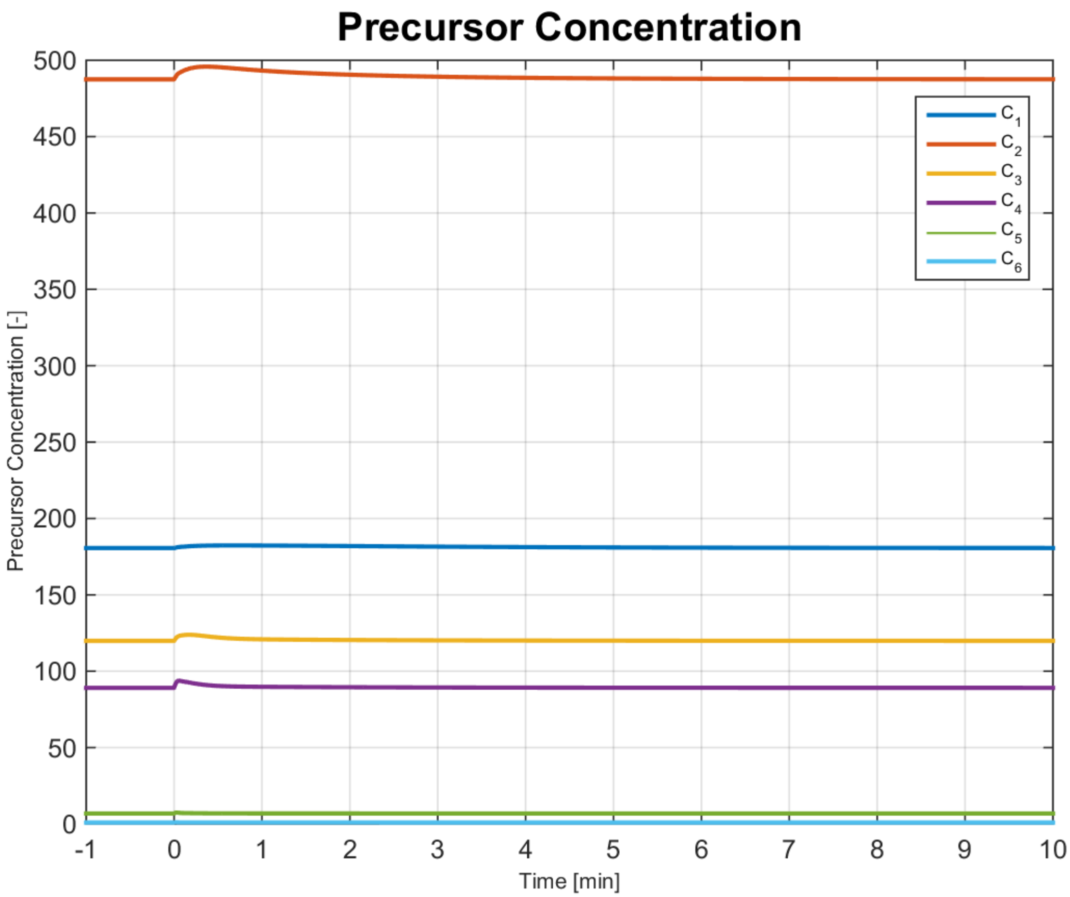

Figure 7.4: Positive reactivity insertion: precursor concentration

Precursor concentrations following the reactivity insertion are provided in Figure 7.4. The concentrations increase shortly after the insertion and slowly return to their nominal values over time.

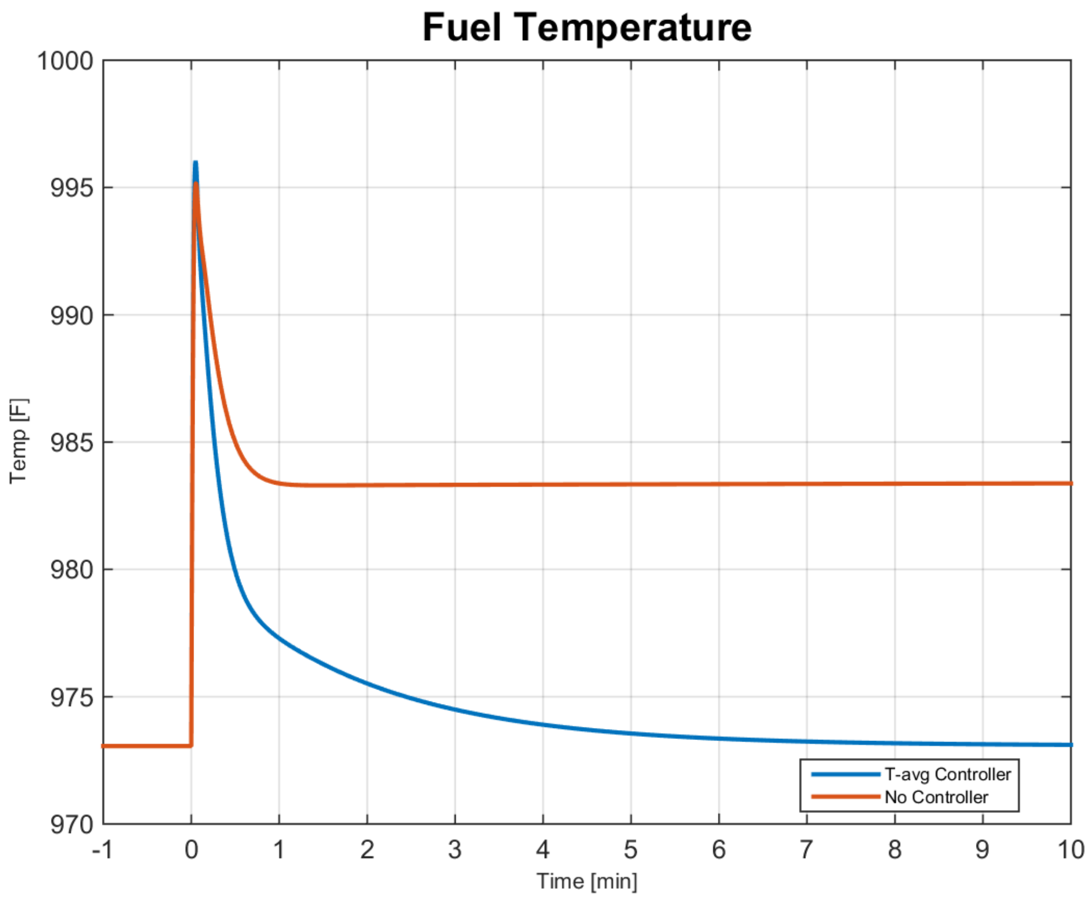

Figure 7.5: Positive reactivity insertion: fuel temperature

The plot of fuel temperature (outer cladding temperature) following reactivity insertion (Figure 7.5) indicates an initial increase in fuel temperature. The increase in fuel temperature also affects the amount of negative reactivity calculated due to the effects of the negative temperature coefficient of the fuel (α_f). The red plot indicates that the final fuel temperature, without the feedback of the T-average controller, increases by about 10 degrees. The blue plot shows the effect of the T-average controller returns the fuel temperature back to its nominal value.

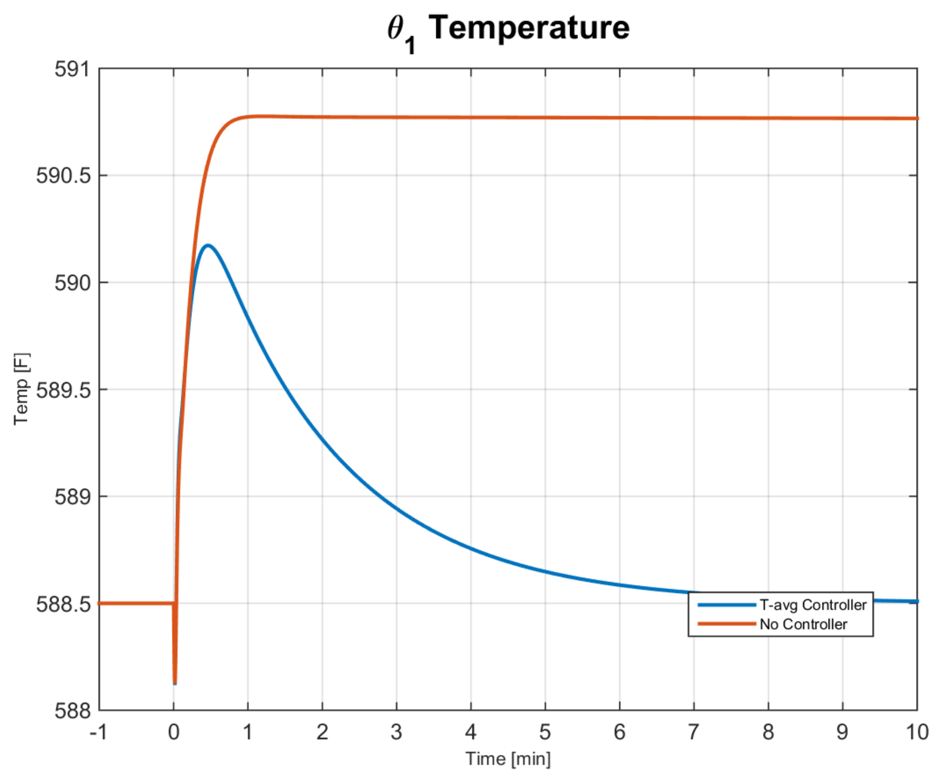

Figure 7.6: Positive reactivity insertion: theta 1 temperature

The same discussion provided for the core inlet temperature (Figure 7.2) applies to the θ_1 node temperature following reactivity insertion. The immediate decrease in temperature is non-physical, resulting from the way the steam generator fluid levels are calculated (Figure 7.12). Fluid levels are calculated as a function of thermal fractional power (Figure 7.3), for immediate power excursions this means the fluid level changes are also immediate. In reality, the fluid level dynamics in response to thermal power are far more delayed. Following the immediate decrease in temperature, the overall response is an increase in the θ_1 node temperature. The plot of the red line indicates the response with no T-average controller engaged and remains at a temperature about two degrees higher. The plot of the blue line indicates the response with the T-average controller engaged, and the response returns to the nominal temperature. The effects of the initial decrease in temperature carry over to the primary node temperatures (Figure 7.9), wall node temperatures (Figure 7.10), and secondary fluid temperatures (Figure 7.11).

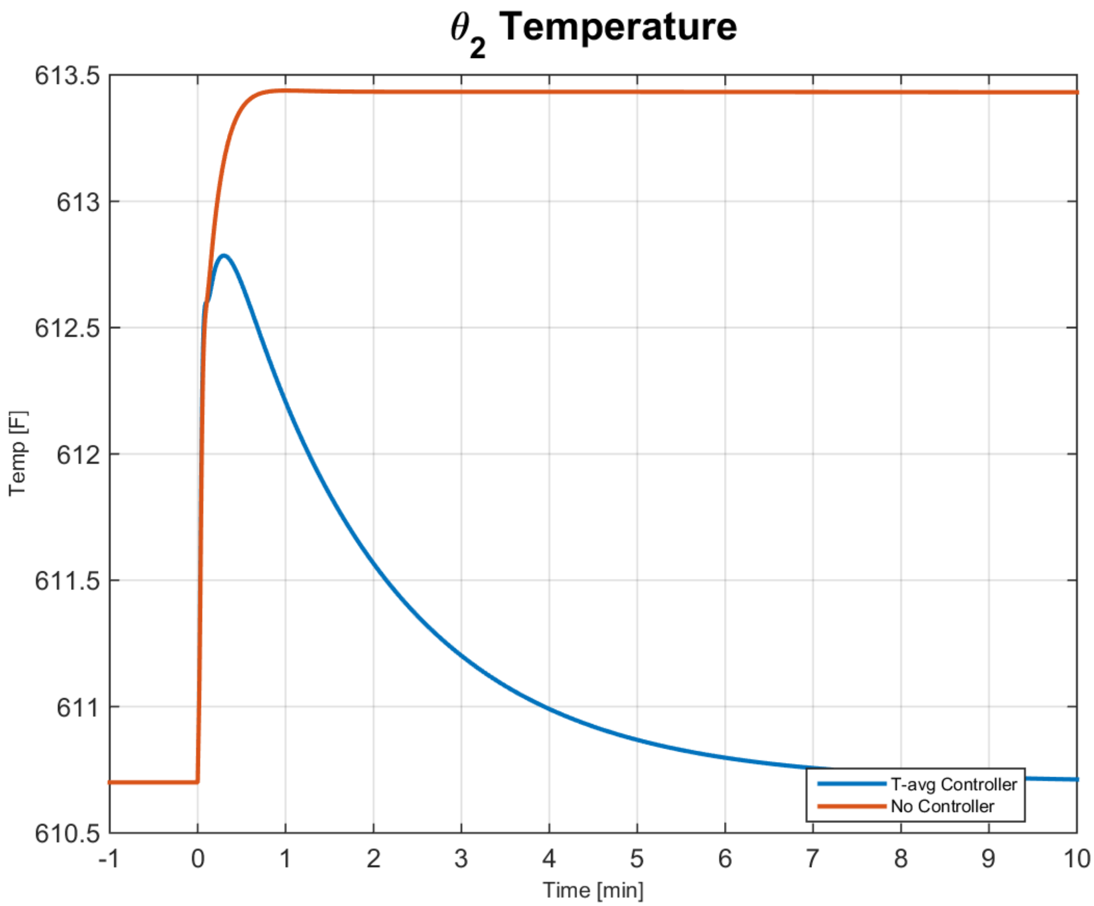

Figure 7.7: Positive reactivity insertion: theta 2 temperature

The θ_2 node (Figure 7.7) increases in temperature in response to the reactivity insertion. The red plot, no T-average controller, yields an overall increase in temperature by about two and a half degrees. The blue plot, T-average controller engaged, returns to the nominal value over time.

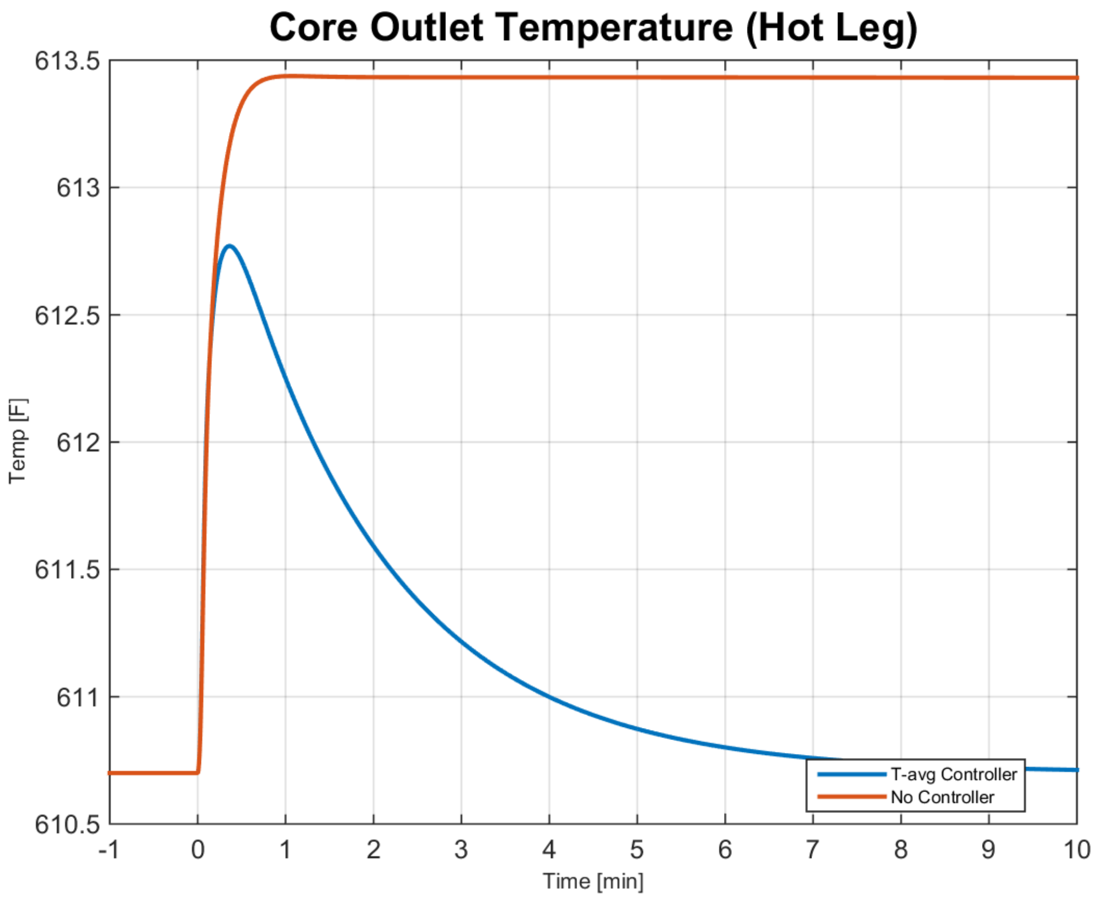

Figure 7.8: Positive reactivity insertion: core outlet temperature

The core outlet temperature (Figure 7.8) increases in temperature in response to the reactivity insertion. The red plot, no T-average controller, yields an overall increase in temperature by about two and a half degrees. The blue plot, T-average controller engaged, returns to the nominal value over time.

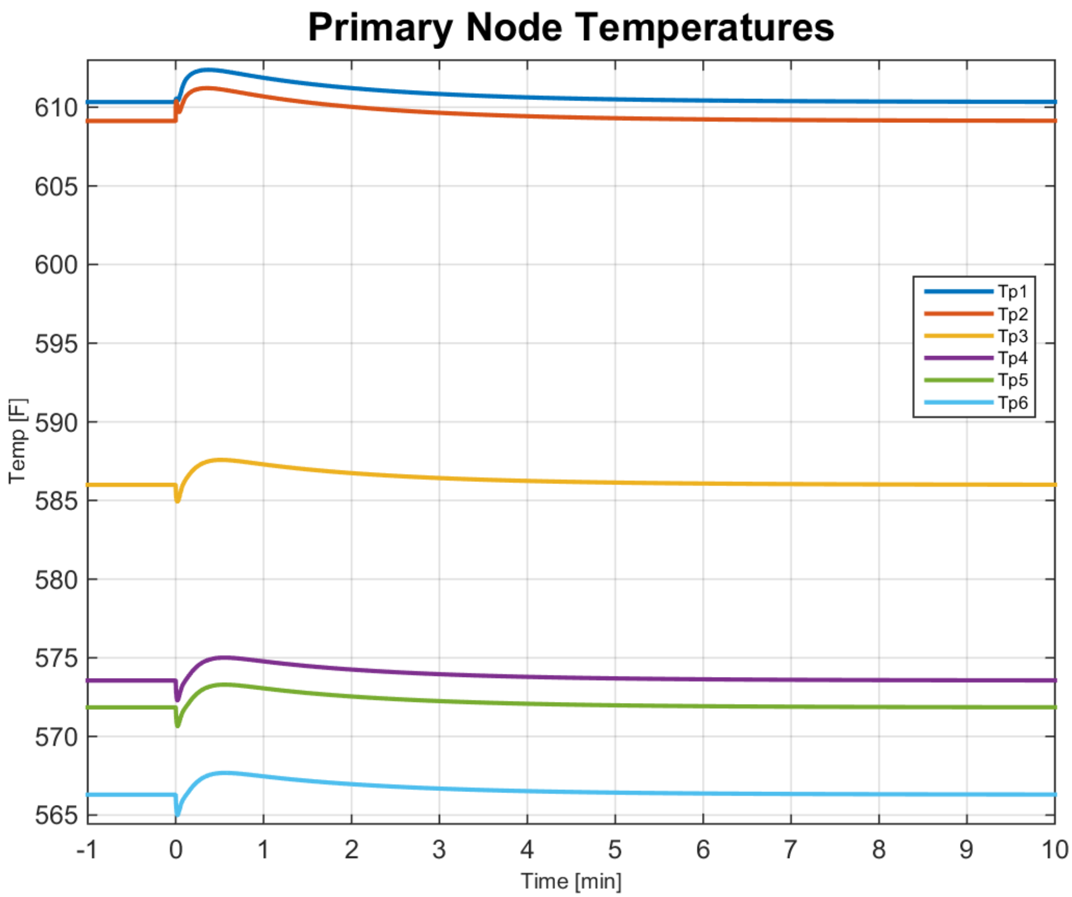

Figure 7.9: Positive reactivity insertion: primary node temperatures

The same discussion provided for the core inlet temperature (Figure 7.2) and the θ_1 node (Figure 7.6) applies to the primary node temperatures (Figure 7.9) following reactivity insertion. The immediate decrease in temperature is non-physical, resulting from the way the steam generator fluid levels are calculated (Figure 7.12). Fluid levels are calculated as a function of thermal fractional power (Figure 7.3), for immediate power excursions this means the fluid level changes are also immediate. In reality, the fluid level dynamics in response to thermal power are far more delayed. Following the immediate decrease in temperature, the overall response is an increase in the primary node temperatures. These temperatures are then brought back to the nominal value over time due to the effects of the T-average controller.

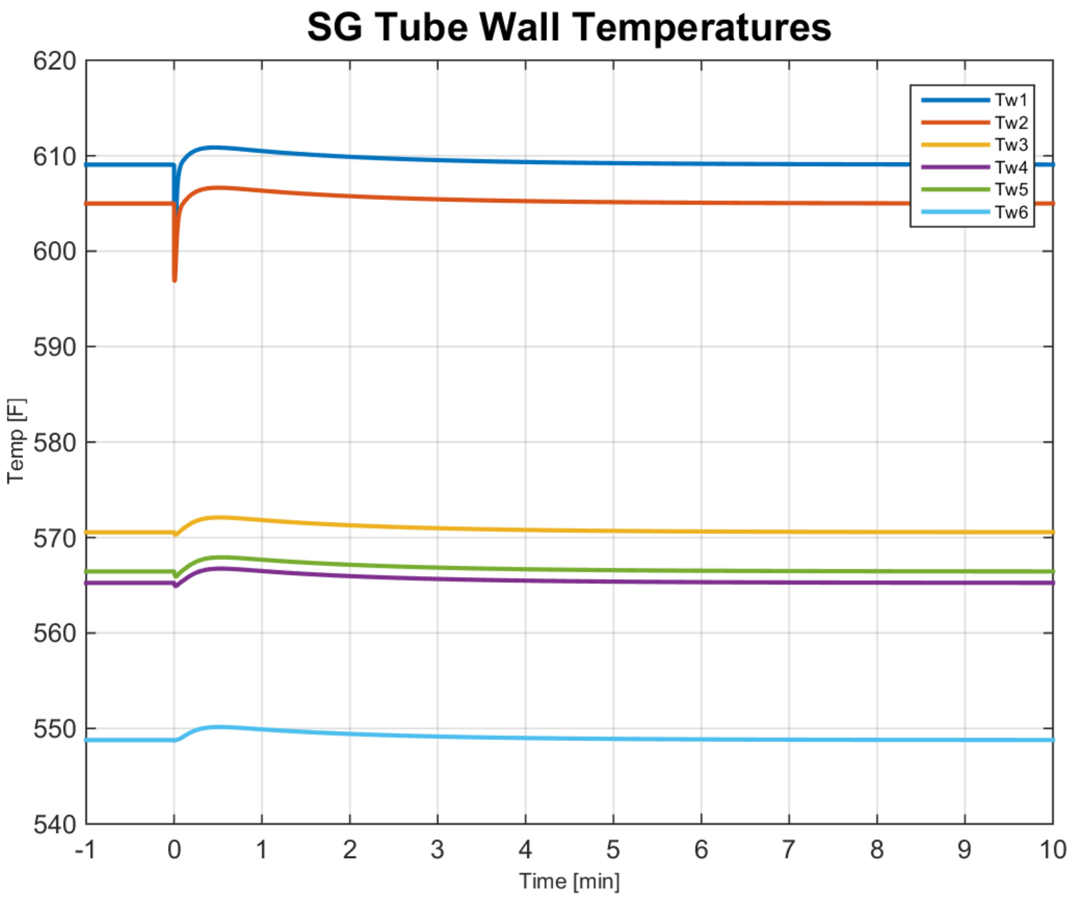

Figure 7.10: Positive reactivity insertion: SG tube wall temperatures

As previously discussed for the primary node temperatures, the tube wall temperatures following reactivity insertion (Figure 7.10) initially decrease. Following the immediate decrease in temperature, the overall response is an increase in the SG tube wall temperatures. These temperatures are then brought back to the nominal value over time due to the effects of the T-average controller.

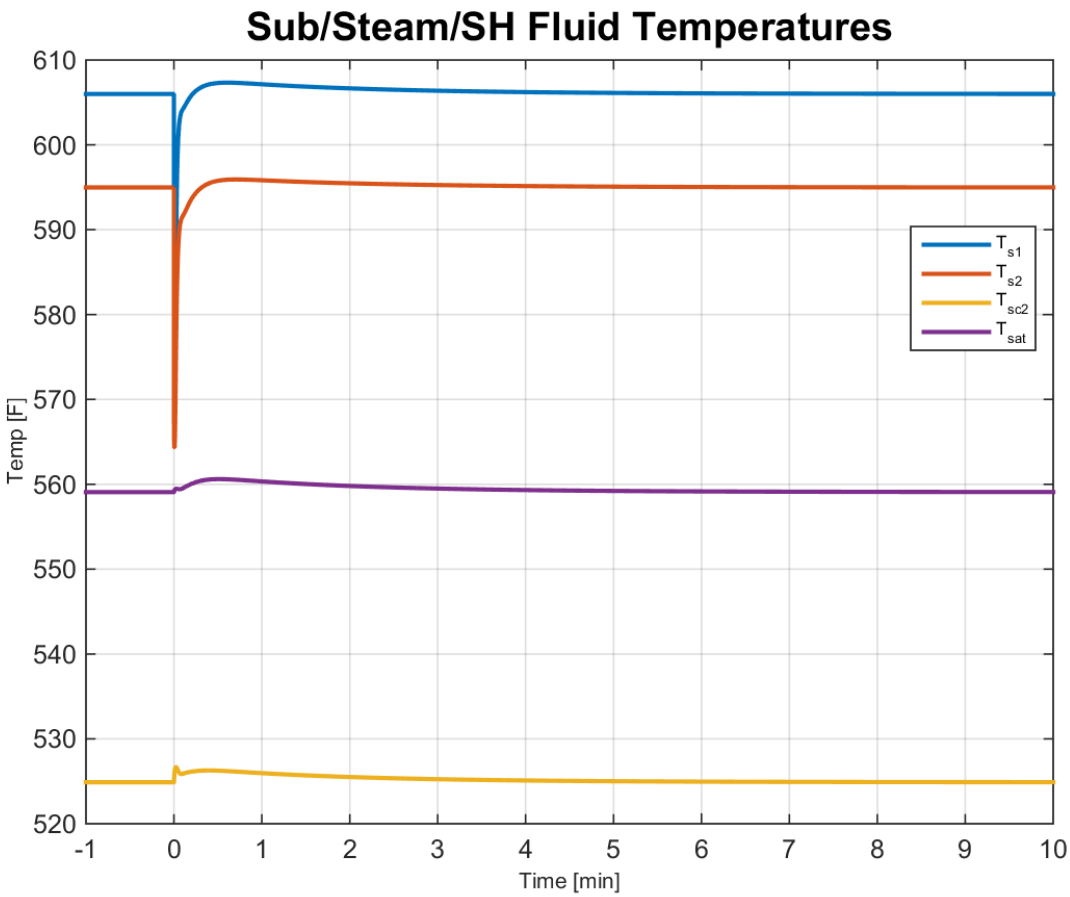

Figure 7.11: Positive reactivity insertion: SG fluid temperatures

As previously discussed for the primary node and tube wall temperatures, the SG fluid temperatures following reactivity insertion (Figure 7.11) initially decrease. Following the immediate decrease in temperature, the overall response is an increase in the SG fluid temperatures. These temperatures are then brought back to the nominal value over time due to the effects of the T-average controller.

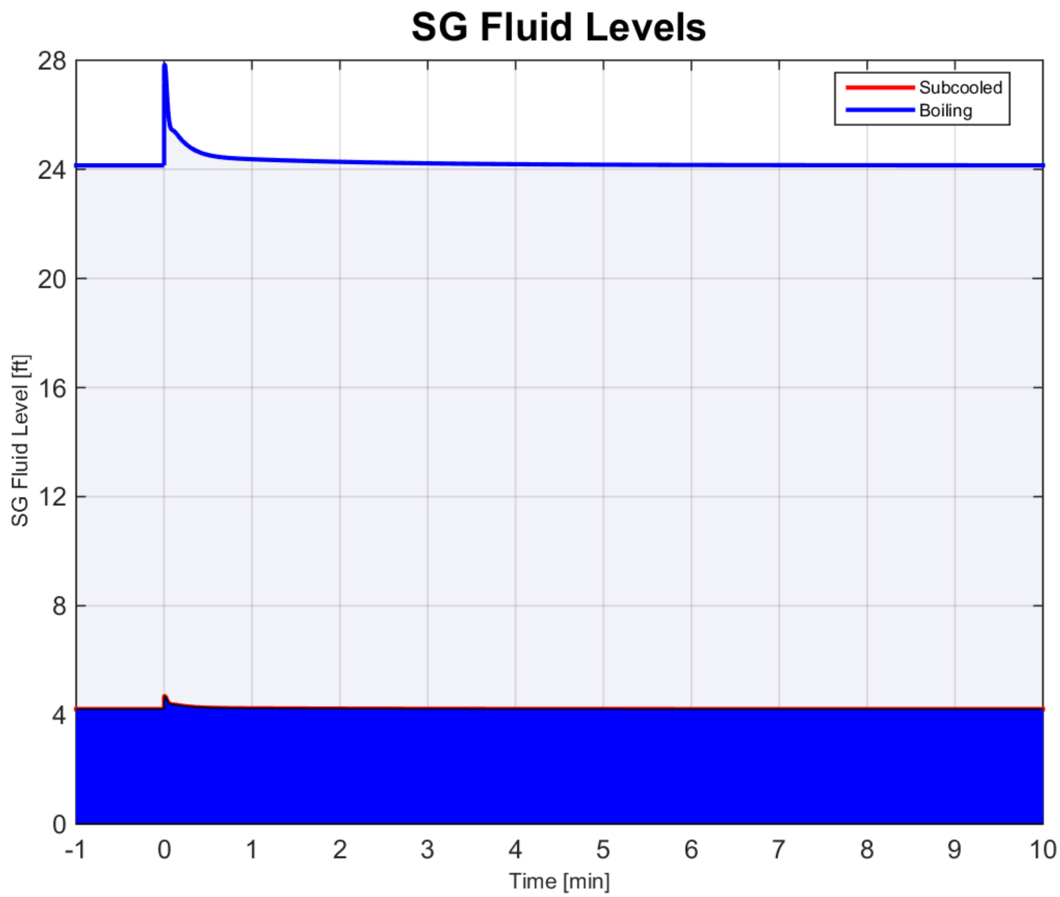

Figure 7.12: Positive reactivity insertion: SG fluid levels

Fluid levels within the steam generator (Figure 7.12) are based on data from the Oconee Nuclear Station (Figure 5.1). Since these data are based on reactor power, for immediate excursions of thermal power this means the fluid level changes are also immediate. In reality, the fluid level dynamics in response to thermal power are far more delayed. As a result, the model is better suited to accommodate gradual power excursions as shown in the second simulation (Section 7.2). Further development of a set of ordinary differential equations representing the fluid levels as a function of many state equations will be required to reproduce realistic dynamics of the steam generator fluid level response to an immediate power excursion.

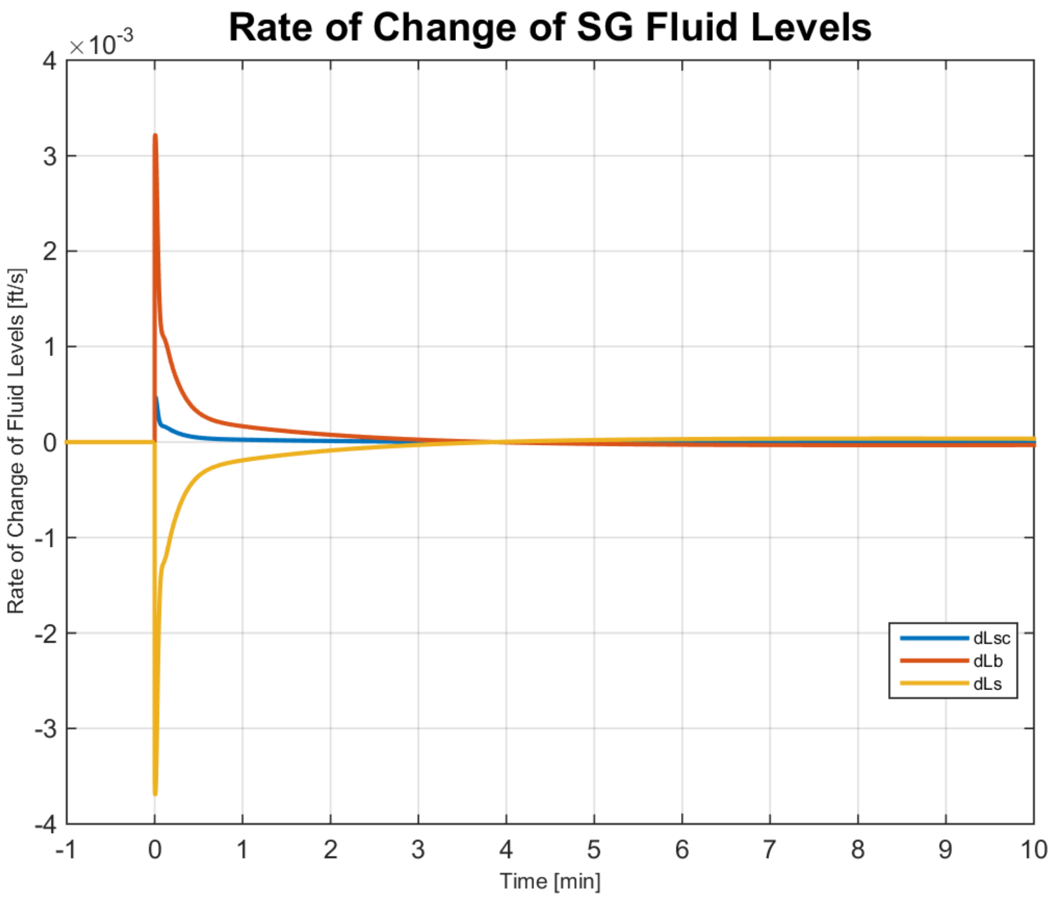

Figure 7.13: Positive reactivity insertion: rate of change of SG fluid levels

As mentioned in in the discussion of the SG fluid levels (Figure 7.12), the rate of change in fluid levels is also immediate. The rate of change of fluid levels within the steam generator are plotted in Figure 7.13.

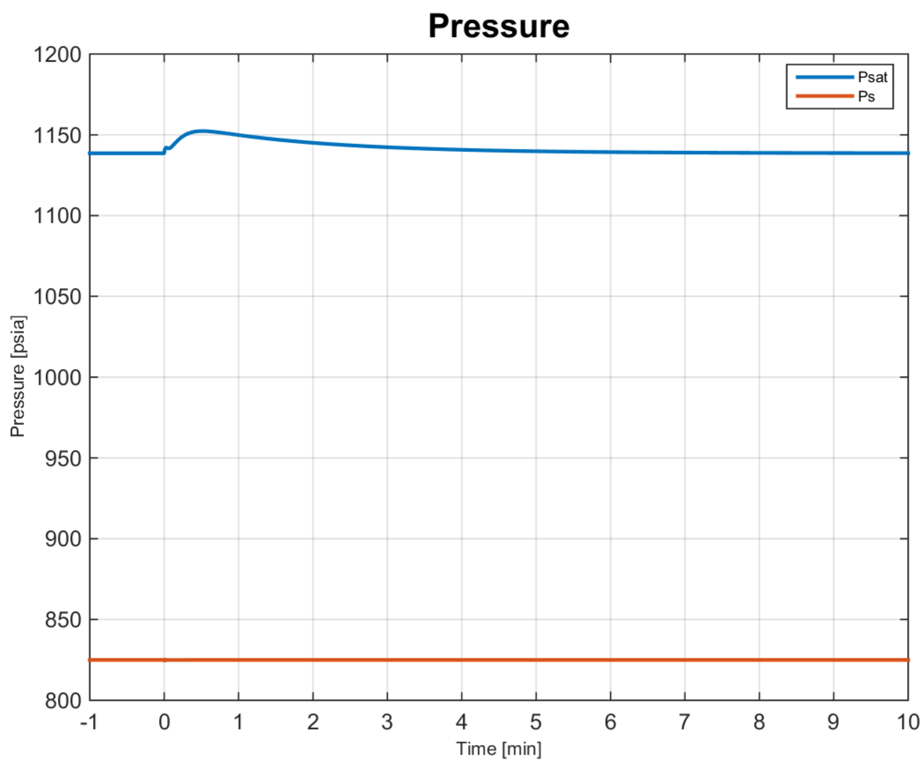

Figure 7.14: Positive reactivity insertion: SG pressure

Saturation pressure and steam pressure are plotted in Figure 7.14. Steam pressure is being controlled (maintained constant) by throttling the main steam control valve (Section 5.2, Equation 5.42). As main steam pressure increases, the steam control valve is opened (increasing steam flow) to relieve pressure back to the user setpoint. Similarly as pressure decreases, the control valve is closed (restricting steam flow) to bottle pressure back up to the user setpoint. The saturation pressure increases with the reactivity insertion and gradually returns to its nominal value over time due to the effects of the T-average controller.

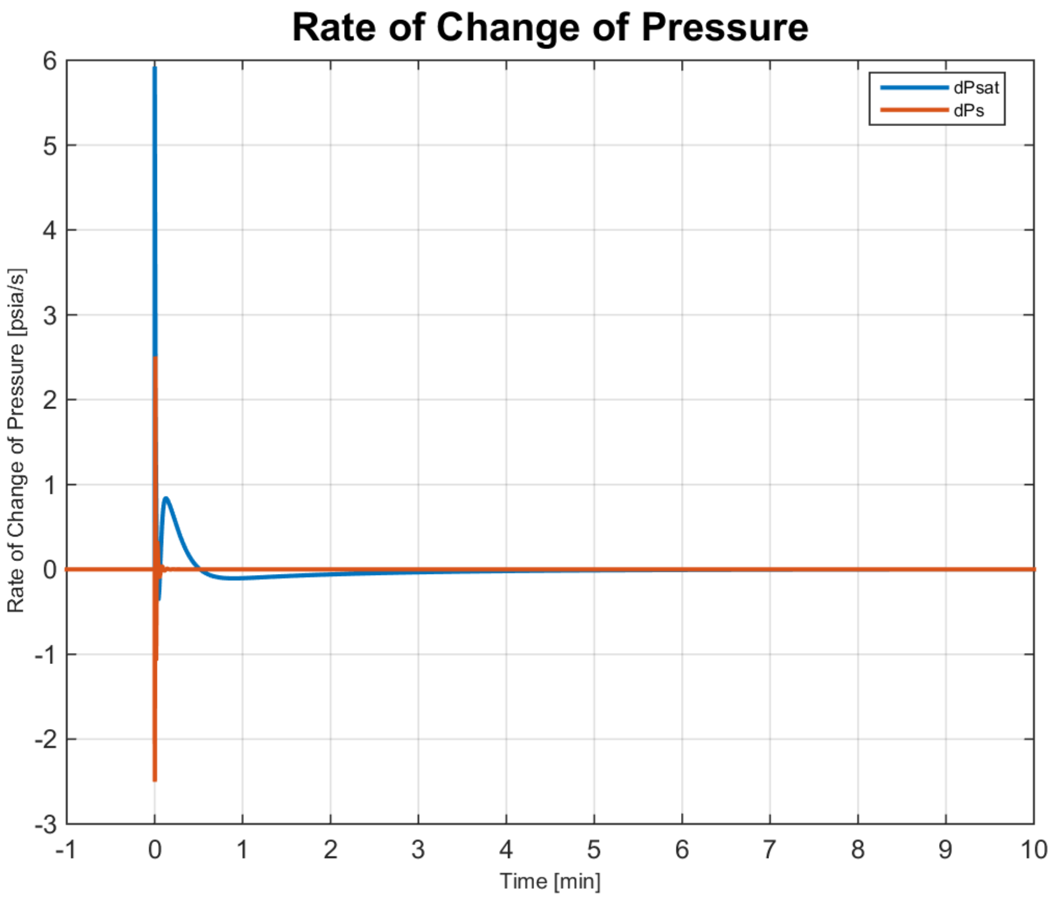

Figure 7.15: Positive reactivity insertion: rate of change of SG pressure

The rate of change of saturation pressure and steam pressure are plotted in Figure 7.15. It can be observed that both signals immediately spike in response to the reactivity insertion, however the effects of the steam pressure controller dampen the steam pressure level very quickly. The saturation pressure has more gradual return to its nominal value.

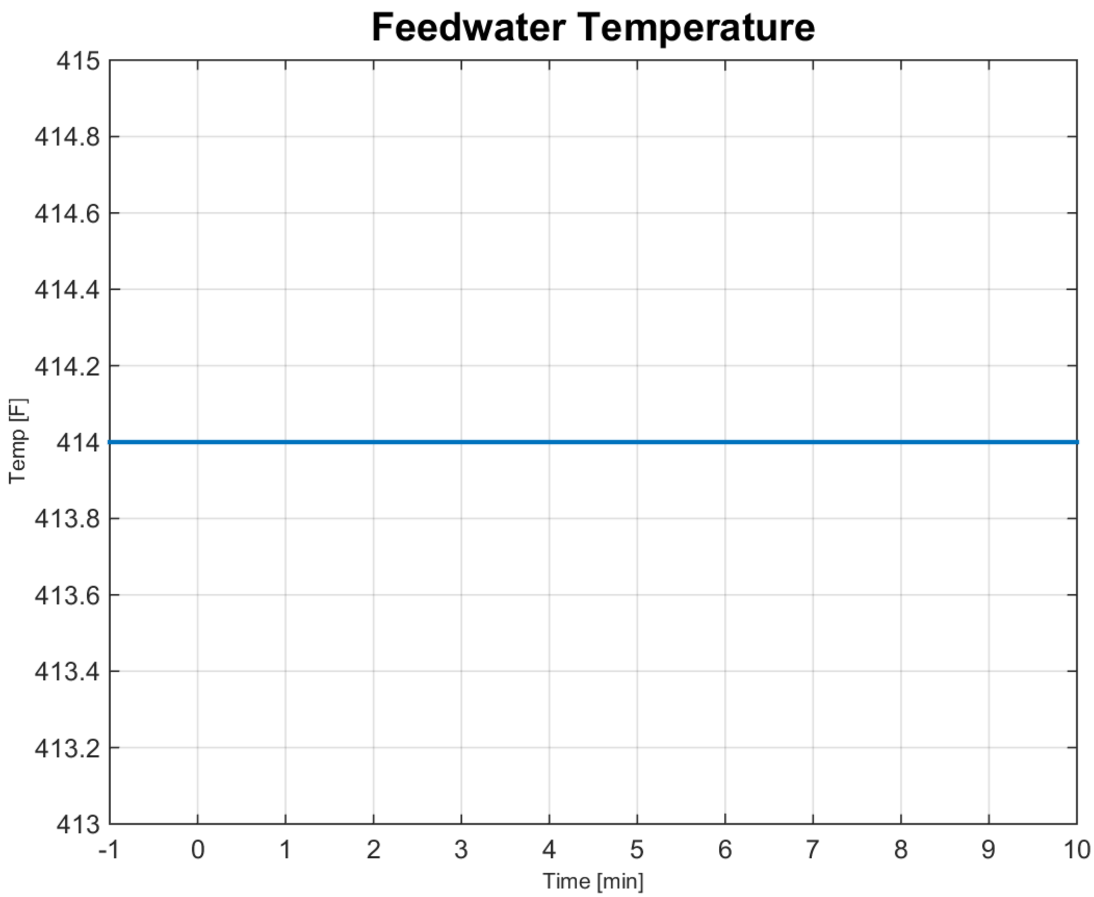

Figure 7.16: Positive reactivity insertion: feedwater temperature

Feedwater temperature is constant and plotted in Figure 7.16.

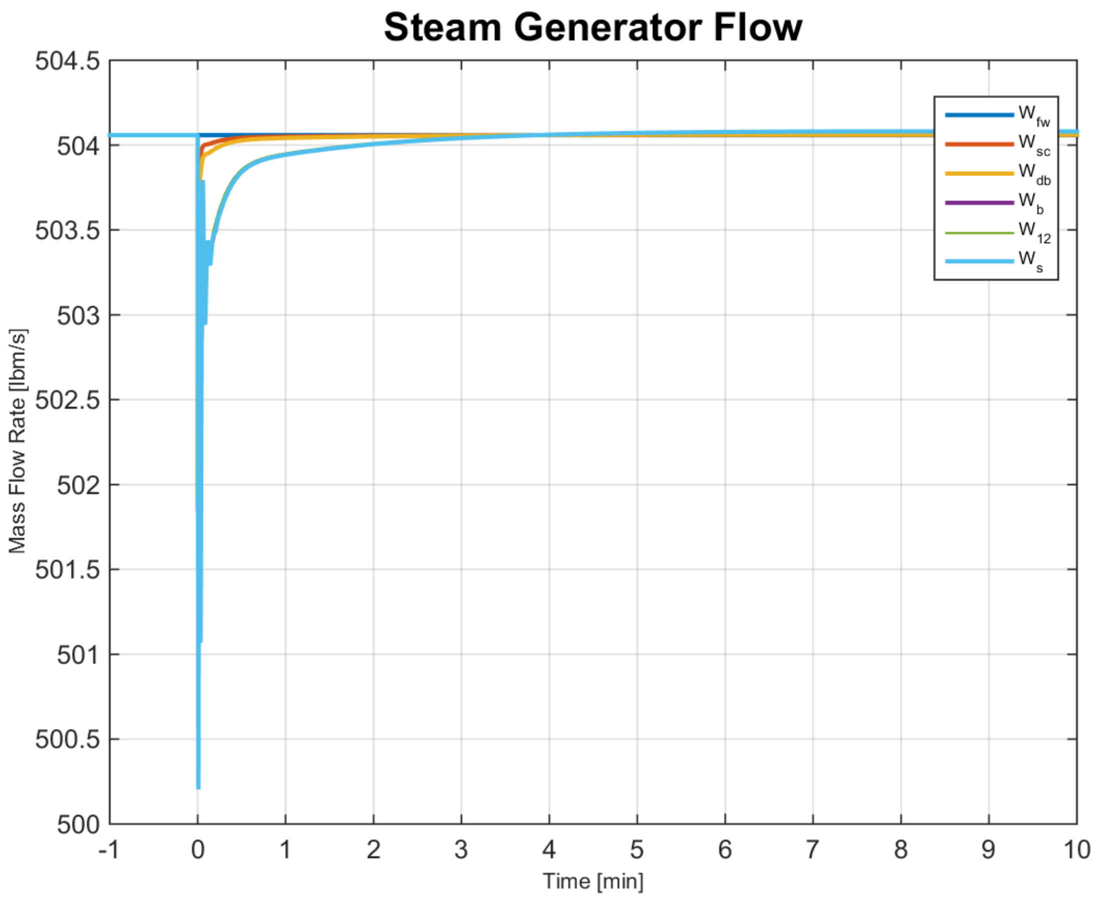

Figure 7.17: Positive reactivity insertion: SG mass flow

Mass flow rates between nodes of the steam generator are provided in Figure 7.17. A large oscillation may be observed in the steam flow W_s as a result of the dynamics of the steam controller.

7.2 Power Ramp

The following transient simulates the system response to a severe power excursion; beginning at 100% power, reduced to 20% power, and returned to 100% power. The transient is conducted by operator manipulation of the feedwater control valve. As feedwater flow is reduced, the resident time of secondary fluid in the subcooled region of the steam generator increases. As a result, the subcooled region does not remove as much heat from the primary fluid which recirculates back to the core. This causes an increase in the core inlet temperature and an overall increase the average primary coolant temperature.

As the average primary coolant temperature increases, the feedback from the T-average controller introduces negative external reactivity. This causes the reactor thermal power to decrease and also reduces the overall ΔT from the core inlet and outlet temperatures.

The reduction of power also coincides with reduced subcooled and saturated fluid levels in the steam generator. At low power levels the majority of heat transfer surface area is in contact with superheated steam.

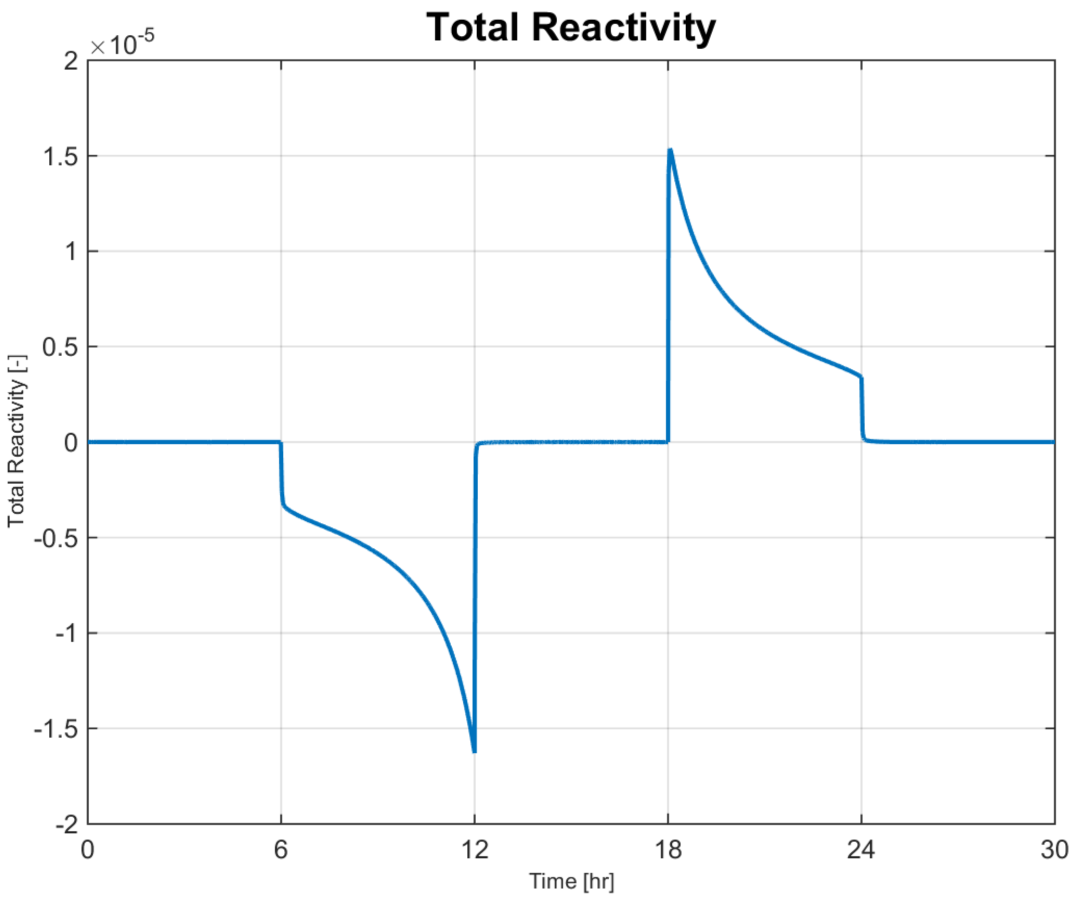

Figure 7.18: Power ramp: total reactivity

The response of reactivity to the power excursion is plotted in Figure 7.18. Starting at hour 6, the power begins to decrease which is accompanied by a gradually decreasing reactivity. At hour 12 the power level remains constant and reactivity stabilizes at zero. The same behavior may be observed from hour 18 to 24 in the reverse orientation.

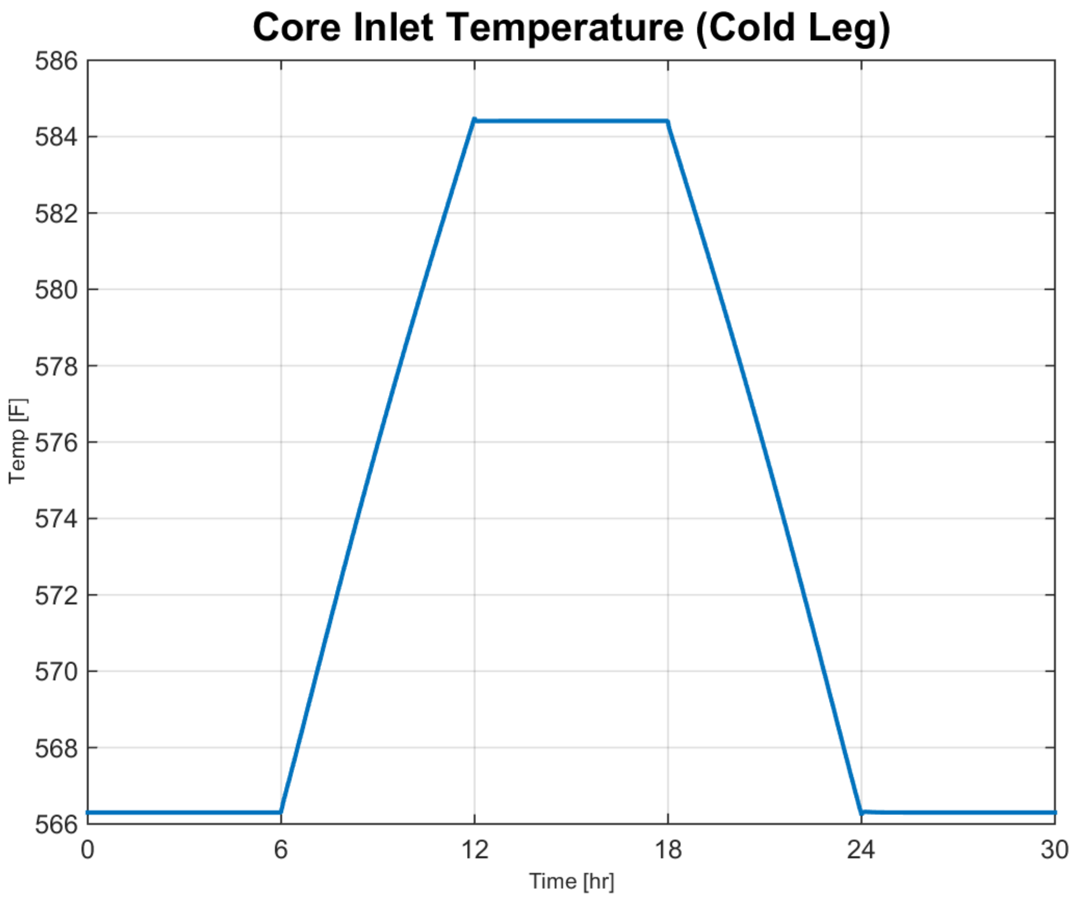

Figure 7.19: Power ramp: core inlet temperature

The core inlet temperature is plotted in Figure 7.19. As feedwater flow is reduced, the residence time of secondary fluid in the subcooled node increases. This reduces its ability to cool the primary fluid which will recirculate across the core. As a result the core inlet temperature increases with a decrease in feedwater flow.

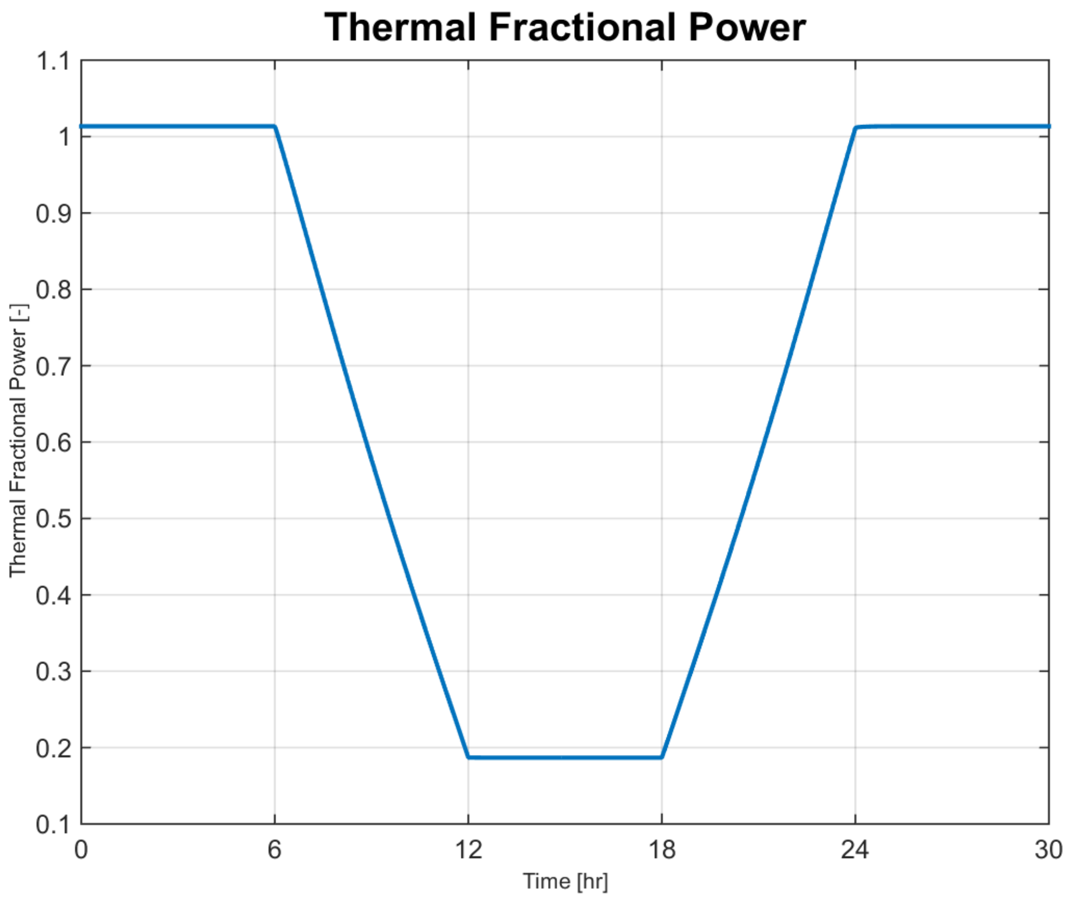

Figure 7.20: Power ramp: thermal fractional power

Thermal fractional power is plotted in Figure 7.20. A reduction in feedflow increases the core inlet temperature which further leads to a mismatch of the average coolant temperature and the T-average setpoint. The T-average controller introduces negative external reactivity and the inlet and outlet core temperatures converge to a much lower ΔT. This reduces the thermal fractional power.

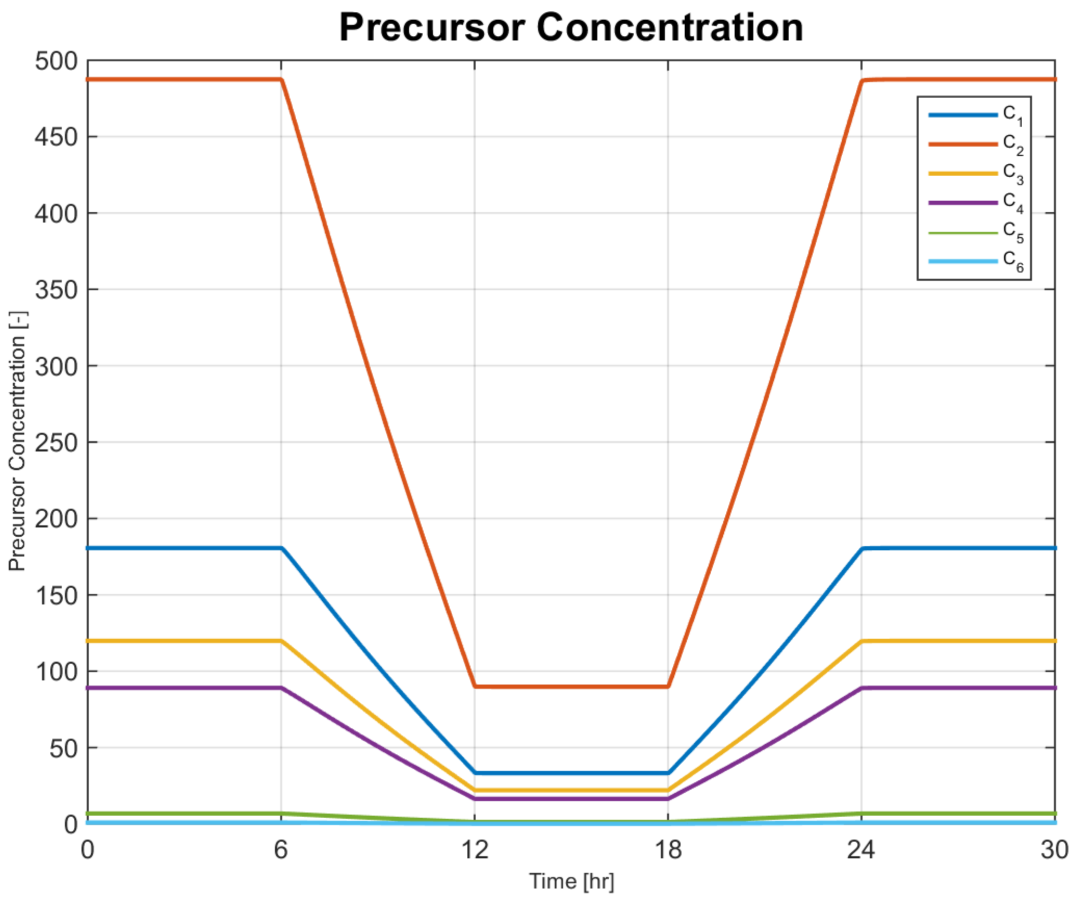

Figure 7.21: Power ramp: precursor concentration

Precursor concentrations are plotted in Figure 7.21. The concentrations are reduced significantly with power.

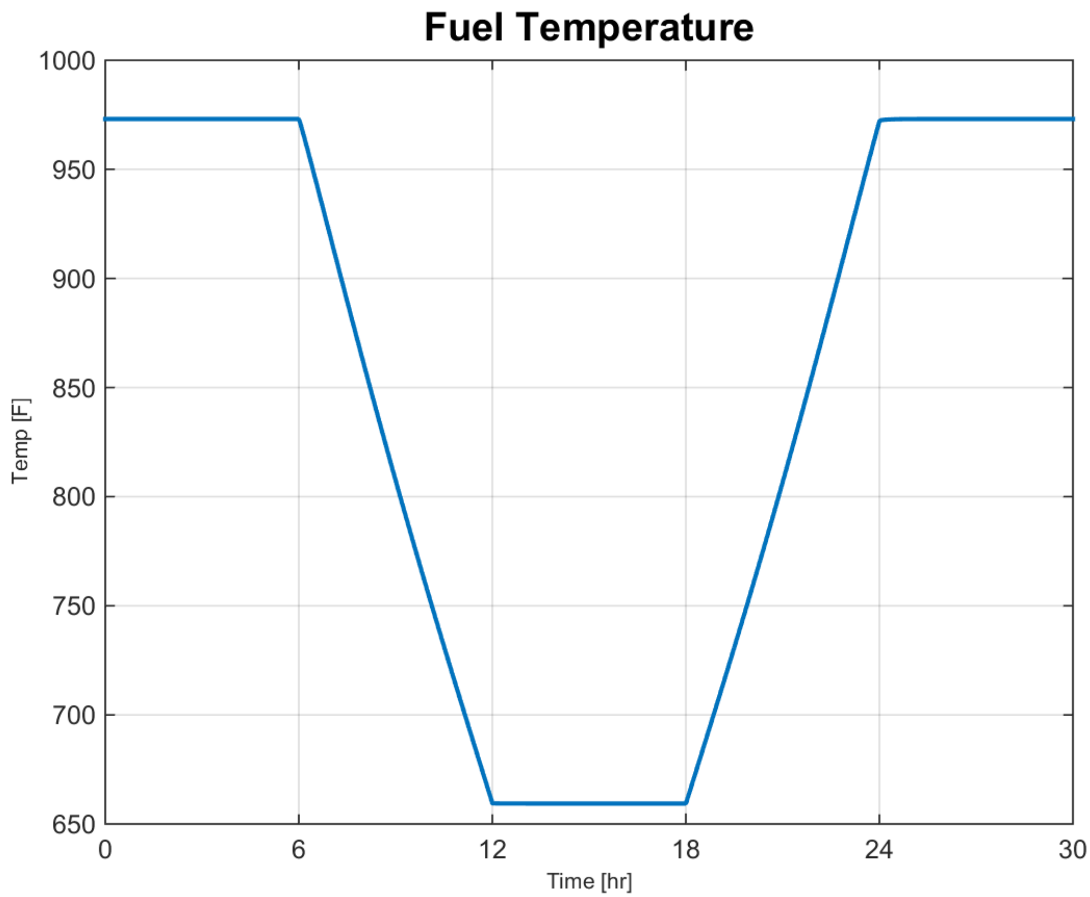

Figure 7.22: Power ramp: fuel temperature

Fuel temperature is plotted in Figure 7.22. Fuel temperature is reduced significantly with thermal power.

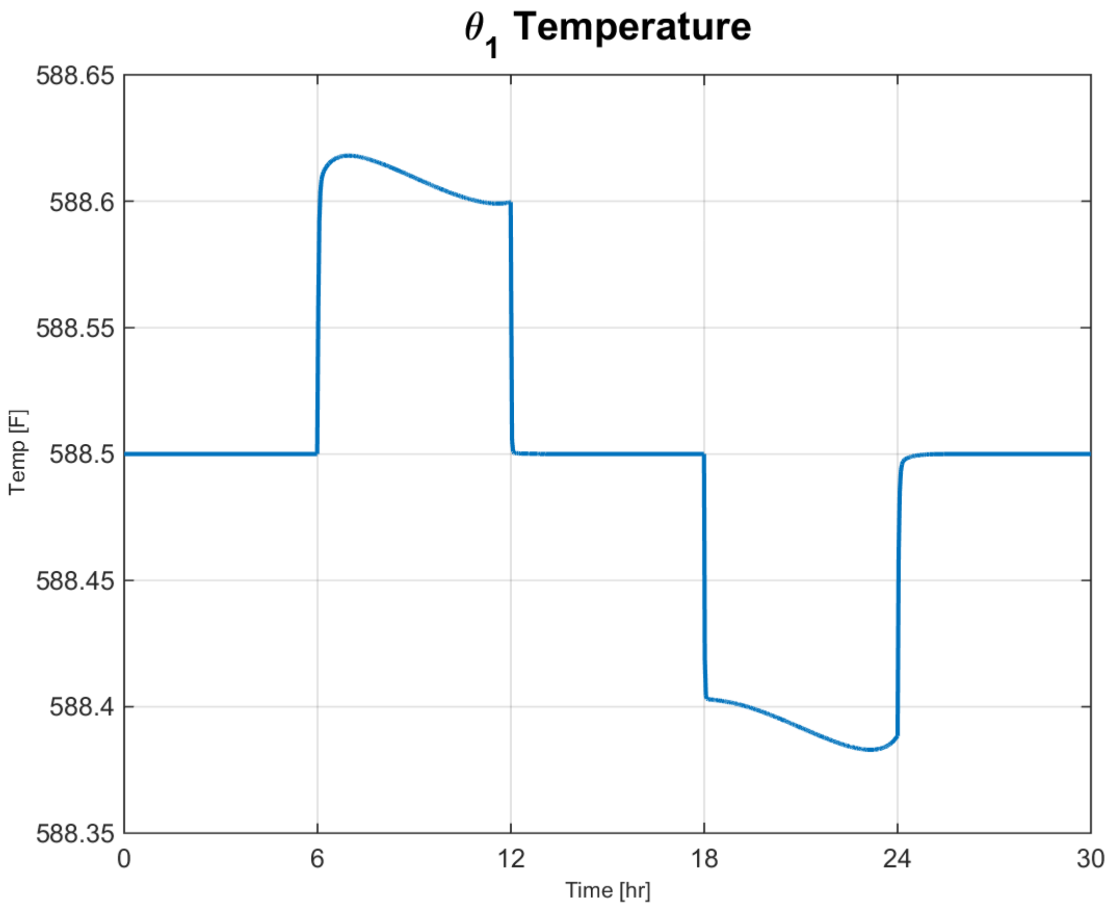

Figure 7.23: Power ramp: theta 1 temperature

Temperature for the θ_1 node remains relatively constant (Figure 7.23) as it is very close to the T-average setpoint. Despite the profile on the plot, the temperature deviates only one tenth of a degree from the nominal value.

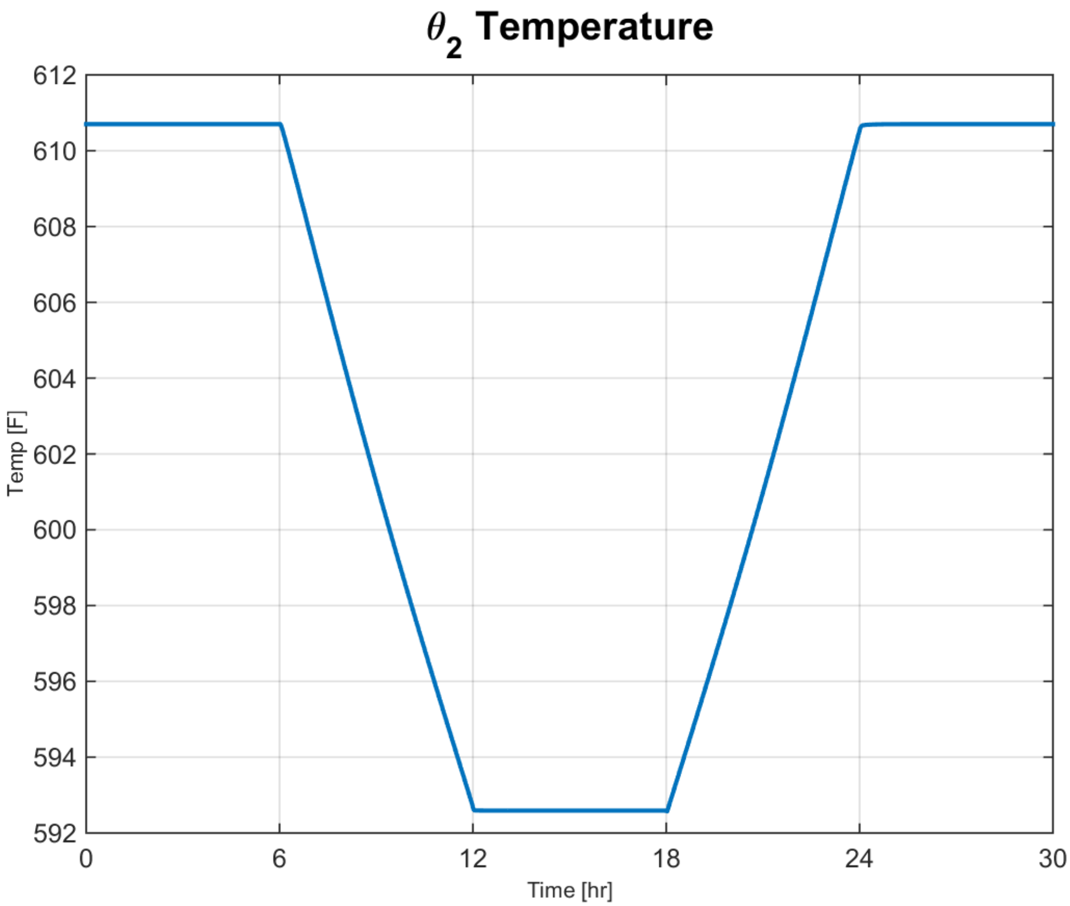

Figure 7.24: Power ramp: theta 2 temperature

Temperature for the θ_2 node (Figure 7.24) is reduced with power. As the core inlet temperature increases, the negative external reactivity introduced by the T-average controller drives the convergence of the primary fluid temperatures closer to the T-average setpoint. As a result the θ_2 node temperature is reduced.

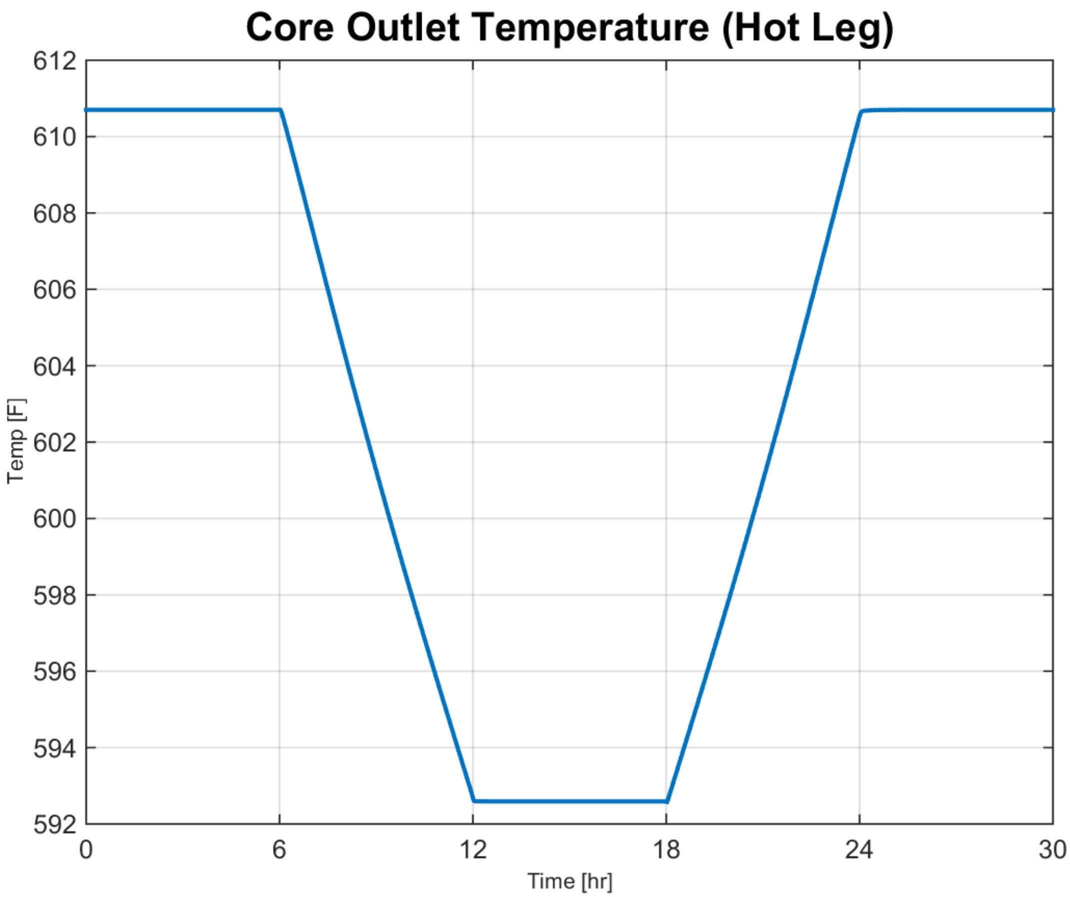

Figure 7.25: Power ramp: core outlet temperature

The core outlet temperature is plotted in Figure 7.25 is reduced with power. As the core inlet temperature increases, the negative external reactivity introduced by the T-average controller drives the convergence of the primary fluid temperatures closer to the T-average setpoint. As a result the core outlet temperature is reduced.

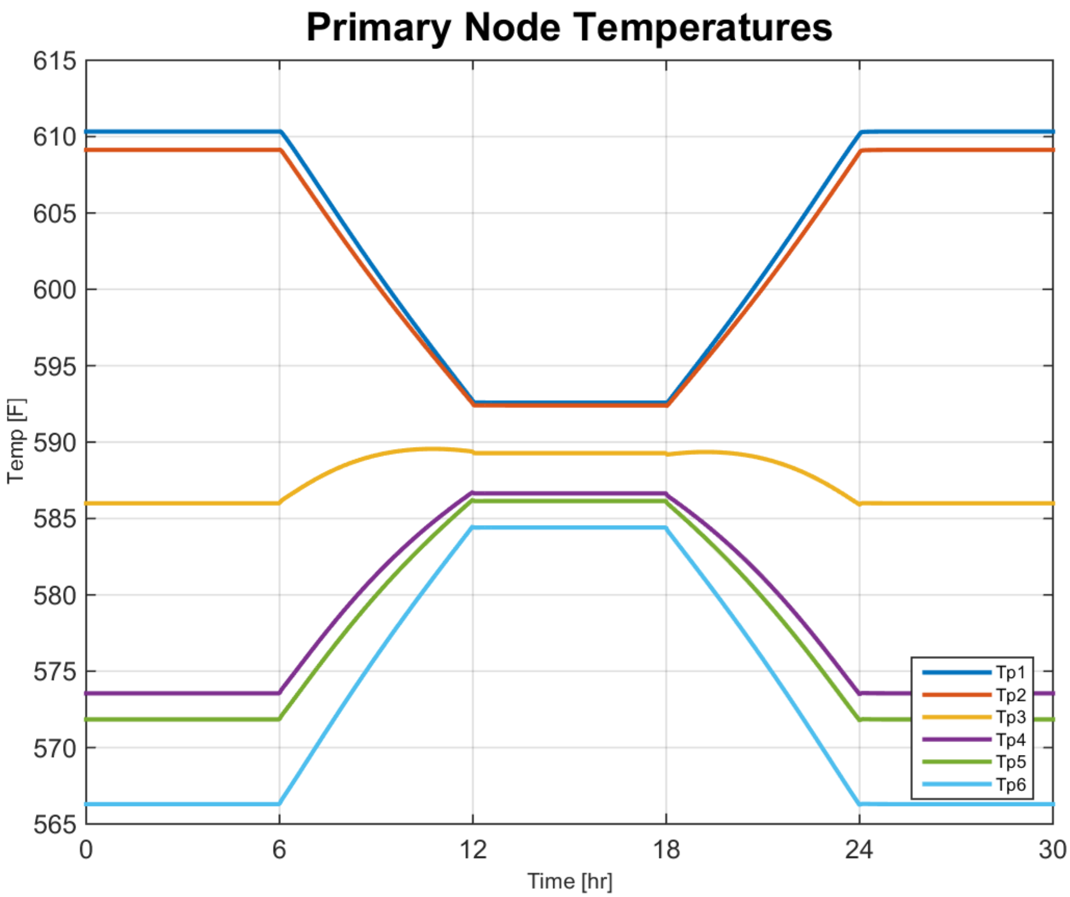

Figure 7.26: Power ramp: primary node temperatures

The primary node temperatures are plotted in Figure 7.26. It can be observed that at low power values the overall ΔT across the primary fluid in the steam generator is reduced. As core power is increased again the overall ΔT increases.

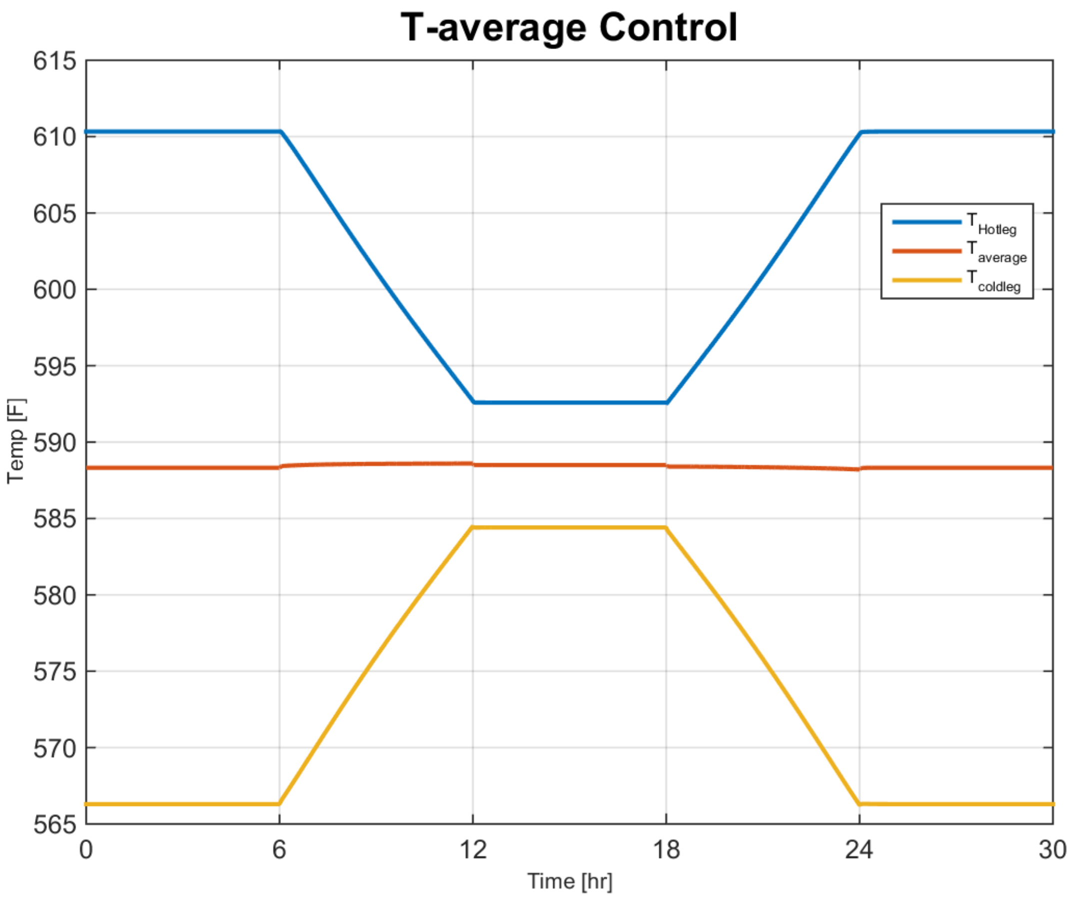

Figure 7.27: Power ramp: T-average controller

The core inlet (coldleg), outlet (hotleg) and average temperatures are plotted in Figure 7.27. It can be observed that at low power values, the average temperature remains constant and the overall ΔT across the primary fluid in the steam generator is reduced. As core power is increased again the overall ΔT increases.

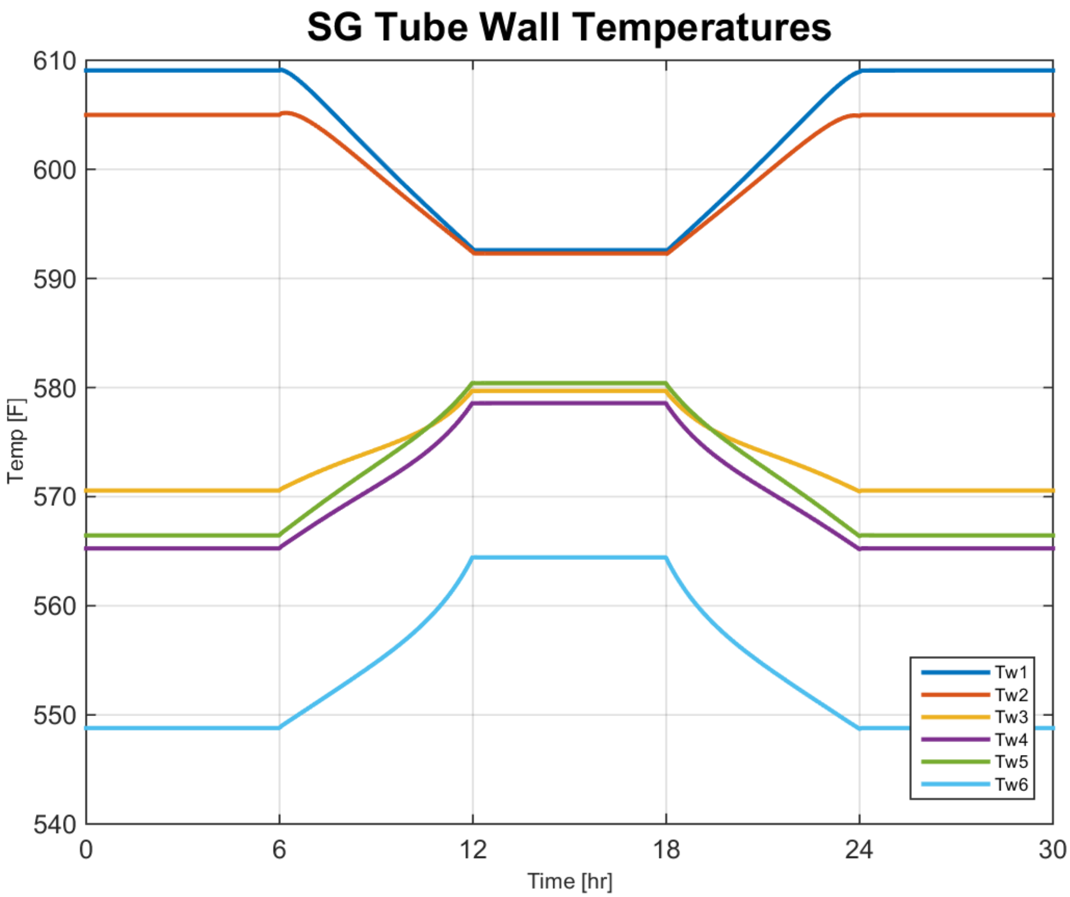

Figure 7.28: Power ramp: SG tube wall temperatures

Steam generator tube wall temperatures are plotted in Figure 7.28. Similar to the primary fluid in the steam generator, the wall temperatures converge toward the T-average setpoint at low power levels and return to their nominal values as power is increased.

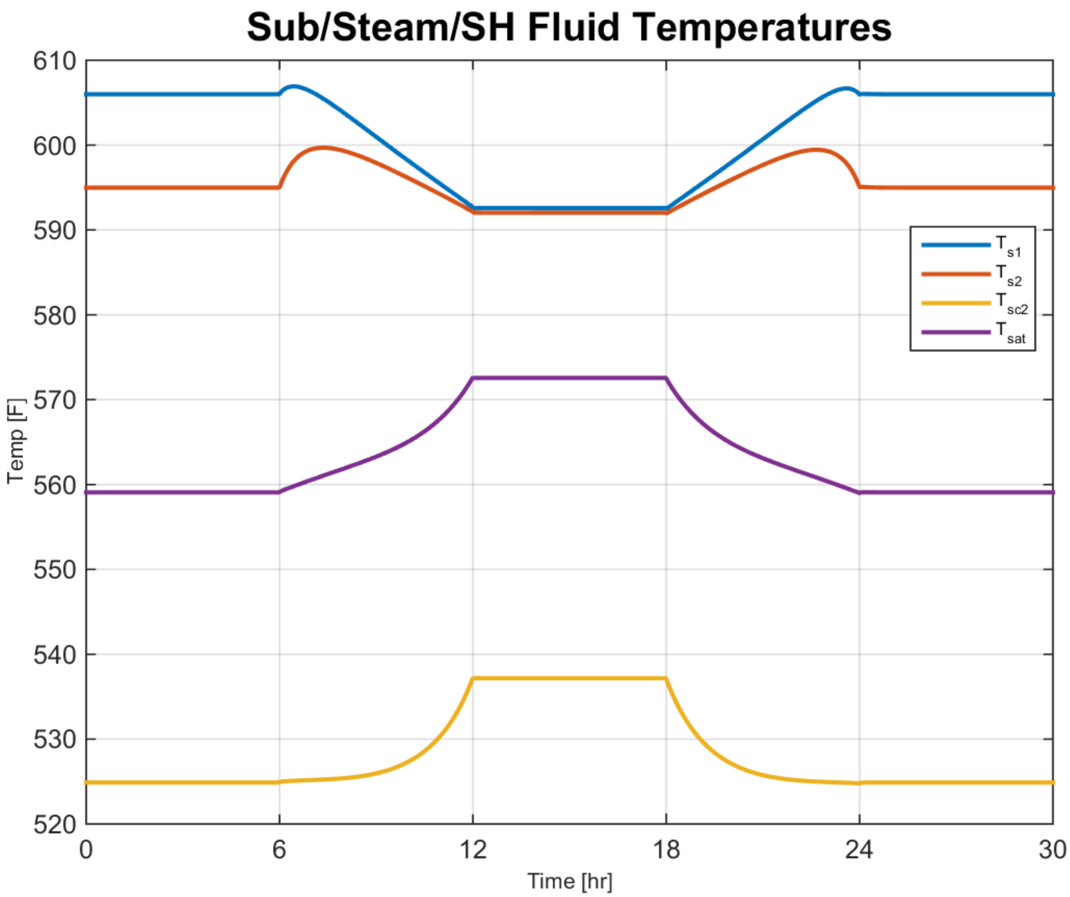

Figure 7.29: Power ramp: SG fluid temperatures

Steam temperatures for nodes within the steam generator are plotted in Figure 7.29. It may be observed that at hour 6 of the transient, the superheated steam nodes increase slightly. This may be due to the dynamics of the pressure controller (Figure 7.32), which temporarily deviate from the 825 psia main steam pressure setpoint.

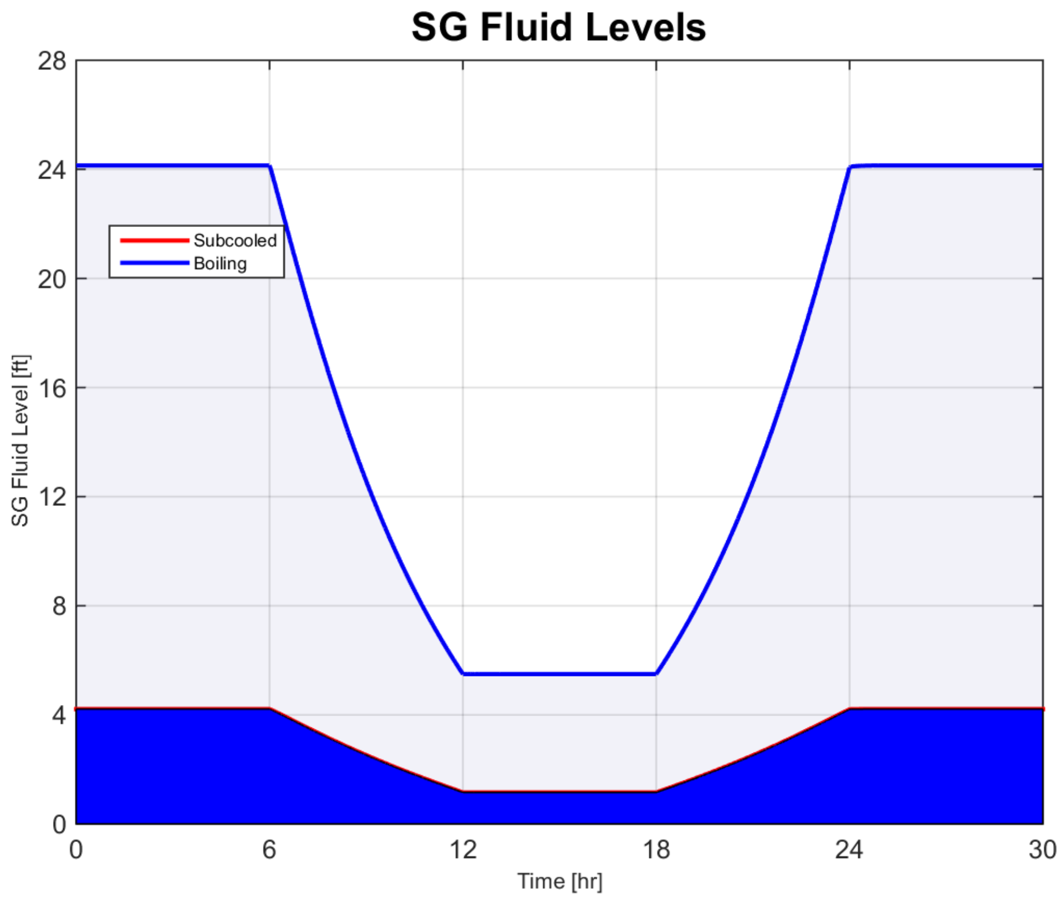

Figure 7.30: Power ramp: SG fluid levels

The steam generator fluid levels (Figure 7.30) are calculated according to reactor power. Therefore as power is reduced, the levels are also reduced. At low power the majority of heat transfer surface area is occupied in the superheated region, as the saturated and subcooled regions are reduced. The heat transfer coefficient of the superheated region is very small compared to that of the saturated region, although at reduced power levels there is less heat removal required.

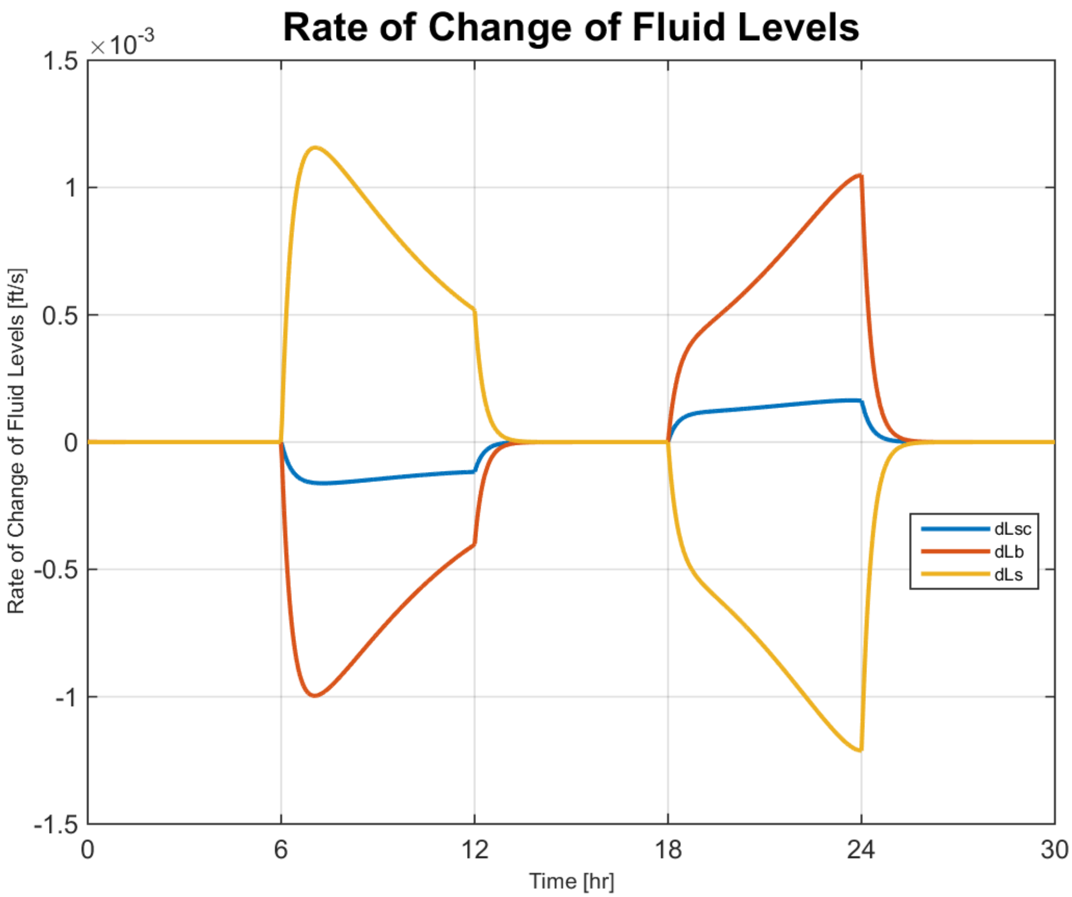

Figure 7.31: Power ramp: rate of change of SG fluid levels

The rate of change of steam generator fluid levels (Figure 7.31) are also calculated according to reactor power.

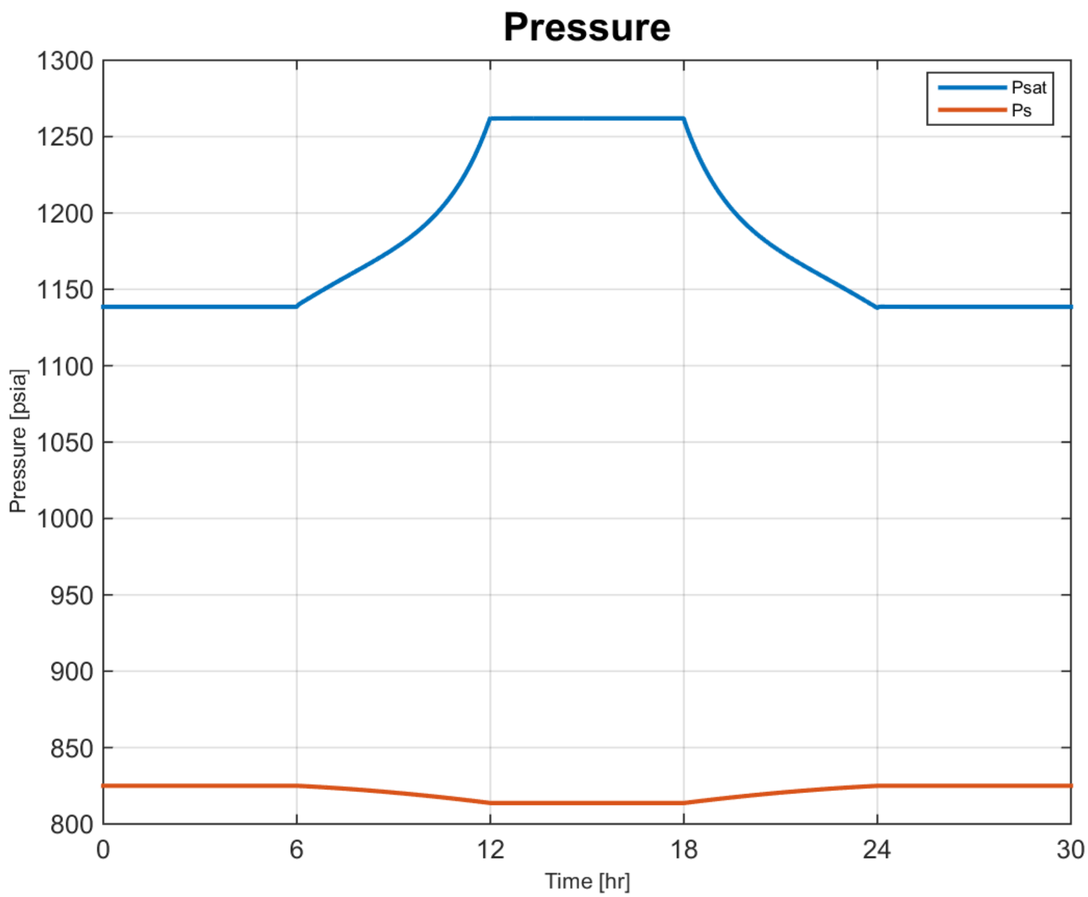

Figure 7.32: Power ramp: SG pressure

Steam pressure and saturation pressure are plotted in Figure 7.32.

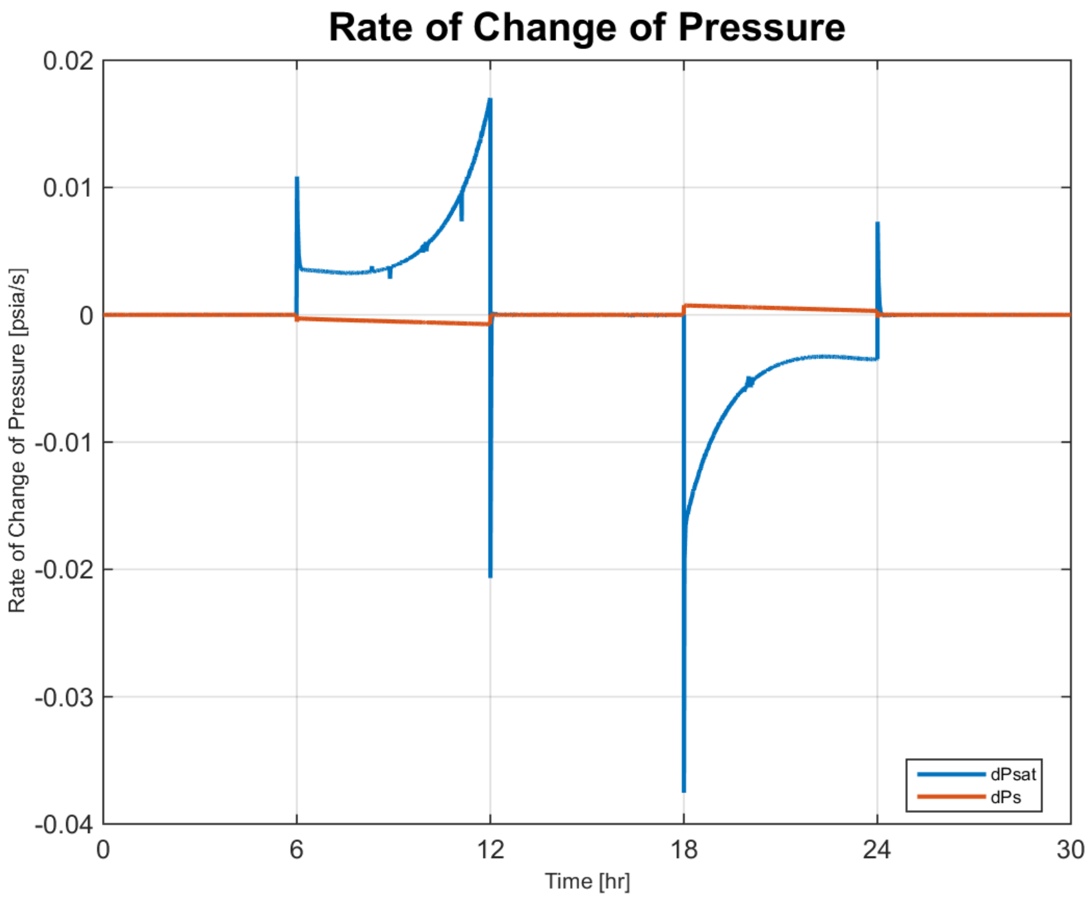

Figure 7.33: Power ramp: Rate of change of SG pressure

Steam and saturated differential pressures are plotted in Figure 7.33. There is some numerical noise embedded within the differential pressure plot, especially between hours 6 and 12. This noise is purely numerical and is largely dependent on which solver type is used, and how small of a timestep is selected. It is not reproducible, subsequent simulations will introduce noise at various times and magnitudes.

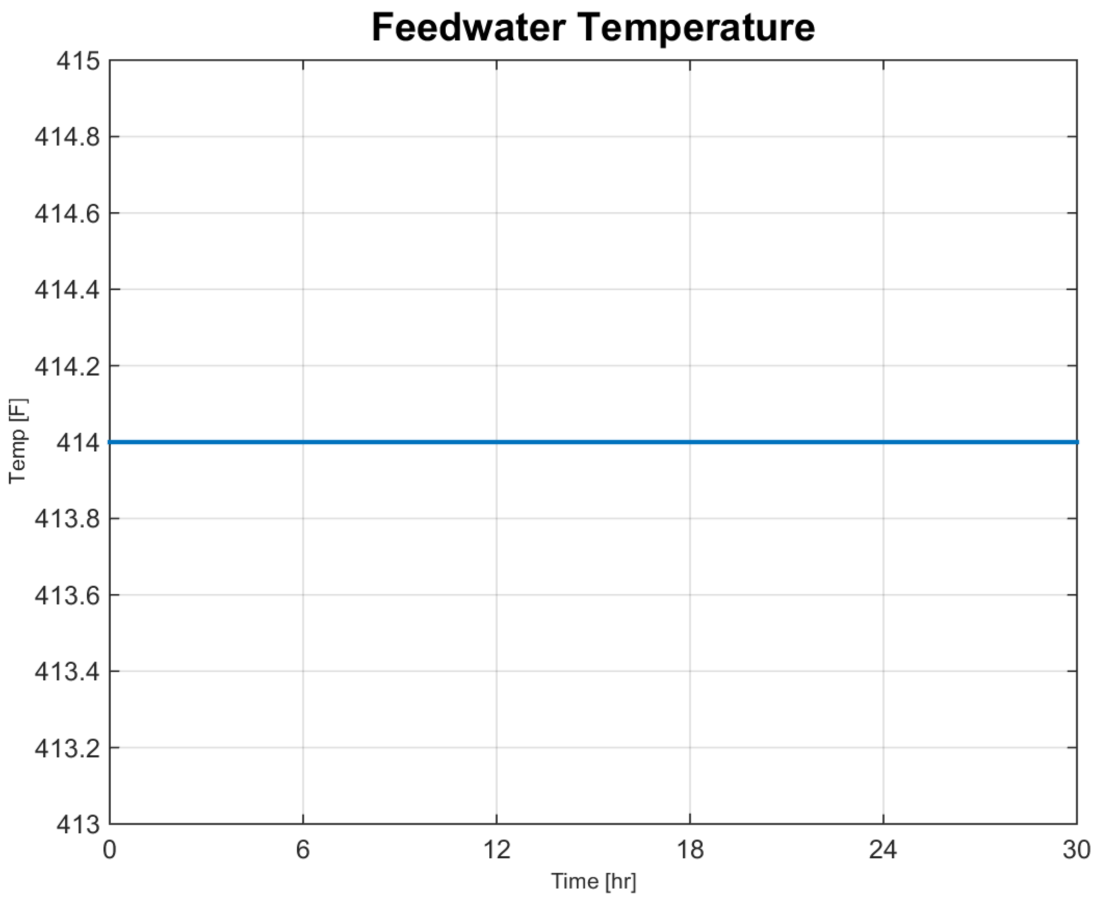

Figure 7.34: Power ramp: feedwater temperature

Feedwater temperature is constant and plotted in Figure 7.34.

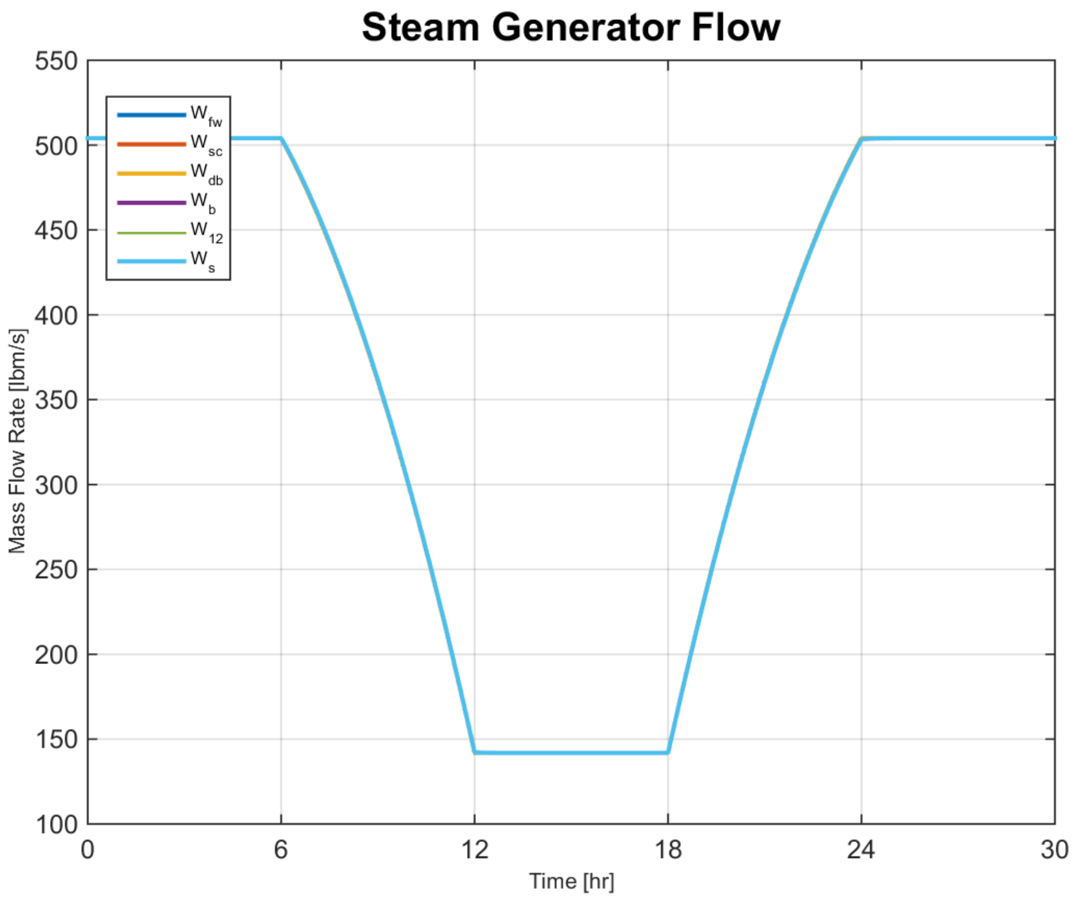

Figure 7.35: Power ramp: SG mass flow

Figure 7.35.

Mass flow rates between nodes of the steam generator are provided in Figure 7.35. The reduction in steam generator flow in what drives the reduction in core power.

Chapter 8

Concluding Remarks & Recommendations for Future Work

The model performance in response to a reactivity insertion and a power excursion have been demonstrated with code output consistent to a physical system. Both controllers achieve their desired action in response to the transients: the T-average controller returns state parameters to their nominal values during a reactivity step insertion, and the standard T-average profile as a function of reactor thermal power is successfully replicated during the power excursion transient. The power excursion also confirms the activity of the pressure controller as it constantly returns the main steam pressure to the user defined setpoint. Although the model satisfies the major research objectives, there remain many areas of improvement which would be of great benefit to the value and scope of the model.

The entire reactor core has been nodalized as a single lump. Although sufficient for the purposes of this simulation, the user may increase the nodalization of the core both radially and axially for increased performance. This suggestion is not critical, but would increase model performance by a small degree. Another area of improvement would be to systematically remove simplifying assumptions. For example there is an assumed constant density in the primary coolant. With the small differences in temperature of the primary nodes, fluid density would change slightly between nodes. Again, this suggestion is not crucial for model performance, however these type of implementations at each step move the code output closer to the true physics.

This research has focused only on two transient simulations, an insertion of reactivity and a power excursion. To further test the capabilities of the model several more simulations must be performed. The developer must validate the code output either by benchmarking it to a code which has already been validated, or by comparing code output to hand calculations. An effort to challenge the limits of the model, and identify its shortcomings, would help to improve it.

The discussion on the T-average controller mentions an additional strategy for reactor control by maintaining a constant hotleg temperature. The literature identifies this control type beneficial as it improves reactor control with the exclusion of chemical shim. Consequently, it negatively affects the performance of the pressurizer due to a large fluctuation of coolant density, causing the pressurizer level to shrink and swell with varying feedwater flows. This places a large demand on the response of the pressurizer and its ability to adequately letdown and charge primary fluid to compensate for the density changes, and maintain constant level. The implementation of a pressurizer model and its control system would improve the overall dynamics of the system model.

Additional development of the BOP is necessary before coupling the output back to the steam generator. There are several inputs to Shankar's model, many of which are not well defined. Each parameter should have a justification for its numerical value before incorporating the BOP within the model; there still remains much work in this area.

Steam generator fluid levels were first coded according to the ODEs of the OTSG model. These did not reproduce any usable results (i.e., levels did not change for any input condition). To ensure that the fluid levels would respond to reactor thermal power, known data from the Oconee nuclear station were used to drive this relationship. Generation mPower is much different than the Oconnee nuclear station and although this may be of some use for a first implementation of the fluid level dynamics, the model requires an ODE for the rate of change of the fluid levels. The development of an ODE that balances feedwater flow, heat transfer, and phase change to the fluid level is mandatory for a true representation of the dynamics of the steam generator.

Additional complexities exist with the manner in which Matlab-Simulink handles initial conditions. Generally when a code is first executed, the system of equations must converge to a solution that is acceptable to all of the signals. For a steady state calculation, the CPU is initially stressed to achieve this state and may require an extremely small timestep for stable advancement. As the calculation begins to converge on a solution the timestep generally opens up and proceeds at a much faster rate. When a second calculation is desired (e.g., transient simulation), the code user will load the final state variables of the converged solution as the new initial conditions. This process is not achievable in the Matlab-Simulink computing environment (R2014b). It puts the code user at a severe disadvantage. The integration blocks within Simulink are provided the option for an initial condition variable, however formulas which are not being integrated, are not provided this option. MathWorks did recently introduce the initial conditions block, although when an initial condition block is provided to each signal, the problem becomes overconstrained and produces a generic error message regardless of how small the timestep is.

Bibliography

[1] M.J. Scarangella. An extended conventional fuel cycle for the b&w mpower small modular nuclear reactor. *2012 Advances in Reactor Physics - Linking Research, Industry and Education (PHYSOR 2012)*, April 2012. 9

[2] M.A. Erighin. A 48-month extended fuel cycle for the b$w mpower small modular nuclear reactor. *2012 Advances in Reactor Physics - Linking Research, Industry and Education (PHYSOR 2012)*, April 2012. 9

[3] Westinghouse Electric Corporation. *The Westinghouse Pressurized Water Reactor Nuclear Power Plant*. Westinghouse Electric Corporation, Pittsburgh, PA, 1984. 10

[4] D.D. Duderstadt and S.S. Hamilton. *Nuclear Reactor Analysis*. John Wiley & Sons Inc., 1976. 12, 33, 40

[5] The babcock & wilcox company, generation mpower snapshot. *www.generationmpower.com*, April 2012. 13

[6] J.A. Halfinger and M.D. Haggerty. The b&w mpower scalable, practical nuclear reactor design. *Nuclear Technology*, 178:164–169, May 2012. 14, 16, 19

[7] S.C. Stultz and J.B. Kitto. *Steam: Its Generation and Use, 41 Edition*. The Babcock & Wilcox Company, 2005. 15, 20, 21, 22, 48

[8] R.H. Perry and D.W. Green. *Perry's Chemical Engineer's Handbook, Seventh Edition*. McGraw-Hill, New York, 1997. 15, 17

[9] W.M. Stacey. *Nuclear Reactor Physics*. John Wiley, June, 2007. 34

[10] J.R. Lamarsh. *Introduction to Nuclear Reactor Theory*. Addison-Wesley, Ney York, 1966. 34

[11] S.J. Ball. Approximate models for distributed-parameter heat-transfer systems. *Transactions, Instrument Society of America*, 3(1):38–47, 1964. 36

[12] T.W. Kerlin. *Dynamic Analysis and Control of Pressurized Water Reactors*. Academic Press, Volume 14, Ney York, 1978. 36

[13] B.R. Upadhyaya and S.P. Perillo. Multi-modular integral pressurized water reactor control and operational reconfiguration for a flow control loop. *Vol. 5, Final Report prepared for the U.S. Department of Energy*, Report No. DE-FG07-ID14895/UTNE/2011-7, 2011 May. 36, 37

[14] K.C. Lish. *Nuclear Power Plant Systems and Equipment*. Industrial Press Inc., New York, 1972. 37, 39, 49, 50

[15] J.D. Malloy. Control system and method for pwr systems. *United States Patent Application Publication*, US 2012/0155594 A1, June 21, 2012. 37, 38

[16] A.T. Chen. A digital simulation for nuclear once through steam generators. *Department of Nuclear Engineering, The University of Tennessee*, 1976. 49

[17] M.J. Moran and H.N. Shapiro. *Fundamentals of Engineering Thermodynamics*. Wiley, Ney York, 2005. 58

[18] P.V. Shankar. Simulation model of a nuclear reactor turbine. *Nuclear Engineering and Design*, 44:269–277, 1977. 63, 64

[19] A. Dutta and I. Thangamani. Simulation model of nuclear power plant-turbine. *Bhabha Atomic Research Centre*, 2006. 63, 64

[20] B.R. Upadhyaya and M. Naghedolfeizi. Dynamic modeling of a pressurized water reactor plant for diagnostics and control. *Department of Nuclear Engineering, The University of Tennessee*, DE-FG07-88ER12824, 1991. 63, 64

Appendix

Appendix A

Reactor Core

A.1 Reactor Design Parameters

Table A.1: Reactor Design Parameters

Parameter	Value	Unit	Value	Unit
thermal power	530.0	[MWt]	502343.1	[$\frac{\text{BTU}}{\text{s}}$]
electric power	180.0	[MWe]	170607.1	[$\frac{\text{BTU}}{\text{s}}$]
core inlet temperature	297.2	[°C]	567.0	[°F]
core outlet temperature	320.0	[°C]	608.0	[°F]
T_{avg} (average coolant temp)	308.61	[°C]	587.5	[°F]
core flow	3779.9	[$\frac{\text{kg}}{\text{s}}$]	8333.3	[$\frac{\text{lbm}}{\text{s}}$]
primary coolant pressure	142.03	[bar]	2060.0	[psia]
primary coolant pressure	14.20	[MPa]	296640.0	[psfa]
primary coolant viscosity	84.611	[μPa-s]	5.686e-05	[$\frac{\text{lbm}}{\text{ft-s}}$]
primary coolant thermal conductivity	0.5426	[$\frac{\text{W}}{\text{m-K}}$]	8.709e-05	[$\frac{\text{BTU}}{\text{s-ft-F}}$]
primary coolant heat capacity	5.7601	[$\frac{\text{kJ}}{\text{kg-C}}$]	1.376	[$\frac{\text{BTU}}{\text{lbm-F}}$]
primary coolant density	704.98	[$\frac{\text{kg}}{\text{m}^3}$]	44.01	[$\frac{\text{lbm}}{\text{ft}^3}$]

Continued on next page

Table A.1 – *Continued from previous page*

Parameter	**Value**	**Unit**	**Value**	**Unit**
vessel diameter	3.9624	[m]	13	[ft]
vessel height	25.3	[m]	83	[ft]
vessel free volume	312.0	[m^3]	11016.8	[ft^3]
fuel centerline temperature	2319	[°C]	4206.2	[°F]
fuel radial temperature	725	[°C]	1337	[°F]
fuel average temperature	1522	[°C]	2771.6	[°F]
clad OD	0.0095	[m]	0.0312	[ft]
fuel pellet diameter	0.0082	[m]	0.0269	[ft]
fuel pins per assembly	264	[No.]	264	[No.]
rod pitch	0.0126	[m]	0.0413	[ft]
assemblies per core	69	[No.]	69	[No.]
total rods in core	19941	[No.]	19941	[No.]
total fuel rods	18216	[No.]	18216	[No.]
active core height	2.413	[m]	7.9	[ft]
fuel heat transfer area	1311.8	[m^2]	14120.6	[ft^2]
fuel matrix	UO_2	[–]	UO_2	[–]
fuel enrichment	< 4.95	[%]	< 4.95	[%]
fuel density	10.543	[$\frac{g}{cm^3}$]	658.20	[$\frac{lbm}{ft^3}$]
fuel volume	2.3168	[m^3]	81.82	[ft^3]
fuel mass	24426.2	[kg]	53850.5	[lbm]
assembly pitch	0.2150	[m]	0.705	[ft]
estimated barrel diameter	2.0425	[m]	6.701	[ft]
total volume of coolant in core	4.07	[m^3]	143.8	[ft^3]
total mass of coolant in core	3129.0	[kg]	6898.3	[lbm]

A.2 Neutronics Model Parameters

Table A.2: Neutronics Model Parameters

Parameter	Description	Value	Unit
α_c	moderator temp coeff	-0.0002	$[\frac{1}{°F}]$
α_f	fuel temp coeff	-1.650e-05	$[\frac{1}{°F}]$
β	Total delayed neutron group fraction	0.0067	$[-]$
β_1	delayed neutron frac group 1	0.000221	$[-]$
β_2	delayed neutron frac group 2	0.001467	$[-]$
β_3	delayed neutron frac group 3	0.001313	$[-]$
β_4	delayed neutron frac group 4	0.002647	$[-]$
β_5	delayed neutron frac group 5	0.000771	$[-]$
β_6	delayed neutron frac group 6	0.000281	$[-]$
Λ	Mean prompt neutron generation time	0.0001	[s]
λ_1	decay const group 1	0.0124	$[\frac{1}{s}]$
λ_2	decay const group 2	0.0305	$[\frac{1}{s}]$
λ_3	decay const group 3	0.111	$[\frac{1}{s}]$
λ_4	decay const group 4	0.301	$[\frac{1}{s}]$
λ_5	decay const group 5	1.14	$[\frac{1}{s}]$
λ_6	decay const group 6	3.01	$[\frac{1}{s}]$
ρ_{fuel}	fuel density	658.2	$[\frac{lbm}{ft^3}]$
ρ_{H_2O}	primary coolant density	44.01	$[\frac{lbm}{ft^3}]$
θ_{1_0}	theta node one coolant temperature	586.3	[°F]
θ_{2_0}	theta node two coolant temperature	608.0	[°F]
A_{fc}	fuel-to-coolant heat transfer area	14120.6	$[ft^2]$
A_{fc_1}	Node 1 fuel-to-coolant heat transfer area	7060.3	$[ft^2]$
A_{fc_2}	Node 2 fuel-to-coolant heat transfer area	7060.3	$[ft^2]$
c_{p_c}	primary coolant heat capacity	1.376	$[\frac{BTU}{lbm\text{-}°F}]$

Continued on next page

Table A.2 – *Continued from previous page*

Parameter	**Description**	**Value**	**Unit**
c_{p_f}	fuel heat capacity	0.059	$[\frac{\text{BTU}}{\text{lbm-}^\circ\text{F}}]$
f	fraction of total power deposited in fuel	0.97	$[-]$
L_{fuel}	active core height	7.9	[ft]
m_c	mass of coolant in core	6898.3	[lbm]
m_{c_1}	coolant mass node 1	3449.1	[lbm]
m_{c_2}	coolant mass node 2	3449.1	[lbm]
m_f	mass of fuel	53850.5	[lbm]
$N_{assembly}$	number of fuel assemblies in core	69	[No.]
N_{fuel}	number of fuel rods	18216	[No.]
N_{total}	total number of rods in core	19941	[No.]
OD_{barrel}	estimated barrel diameter	6.701	[ft]
OD_{clad}	outer diameter of fuel cladding	0.0312	[ft]
OD_{pellet}	fuel pellet diameter	0.0269	[ft]
$P_{assembly}$	assembly pitch	0.705	[ft]
P_{fuel}	fuel rod pitch	0.0413	[ft]
P_0	nominal thermal power	502343	$[\frac{\text{BTU}}{\text{s}}]$
T_{avg}	T_{avg} average coolant temp	588.5	$[^\circ\text{F}]$
T_f	fuel temperature	973.061	$[^\circ\text{F}]$
T_{f0}	nominal fuel temperature	973.061	$[^\circ\text{F}]$
U_{fc}	overall heat transf coefficient	0.0909444	$[\frac{\text{BTU}}{\text{s-ft}^2\text{-}^\circ\text{F}}]$
W_c	Core Flow	8333.3	$[\frac{\text{lbm}}{\text{s}}]$

Appendix B

Steam Generator Design Parameters

Table B.1: Steam Generator Design Parameters

Parameter	Description	Value	Unit
A_{dc}	total downcomer cross-sectional area	30.35	$[\text{ft}^2]$
A_r	total riser area	33.13	$[\text{ft}^2]$
A_s	cross sectional SG shellside area	13.18	$[\text{ft}^2]$
A_{wsc}	surface area from wall to subcooled	2247.22	$[\text{ft}^2]$
A_{sit}	total surface area inner tube	26727.5	$[\text{ft}^2]$
A_{sot}	total surface area outer tube	29990.4	$[\text{ft}^2]$
$c_{p_{fw}}$	feedwater heat capacity	1.122	$[\frac{\text{BTU}}{^\circ\text{F-lbm}}]$
c_{p_p}	primary fluid heat capacity	1.37661	$[\frac{\text{BTU}}{^\circ\text{F-lbm}}]$
$c_{p_{sc}}$	subcooled fluid heat capacity	1.138	$[\frac{\text{BTU}}{^\circ\text{F-lbm}}]$
c_{p_w}	inconel heat capacity	0.109	$[\frac{\text{BTU}}{^\circ\text{F-lbm}}]$
c_{p_s}	steam heat capacity	0.762	$[\frac{\text{BTU}}{^\circ\text{F-lbm}}]$
C_{st}	adjustable pressure control variable	10	$[-]$
D_{is}	diameter inside shell	3.5	[ft]
D_{it}	internal tube diameter	4.642e-02	[ft]
D_{os}	diameter outside shell	6.84	[ft]

Continued on next page

Table B.1 – *Continued from previous page*

Parameter	**Description**	**Value**	**Unit**
D_{ot}	outer tube diameter	5.208e-02	[ft]
D_r	riser internal diameter	3.5	[ft]
h_{fg}	heat of vaporization used for dLb/dt	664.9	$[\frac{\text{BTU}}{\text{lbm}}]$
h_{pw}	primary to wall htc	1.807	$[\frac{\text{BTU}}{\text{s-ft}^2\text{-}^\circ\text{F}}]$
h_{wb}	htc wall to boiling node	2.16647	$[\frac{\text{BTU}}{\text{s-ft}^2\text{-}^\circ\text{F}}]$
h_{ws}	htc wall to steam node	0.6672	$[\frac{\text{BTU}}{\text{s-ft}^2\text{-}^\circ\text{F}}]$
h_{wsc}	htc wall to subcooled node	1.18	$[\frac{\text{BTU}}{\text{s-ft}^2\text{-}^\circ\text{F}}]$
k_c	pressure control valve coefficient	5	$[-]$
K_B	partial boiling density wrt pressure	-5.300e-05	$[\frac{\text{ft}^2}{\text{s}^2}]$
K_1	partial Tsat wrt sc pressure	8.023e-04	$[\frac{\text{F-ft}^2}{\text{lbf}}]$
K_{sc}	partial sc density wrt sc pressure	-5.300e-05	$[\frac{\text{ft}^2}{\text{s}^2}]$
ρ_b	boiling fluid density	45.14	$[\frac{\text{lbm}}{\text{ft}^3}]$
ρ_f	boiling density	45.138	$[\frac{\text{lbm}}{\text{ft}^3}]$
ρ_{fw}	feedwater density	53.47	$[\frac{\text{lbm}}{\text{ft}^3}]$
ρ_p	primary fluid density	44.75	$[\frac{\text{lbm}}{\text{ft}^3}]$
ρ_s	steam density	1.5358	$[\frac{\text{lbm}}{\text{ft}^3}]$
ρ_{sc}	subcooled fluid density	50.76	$[\frac{\text{lbm}}{\text{ft}^3}]$
ρ_w	inconel 690 density	526	$[\frac{\text{lbm}}{\text{ft}^3}]$
L	active SG tube length	28	[ft]
L_b	boiling length	19.9302	[ft]
L_s	steam length	3.85776	[ft]
L_{sc}	subcooled length	4.21202	[ft]
M_{stm}	molar weight of steam	18	$[\frac{\text{lbm}}{\text{lbmol}}]$
N	number of tubes	6546	$[-]$
P_s	steam pressure	825	[psia]
P_{set}	steam pressure setpoint	825	[psia]

Continued on next page

Table B.1 – *Continued from previous page*

Parameter	Description	Value	Unit
P_{sat}	saturated pressure	1138.56	[psia]
$\frac{\mathrm{dP_{sc}}}{\mathrm{dt}}$	rate of change of sc pressure	0.0	$[\frac{\mathrm{psia}}{\mathrm{s}}]$
P_{sc}	subcooled pressure	-1602.11	[psia]
R	universal gas constant	10.7316	$[\frac{\mathrm{ft^3\text{-}psia}}{\mathrm{R\text{-}lbmol}}]$
R_{is}	downcomer outer diameter	7.5	[ft]
R_{it}	internal tube radius	2.321e-02	[ft]
R_{os}	downcomer inner diameter	3.75	[ft]
R_{ot}	outer tube radius	2.604e-02	[ft]
R_r	riser internal radius	1.75	[ft]
R_{th}	riser thickness	0.125	[ft]
RPV_{od}	RPV outer diameter	13.0	[ft]
RPV_{th}	RPV thickness	0.416667	[ft]
t_s	pressure control time constant	1	$[\frac{1}{\mathrm{s}}]$
T_{sat}	saturation temperature	559.079	[°F]
T_{th}	tube wall thickness	2.833e-03	[ft]
W_{sc}	subcooled flow	504.059	$[\frac{\mathrm{lbm}}{\mathrm{s}}]$
W_{db}	transition to boiling flow	504.059	$[\frac{\mathrm{lbm}}{\mathrm{s}}]$
W_b	boiling flow	504.059	$[\frac{\mathrm{lbm}}{\mathrm{s}}]$
W_p	primary flow	8333.33	$[\frac{\mathrm{lbm}}{\mathrm{s}}]$
W_{fw}	feedwater flow	504.059	$[\frac{\mathrm{lbm}}{\mathrm{s}}]$
W_s	steam flow	504.059	$[\frac{\mathrm{lbm}}{\mathrm{s}}]$
W_{s_0}	nominal steam flow	504.058	$[\frac{\mathrm{lbm}}{\mathrm{s}}]$
Z_{ss}	steam expansion coefficient	0.8313	$[-]$

Appendix C

Balance of Plant

Table C.1: Balance of Plant Model Inputs

Parameter	Description	Value	Unit
A_{K2}	constant which relates the flow and pressure drop in a turbine with many stages	3.0326	$[-]$
H_{FW}	heat transfer coefficient of feedwater heaters	215.0	$[\frac{\text{BTU}}{\text{lbm}}]$
H_R	heat transfer coefficient of reheater	0.513996	$[\frac{\text{BTU}}{\text{lbm}}]$
h_C	enthalpy of main steam at nozzle chest	1271.21	$[\frac{\text{BTU}}{\text{lbm}}]$
h_R	enthalpy of fluid at reheater	1273.67	$[\frac{\text{BTU}}{\text{lbm}}]$
h_S	enthalpy of main steam at throttle valve	1272.48	$[\frac{\text{BTU}}{\text{lbm}}]$
h_2	enthalpy of main steam at moisture separator	1234.77	$[\frac{\text{BTU}}{\text{lbm}}]$
h_2'	enthalpy of main steam at isentropic end points from pressure P_C	1146.79	$[\frac{\text{BTU}}{\text{lbm}}]$
h_4'	enthalpy of main steam at isentropic end points from pressure P_R	898.0	$[\frac{\text{BTU}}{\text{lbm}}]$
h_f	enthalpy of saturated water in the reheater feedwater	423.022	$[\frac{\text{BTU}}{\text{lbm}}]$
h_{fw}'	enthalpy of saturated water leaving heater 1	73.2943	$[\frac{\text{BTU}}{\text{lbm}}]$

Continued on next page

Table C.1 – *Continued from previous page*

Parameter	Description	Value	Unit
h_{fw}	enthalpy of saturated water leaving heater 2	76.0037	$[\frac{\text{BTU}}{\text{lbm}}]$
h_0	enthalpy of saturated water in the condenser	69	$[\frac{\text{BTU}}{\text{lbm}}]$
h_{fg}	latent heat of vaporization in the reheater feedwater	1.278e-03	$[\frac{\text{BTU}}{\text{lbm}}]$
h_g	enthalpy of saturated steam in the reheater feedwater	1204.86	$[\frac{\text{BTU}}{\text{lbm}}]$
J	constant to relate mechanical energy and heat energy	1.285e-03	$[\frac{\text{BTU}}{\text{ft-lbf}}]$
K_3	throttling valve coefficient	1.8	$[-]$
K_{BHP}	coefficient which indicates the amount of bled steam from the high pressure turbine	0.1634	$[-]$
K_{BLP}	coefficient which indicates the amount of bled steam from the low pressure turbine	0.2174	$[-]$
η_{HP}	isentropic efficiency of the high pressure turbine	0.86	$[-]$
η_{LP}	isentropic efficiency of the low pressure turbine	0.86	$[-]$
ρ_2	density of steam at the HP turbine outlet	0.830115	$[\frac{\text{lbm}}{\text{ft}^3}]$
ρ_c	density of steam in the nozzle chest	0.922298	$[\frac{\text{lbm}}{\text{ft}^3}]$
ρ_R	density of steam in the reheater	0.729078	$[\frac{\text{lbm}}{\text{ft}^3}]$
P_C	pressure in nozzle chest	504.116	[psia]
P_R	pressure in reheater	397.022	[psia]
P_S	pressure in main steam line	825	[psia]
Q_{H1}	heat transfer rate in the reheater	2164.59	$[\frac{\text{BTU}}{\text{s}}]$
Q_{H2}	heat transfer rate in the reheater	1365.67	$[\frac{\text{BTU}}{\text{s}}]$

Continued on next page

Table C.1 – *Continued from previous page*

Parameter	**Description**	**Value**	**Unit**
Q_R	heat transfer rate in the reheater	23920.4	$[\frac{\text{BTU}}{\text{s}}]$
R	universal gas constant	0.563880	$[\frac{\text{ft}^3\text{-lbf}}{\text{F-lbm-in}^2}]$
T_{H1}	time constant associated with heater No. 1	100	$[\frac{1}{s}]$
T_{H2}	time constant associated with heater No. 2	65	$[\frac{1}{s}]$
T_{H2P}	time constant associated with shell side of heater No. 1	10	$[\frac{1}{s}]$
T_{R1}	time constant associated with reheater flow rate	3	$[\frac{1}{s}]$
T_{R2}	time constant associated with reheater heat transfer rate	10	$[\frac{1}{s}]$
T_{w2}	time constant associated with HP turbine	2	$[\frac{1}{s}]$
T_{w3}	time constant associated with with LP turbine	10	$[\frac{1}{s}]$
V_C	total effective volume of the nozzle chest	200	$[\text{ft}^3]$
V_R	total effective volume of the reheater	2000	$[\text{ft}^3]$
ν_f	specific volume of saturated water	0.0184	$[\frac{\text{ft}^3}{\text{lbm}}]$
ν_g	specific volume of saturated steam	1.16182	$[\frac{\text{ft}^3}{\text{lbm}}]$
w_1	steam flow into nozzle chest	423.409	$[\frac{\text{lbm}}{\text{s}}]$
w_2	steam flow from nozzle chest to HP turbine	423.409	$[\frac{\text{lbm}}{\text{s}}]$
w_2'	fluid flow from moisture separator to reheater	367.492	$[\frac{\text{lbm}}{\text{s}}]$
w_2''	steam flow from HP turbine to moisture separator	354.224	$[\frac{\text{lbm}}{\text{s}}]$
w_3	steam flow from reheater to LP turbine	367.492	$[\frac{\text{lbm}}{\text{s}}]$
w_3'	fluid flow from low pressure turbine to condenser	287.599	$[\frac{\text{lbm}}{\text{s}}]$

Continued on next page

Table C.1 – *Continued from previous page*

Parameter	**Description**	**Value**	**Unit**
w_{BHP}	high pressure turbine bleed flow	69.1851	$[\frac{\text{lbm}}{\text{s}}]$
w_{BLP}	bleed flow from low pressure turbine to heater one	79.8928	$[\frac{\text{lbm}}{\text{s}}]$
w_{MS}	bleed flow from moisture separator to heater two	-13.2679	$[\frac{\text{lbm}}{\text{s}}]$
w_{PR}	bypass flow from main steam entering reheater	80.6494	$[\frac{\text{BTU}}{\text{lbm}}]$
w'_{PR}	bypass flow from main steam leaving reheater and entering heater two	80.6494	$[\frac{\text{BTU}}{\text{lbm}}]$
W_{fw}	feedwater flow rate	504.059	$[\frac{\text{lbm}}{\text{s}}]$
x	enthalpy ratio	1.03746	$[-]$

Appendix D

Model Output

Table D.1: Steady State Model Output

ID	Param	Description	Value	Unit
cor-01	ρ_{tot}	total reactivity	-1.73929e-12	[-]
cor-02	T_{cl}	coldleg temperature	566.3	[°F]
cor-03	P_{th}	thermal power	1.0135	[MWt]
cor-04	β_1	first delayed group	180.631	[-]
cor-05	β_2	second delayed group	487.475	[-]
cor-06	β_3	third delayed group	119.885	[-]
cor-07	β_4	fourth delayed group	89.127	[-]
cor-08	β_5	fifth delayed group	6.85443	[-]
cor-09	β_6	sixth delayed group	0.946154	[-]
cor-10	T_f	fuel ht temperature	973.061	[°F]
cor-11	θ_1	lower node	588.5	[°F]
cor-12	θ_2	upper node	610.7	[°F]
cor-13	T_{hl}	hotleg temperature	610.7	[°F]
stg-01	T_{p1}	primary temperature node 1	610.331	[°F]

Continued on next page

Table D.1 – *Continued from previous page*

ID	Param	Description	Value	Unit
stg-02	T_{p2}	primary temperature node 2	609.129	[°F]
stg-03	T_{p3}	primary temperature node 3	585.995	[°F]
stg-04	T_{p4}	primary temperature node 4	573.554	[°F]
stg-05	T_{p5}	primary temperature node 5	571.845	[°F]
stg-06	T_{p6}	primary temperature node 6	566.3	[°F]
stg-07	T_{w1}	sg tube wall temperature node 1	609.06	[°F]
stg-08	$T_{\cdot w2}$	sg tube wall temperature node 2	604.985	[°F]
stg-09	T_{w3}	sg tube wall temperature node 3	570.556	[°F]
stg-10	T_{w4}	sg tube wall temperature node 4	565.251	[°F]
stg-11	T_{w5}	sg tube wall temperature node 5	566.446	[°F]
stg-12	T_{w6}	sg tube wall temperature node 6	548.789	[°F]
stg-13	T_{s1}	steam temperature node 1	605.992	[°F]
stg-14	T_{s2}	steam temperature node 2	594.981	[°F]
stg-15	T_{sc2}	subcooled temperature node 2	524.892	[°F]
stg-16	T_{pin}	primary inlet temperature	610.7	[°F]
stg-17	$\frac{dL_{sc}}{dt}$	rate of subcooled length	-8.35988e-11	$[\frac{ft}{s}]$
stg-18	L_{sc}	subcooled length	4.21202	[ft]
stg-19	$\frac{dL_{b}}{dt}$	rate of boiling length	-5.51697e-10	$[\frac{ft}{s}]$
stg-20	L_{b}	boiling length	19.9302	[ft]
stg-21	$\frac{dL_{s}}{dt}$	rate of steam pressure	6.35298e-10	$[\frac{ft}{s}]$
stg-22	L_{s}	steam pressure	3.85776	[ft]
stg-23	$\frac{dP_{sc}}{dt}$	rate of subcooled pressure	1.33452e-11	$[\frac{psfa}{s}]$
stg-24	P_{sc}	subcooled pressure	-230704	[psfa]
stg-25	$\frac{dP_{sat}}{dt}$	rate of saturated pressure	0.000175242	$[\frac{psfa}{s}]$

Continued on next page

Table D.1 – *Continued from previous page*

ID	Param	Description	Value	Unit
stg-26	$\mathrm{P_{sat}}$	saturated pressure	163953	[psfa]
stg-27	$\mathrm{T_{sat}}$	saturation temperature	559.079	[°F]
stg-28	$\frac{\mathrm{dP_s}}{\mathrm{dt}}$	rate of steam pressure	-1.043e-04	$[\frac{\mathrm{psfa}}{\mathrm{s}}]$
stg-29	$\mathrm{P_s}$	steam pressure	118800	[psfa]
stg-30	$\mathrm{T_{fw}}$	feedwater temperature	414	[°F]
stg-31	$\mathrm{W_{fw}}$	feedwater flow	504.059	$[\frac{\mathrm{lbm}}{\mathrm{s}}]$
stg-32	$\mathrm{W_{sc}}$	subcooled flow	504.059	$[\frac{\mathrm{lbm}}{\mathrm{s}}]$
stg-33	$\mathrm{W_{db}}$	transition to boiling flow	504.059	$[\frac{\mathrm{lbm}}{\mathrm{s}}]$
stg-34	$\mathrm{W_b}$	boiling flow	504.059	$[\frac{\mathrm{lbm}}{\mathrm{s}}]$
stg-35	$\mathrm{W_{12}}$	flow between superheat nodes	504.059	$[\frac{\mathrm{lbm}}{\mathrm{s}}]$
stg-36	$\mathrm{W_s}$	main steam flow	504.059	$[\frac{\mathrm{lbm}}{\mathrm{s}}]$
stg-37	$\mathrm{K_b}$	partial boiling density wrt pressure	-5.3e-05	$[\frac{\mathrm{ft}^2}{\mathrm{s}^2}]$
stg-38	$\mathrm{K_1}$	Tsat wrt sc pressure	8.023e-04	$[\frac{\mathrm{F\text{-}ft}^2}{\mathrm{lbf}}]$
stg-39	$\frac{1}{\mathrm{K_1}}$	inverted Tsat wrt sc pressure	1246.42	$[\frac{\mathrm{lbf}}{\mathrm{F\text{-}ft}^2}]$
stg-40	$\mathrm{K_{sc}}$	partial sc density wrt sc pressure	-5.3e-05	$[\frac{\mathrm{ft}^2}{\mathrm{s}^2}]$
stg-41	$\frac{1}{\mathrm{K_{sc}}}$	inverted partial sc density wrt sc pressure	-18867.9	$[\frac{\mathrm{s}^2}{\mathrm{ft}^2}]$
stg-42	$\mathrm{W_s}$	steam pressure control	504.059	$[\frac{\mathrm{lbm}}{\mathrm{s}}]$
stg-43	P_{th}	thermal fractional power	101.35	[–]
stg-44	$\frac{1}{\mathrm{T_{sat}}}$	inverted saturation temperature	1.789e-03	$[\frac{1}{°\mathrm{F}}]$
stg-45	$\frac{1}{\mathrm{L_{sc}}}$	inverted subcooled length	0.237416	$[\frac{1}{\mathrm{ft}}]$
cst-01	$\frac{\mathrm{dh_c}}{\mathrm{dt}}$	rate of enthalpy change in steam chest	-1.522e-08	$[\frac{\mathrm{BTU}}{\mathrm{lbm\text{-}s}}]$
cst-02	$\mathrm{h_c}$	enthalpy of main steam at nozzle chest	1272.48	$[\frac{\mathrm{BTU}}{\mathrm{lbm}}]$
cst-03	$\frac{\mathrm{d}\rho_\mathrm{c}}{\mathrm{dt}}$	rate of change of steam density in chest	-1.18009e-11	$[\frac{\mathrm{lbm}}{\mathrm{ft}^3\text{-}\mathrm{s}}]$
cst-04	ρ_c	steam density in nozzle chest	0.922298	$[\frac{\mathrm{lbm}}{\mathrm{ft}^3}]$

Continued on next page

Table D.1 – *Continued from previous page*

ID	Param	Description	Value	Unit
cst-05	$\frac{1}{\rho_c}$	inverse steam density in chest	1.08425	$[\frac{ft^3}{lbm}]$
cst-06	w_2	steam flow exiting nozzle chest	423.409	$[\frac{lbm}{s}]$
cst-07	P_C	Pressure in nozzle chest	72592.7	[psfa]
cst-08	x	steam quality into moisture separator	1.03746	[–]
cst-09	ρ_2	steam density into moisture separator	0.830115	$[\frac{lbm}{ft^3}]$
cst-10	ν_g	specific volume of saturated steam	1.16182	$[\frac{ft^3}{lbm}]$
cst-11	h_f	enthalpy of saturated water in the reheater feedwater	423.022	$[\frac{BTU}{lbm}]$
cst-12	h_{fg}	specific enthalpy change of evaporation in the reheater fluid	1.278e-03	$[\frac{BTU}{lbm}]$
hpt-01	$\frac{dw_2''}{dt}$	rate of change of mass flow into moisture separator	4.790e-10	$[\frac{lbm}{s^2}]$
hpt-02	w_2''	mass flow into moisture separator	354.224	$[\frac{lbm}{s}]$
hpt-03	w_{BHP}	bleed flow from high pressure turbine to heater 2	69.1851	$[\frac{lbm}{s}]$
hpt-04	h_2	enthalpy of main steam at moisture separator	1234.77	$[\frac{BTU}{lbm}]$
hpt-05	h_2'	enthalpy of main steam at isentropic end points from pressure P_C	1146.79	$[\frac{BTU}{lbm}]$
msr-01	w_{MS}	flow exiting hotwell of moisture separator to heater 2	-13.2679	$[\frac{lbm}{s}]$
msr-02	w_2'	steam flow from moisture separator to reheater	367.492	$[\frac{lbm}{s}]$
rhr-01	$\frac{d\rho_R}{dt}$	rate of change of density of steam in reheater	-7.60338e-13	$[\frac{lbm}{ft^3\text{-}s}]$
rhr-02	ρ_R	density of steam in reheater	0.729078	$[\frac{lbm}{ft^3}]$
rhr-03	$\frac{1}{\rho_R}$	inverse reheater steam density	1.3716	$[\frac{ft^3}{lbm}]$

Continued on next page

Table D.1 – *Continued from previous page*

ID	Param	Description	Value	Unit
rhr-04	$\frac{dh_R}{dt}$	change in enthalpy of main steam in reheater	-1.50473e-10	$[\frac{BTU}{lbm\text{-}s}]$
rhr-05	h_R	enthalpy of main steam in reheater	1269.95	$[\frac{BTU}{lbm}]$
rhr-06	$\frac{1}{h_R}$	inverse enthalpy of main steam in reheater	7.874e-04	$[\frac{lbm}{BTU}]$
rhr-07	P_R	pressure in reheater	57171.1	[psfa]
rhr-08	w_3	steam flow from reheater to low pressure turbine	367.492	$[\frac{lbm}{s}]$
rhr-09	h_g	enthalpy	1204.86	$[\frac{BTU}{lbm}]$
rhr-10	$\frac{dW_{1PR}}{dt}$	change in flow from reheater to heater 2	-8.96089e-11	$[\frac{lbm}{s^2}]$
rhr-11	W_{1PR}	flow from reheater to heater 2	80.6494	$[\frac{lbm}{s}]$
rhr-12	$\frac{dQ_R}{dt}$	change in heat transfer rate in reheater	2.847e-08	$[\frac{BTU}{s^2}]$
rhr-13	Q_R	heat transfer rate in reheater	23920.4	$[\frac{BTU}{s}]$
rhr-14	T_R	temperature of reheater fluid	913.542	[°F]
lpt-01	$\frac{dw'_3}{dt}$	change in steam flow from low pressure turbine to condenser	-2.02711e-10	$[\frac{lbm}{s^2}]$
lpt-02	w'_3	steam flow from low pressure turbine to condenser	287.599	$[\frac{lbm}{s}]$
lpt-03	w_{BLP}	bleed flow from low pressure turbine to heater 1	79.8928	$[\frac{lbm}{s}]$
fha-01	$\frac{dh'_{fw}}{dt}$	change in feedwater enthalpy	-2.37181e-12	$[\frac{BTU}{lbm\text{-}s}]$
fha-02	h'_{fw}	feedwater enthalpy	73.2943	$[\frac{BTU}{lbm}]$
fha-03	h_0	heat transfer rate in heater 1	69	$[\frac{BTU}{s}]$
fha-04	Q_{H1}	feedwater flow	2164.59	$[\frac{lbm}{s}]$
fhb-01	$\frac{dh_{fw}}{dt}$	change of enthalpy in fluid leaving heater 2	-4.73654e-12	$[\frac{BTU}{lbm\text{-}s}]$
fhb-02	h_{fw}	enthalpy of fluid leaving heater 2	76.0037	$[\frac{BTU}{lbm}]$
fhb-03	Q_{H2}	heat transfer rate in heater 2	1365.67	$[\frac{BTU}{s}]$

Continued on next page

Table D.1 – *Continued from previous page*

ID	Param	Description	Value	Unit
fhb-04	$\frac{\mathrm{dw}'_{\mathrm{HP}}}{\mathrm{dt}}$	change in flow from heater 2 wet well to heater 1	-7.29386e-11	$[\frac{\mathrm{lbm}}{\mathrm{s}^2}]$
fhb-05	$\mathrm{W}'_{\mathrm{HP}}$	flow from heater 2 wet well to heater 1	136.567	$[\frac{\mathrm{lbm}}{\mathrm{s}}]$

Vita

Jeff Kapernick was born in San Diego, California in 1982. He grew up in Leucadia where he attended Pacific View elementary, Digueno middle school and in 1996 his family moved to Los Alamos, New Mexico where he attended Los Alamos High School.

In 2007 He received a B.S. degree in biology from the University of New Mexico. He returned to San Diego and worked briefly in the biotechnical industry before deciding to return to college in pursuit of a nuclear engineering degree. In 2013 he received a B.S. degree in nuclear engineering from Oregon State Univeristy. Following graduation he attended the University of Tennessee as a graduate student working toward a M.S. degree in nuclear engineering. His professional work experience and interests include reactor system modeling, severe accident and safety analysis, thermal hydraulics, reactor operations, reactor physics and core design.